ISBN 978-82-326-1567-4 (printed version)
ISBN 978-82-326-1566-7 (electronic version)
ISSN 1503-8181

Doctoral theses at NTNU, 2016:114

Erlend Grytli Tveten

Manipulating Spins in Antiferromagnets with External Forces

NTNU
Norwegian University of
Science and Technology

NTNU
Norwegian University of
Science and Technology

Doctoral theses at NTNU, 2016:114

NTNU

NTNU
Norwegian University of
Science and Technology
Faculty of Natural Sciences and Technology
Department of Physics

NTNU
Norwegian University of
Science and Technology

Erlend Grytli Tveten

Manipulating Spins in Antiferromagnets with External Forces

Thesis for the degree of Philosophiae Doctor

Trondheim, April 2016

Norwegian University of Science and Technology
Faculty of Natural Sciences and Technology
Department of Physics

NTNU
Norwegian University of
Science and Technology

NTNU
Norwegian University of Science and Technology

Thesis for the degree of Philosophiae Doctor

Faculty of Natural Sciences and Technology
Department of Physics

ISBN 978-82-326-1567-4 (printed version)
ISBN 978-82-326-1566-7 (electronic version)
ISSN 1503-8181

Doctoral theses at NTNU, 2016:114

Printed by Skipnes Kommunikasjon as

Abstract

This thesis presents five papers on theoretical spintronics. Four of the papers describe antiferromagnets and the interactions between the magnetic order parameter and external forces induced by charge currents, spin waves, magnetic fields, and stochastic temperature fluctuations. The fifth paper studies the ultrafast magnetic response of a ferromagnet after rapid heating by a laser pulse.

A significant part of the presented work is devoted to describing dynamics of the antiferromagnetic order parameter. To this end, we develop the conceptually simple collective coordinate equations of motion and demonstrate that the dynamics of antiferromagnetic textures are equivalent to the inertial motion of classical particles subject to external forces and dissipation-induced friction. We apply the collective coordinate method to describe the dynamics of antiferromagnetic domain walls. First, we study a domain wall under the influence of a charge current. Second, we describe the interactions between a domain wall and antiferromagnetic spin waves and show that the resulting domain wall dynamics depend crucially on the polarization of the spin waves. Third, we demonstrate the possibility of accurately controlling the position of an antiferromagnetic domain wall using external magnetic fields. The interactions between inhomogeneous magnetic fields and antiferromagnetic domain walls result from the intrinsic magnetization of textures in the order parameter.

By applying the fluctuation-dissipation theorem, we include finite temperature effects to the dynamic equations of motion for a homogeneous antiferromagnet. We calculate that the heat current between an antiferromagnetic insulator and an adjacent normal metal is substantial and carried by a staggered spin current. We complete the transition to the high-temperature regime by developing a theory of out-of-equilibrium ultrafast spin dynamics in a ferromagnetic metal based on electron-magnon scattering. The theory includes the effects from a nonthermalized magnon distribution function and the out-of-equilibrium spin accumulation among the itinerant electrons.

To friends and family

Being a PhD student is not just a job, but also a lifestyle. It is hard to let go of your project when you leave the work desk in the afternoon. Quite often, I have found solutions to my problems while walking home with a wandering mind. Now, this period of my life is reaching its end, and I am left with mixed feelings of relief and melancholy. Relief because I have reached an important milestone, and melancholy because the fifth floor in the science building at NTNU has been my second home for four years. Here, I have met some of my best friends, for which I am most grateful.

Foremost, I would like to express my deepest gratitude to my supervisor, Professor Arne Brataas. Thank you for all your help and support, your patience when the work went slowly, and your indisputable physical insight. I am most grateful to you for giving me the opportunity to take part in your scientific network and visit conferences, summer schools, and other research groups all over the world.

My sincere acknowledgement goes to all my co-authors and in particular to postdoc Alireza Qaiumzadeh. Thank you very much for the countless hours of vivid discussions in front of the blackboard in the lunch room and for the invaluable support in the first years of my PhD. I would also like to thank Oleg Tretiakov, Hans Skarsvåg, Eirik Fjærbu, Tristan Müller, and Jacob Linder for the great collaboration with my papers. My appreciation also goes to Professor Yaroslav Tserkovnyak, Scott Bender, and So Takei for their hospitality during my visit at the University of California in Los Angeles in the spring of 2014. The collaboration with the UCLA group is definitely one of the highlights of my time as a PhD student.

Thanks to my office inmates Hans, Camilla, Lars, and André for all the discussions, practical jokes, sporting events, chess games, and the general fun that have made my work days brighter. Without friends like you, the everyday life as a PhD student would be dark and miserable indeed. Many thanks also to Peder, William, Severin, Eirik, Stefan, Peter, Sol, Sverre, Therese, and Cecilia, for contributing to the great social environment at the theory section, and to Eli, Inger, Peder, Magni, and Solveig at the department administration for always meeting my problems with a smile.

In addition, I would like to thank my parents Ingvil and Kjell Erik and my two sisters Silje and Åsa, for bringing me up in a family that cherishes knowledge, discussion, and the ability to regard every problem from a meta perspective to reveal the bigger picture. Finally, my deepest love goes to the two girls that are the moon and the stars of my night sky. My beautiful fiancée and the love of my life, Carina. You have stood by my side when the days have been rough and the hours have been long. I would not have reached this far without your love and support or your delicious lunch packages. I am deeply grateful for having you in my life. A special place in my heart is occupied by my lovely daughter Eirin. Your smiles and laughter remind me that there are much more important things in life than work.

Erlend Grytli Tveten
Trondheim, February 2016

To the non-physicist

Most people are familiar with the elusive particles called *electrons*. They are popularly visualized as orbiting around the atomic nuclei almost like a miniature analog of the planets in the solar system. In metals, the outermost electrons are so loosely bound to the nuclei that they roam freely around in the crystal grid of atoms and form a sea of charged particles. Because of their elementary charge, an electric potential (voltage) can transform this electron sea into a flowing river of charge current, which humanity has learned to exploit for electricity.

However, the charge-current river does not run still. There is resistance. The electrons crash into each other emitting light and heating up their proximity. Sometimes, the heat or the light from electricity is a desirable effect, for example on cold and dark Norwegian winter nights. In other situations, the electronic heat waste is a nuisance, for example when your laptop burns your thighs or your smart phone needs recharging twice a day. For the electronics industry, the ability to process information with less energy loss is one of the foremost technological challenges of our time because information processing represents a significant share of our total energy consumption.

Now, imagine that we could send information as ripples on the surface of a calm electron sea instead of along violent rivers of colliding electrons. In addition to its charge, the electron possesses another fundamental property, namely its *spin*. Because electrons are "point-like" particles, the electron spin is a property that arises from quantum mechanics. Still, we typically visualize the electron as a small spherical particle rotating around its own axis. The axis of rotation is called the spin axis. Because electrons in magnetic materials influence each other through their spins, it is possible to transmit signals without moving the electrons at all.

There exists a special type of materials, called ferromagnets, in which it is energetically favorable for an electron to align its spin axis along the spin axes of its neighboring electrons. A huge ensemble of quantum spins with their spin axes aligned is responsible for a macroscopic phenomenon that has been well known for thousands of years: *magnetism*. The subfield of condensed matter physics that deals with *nano*-magnetism is called "spin electronics", or *spintronics*. In addition to revealing the complex interplay between electron spins, charges, and magnetic fields, the technological goal of spintronics is to develop devices for information processing that are faster, more energy efficient, and more flexible than those which are predominantly used today.

The main focus of this thesis is on a different type of magnetic materials, called antiferromagnets. In these materials, it is energetically favorable for neighboring electrons to align their spins in an antiparallel configuration. Because the spins in this way cancel each other out, antiferromagnets, in contrast to ferromagnets, have no macroscopic magnetization and will not stick to your refrigerator door. In this thesis, I describe the highly ordered spin state of these materials and their interactions with charges, currents, and magnetic fields. Many of the presented phenomena are richer, faster, and more interesting than their analogous ferromagnetic counterparts.

List of papers

Paper [1]
"Staggered Dynamics in Antiferromagnets by Collective Coordinates",
Erlend G. Tveten, Alireza Qaiumzadeh, Oleg A. Tretiakov, and Arne Brataas,
Physical Review Letters **110**, 127208 (2013).

Paper [2]
"Antiferromagnetic Domain Wall Motion Induced by Spin Waves",
Erlend G. Tveten, Alireza Qaiumzadeh, and Arne Brataas,
Physical Review Letters **112**, 147204 (2014).

Paper [3]
"Electron-magnon scattering in magnetic heterostructures far out of equilibrium",
Erlend G. Tveten, Arne Brataas, and Yaroslav Tserkovnyak,
Physical Review B **92**, 180412(R) (2015).
This paper was chosen as an *Editor's Suggestion* in the 18$^{\text{th}}$ issue of PRB in 2015.

Paper [4]
"Heat transport between antiferromagnetic insulators and normal metals",
Arne Brataas, Hans Skarsvåg, Erlend G. Tveten, and Eirik L. Fjærbu,
Physical Review B **92**, 180414(R) (2015).

Paper [5]
"Intrinsic magnetization of antiferromagnetic textures",
Erlend G. Tveten, Tristan Müller, Jacob Linder, and Arne Brataas,
Physical Review B **93**, 104408 (2016).

My contribution to the papers

When listed as the first author, I have contributed significantly to all parts of the paper. For these papers [1–3, 5], I have done the majority of the analytical work, developed the models used for the numerical analyses in the papers, produced the figures, and organized the discussion with the co-authors. I have also written most of the text in the papers and led the subsequent correspondence in the review processes.

For paper [4], I have participated in the discussion and quality control of the analytical results and participated in writing the paper. The analytical work and the formulation of the model is mainly the work of the first author.

Preface

This thesis concludes four years of study at the division for theoretical condensed matter physics at the Department of Physics at the Norwegian University of Science and Technology (NTNU). The scientific work presented in this thesis can be categorized within *spintronics*, a subfield of condensed matter physics that describes physical phenomena originating from the spin properties of the electrons. As the title suggests, the main focus of this thesis is on a class of highly ordered magnetic materials called *antiferromagnets*, which exhibit no macroscopic magnetization, in contrast to the more commonly known *ferromagnets*.

The thesis is organized as follows. The main body of scientific work submitted for the degree of Philosophiae Doctor are the five papers [1–5] that are presented at the end of this dissertation. [1, 2] are published in Physical Review Letters and [3–5] are published in the Physical Review B.

In the introductory chapters of this thesis, I present the most important concepts and motivations behind the five succeeding papers. These introductory chapters do not include any new results. Nor do they include any significant supplemental discussions of the main results in the published articles, which are assumed to stand on their own. The main purpose of the introductory part of this thesis is rather to present theoretical and conceptual formalism that, hopefully, can be helpful for new PhD students who are faced with similar problems as those that are presented in my papers.

The introductory chapters consider the papers in conceptual rather than chronological order. At the beginning of each chapter, I present a short motivation for the subsequent discussion and define the context with respect to the appended papers. At the end of each chapter, I include a short outlook that discusses the consequences of the presented work and guides the reader to follow-up literature.

Chapter 1 includes a short layman's introduction to the field of (antiferromagnetic) spintronics.

Chapter 2 discusses the definition of the antiferromagnetic order parameter, the transition from discrete spins to the continuum limit, and the presence of domains and domain walls in antiferromagnets. In this chapter, two important concepts from Paper [5] are presented: the intrinsic magnetization of textured antiferromagnets and the nonequivalence of two different parametrization procedures for the antiferromagnetic continuum fields.

Chapter 3 describes interactions between antiferromagnetic textures and external forces such as currents, fields, and spin waves. From Paper [1], I present the collective coordinate description of antiferromagnetic dynamics, demonstrating that antiferromagnetic textures can be viewed as inertial quasiparticles that react to external current- and magnetic field-induced forces. This chapter also includes two central concepts from the theory of spin-wave-induced antiferromagnetic domain wall motion in Paper [2]: the spin wave response to a localized excitation field and the difference between linearly polarized and circularly polarized antiferromagnetic spin waves.

Chapter 4 includes finite-temperature effects to the dynamic equations for an antiferromagnetic insulator. From Paper [4], I present the fluctuation-dissipation theorem and discuss how the interfacial heat currents between an antiferromagnetic insulator and adjacent normal metals differ from the analogous problem in ferromagnetic insulators.

Chapter 5 describes the high-temperature regime of laser-induced ultrafast spin dynamics. In this chapter, I leave the antiferromagnetic models to describe the ultrafast demagnetization of a ferromagnetic metal via electron-magnon scattering. Two important concepts from Paper [3] are introduced in this chapter: the nonthermalized distribution of the excited magnons and the out-of-equilibrium spin accumulation among the itinerant electrons.

There exists a natural progression from the effective zero-temperature equilibrium considerations in Paper [5], via the external-force-induced domain wall motion in Papers [1, 2], and the small stochastic temperature fluctuations in Paper [4], to, finally, the extreme high-energy limit of ultrafast magnetization dynamics in Paper [3]. The same path also progresses from a classical description of spin vectors on a lattice to a fully quantum mechanical treatment of collective spin excitations. Although the main focus of this thesis is on antiferromagnetic dynamics, Paper [3] deviates from this focus and describes ultrafast spin dynamics in a ferromagnetic metal. However, as I discuss at the end of Chapter 5, a natural next step is to extend this theory to multi-sublattice models. This extension provides the connection to the other articles which focus on antiferromagnets.

Note on the numerical analyses
In Papers [1–3] and [5], I have performed numerical calculations to test the validity of the analytical results. The numerical models have been made in the mathematical computation program *Mathematica*[1]. After spatial discretization (energy discretization in [3]), the equations of motion have been solved using a partial differential equation algorithm that utilizes the numerical method of lines with an adaptive time control. Because the numerical analyses are considered supplemental to the analytical main work of this thesis, I will not describe in detail the numerical method or results from the numerical analyses in these introductory chapters.

Note on the figures
All figures in this thesis have been produced by myself using *Mathematica*, the open-source vector graphics editor *Inkscape*[2], or *Microsoft PowerPoint*, except Fig. 4.1, which has been produced by the second author of Paper [4].

[1] Wolfram Research, Inc., Mathematica, Version 9.0, Champaign, IL (2012).
[2] `http://inkscape.org`

Contents

Chapter 1

Introduction

"We live in a society exquisitely dependent on science and technology, in which hardly anyone knows anything about science and technology."

Carl Sagan, Skeptical Inquirer (1990)

In this chapter, I introduce and motivate the field of *spintronics* and, in particular, the subfield of *antiferromagnetic* spintronics, which is the main focus of this thesis. Sec. 1.1 briefly presents the historical and present technological challenges of *information processing*, which is arguably one of the most defining features of the modern world. In Sec. 1.2, I present the idea of utilizing the electron *spin* as an information carrier, which is the main objective of spintronics research. Sec. 1.3 discusses the differences between ferromagnetic and antiferromagnetic materials and motivates the new and upcoming field of antiferromagnetic spintronics. In Sec. 1.4, I present an outline of the subsequent introductory chapters of this thesis.

1.1 Information processing and energy consumption

One of the strongest driving forces for human technological development is the ability to share, store, and process *information*. Throughout human history, our information processing has evolved from ancient oral storytelling, via the written languages and the printing press from the 15th century, to analog recordings of images, sounds, and live video in the early 20th century. Today, the vast majority of the information we share is stored and processed in a digital language, meaning that information is encoded in memory bits and transistors that only have two states: "1" (on) or "0" (off).

50 years have passed since Gordon R. Moore's famous prediction [6] that the number of transistors per integrated circuit would grow exponentially fast due to the technological development in the semiconductor electronics industry. Indeed, up until today (2016), we have seen a doubling of the processing power of computers roughly every 18 months [7]. In the recent years, however, there is a tendency that this rapid technological development, which has mainly been fueled by more efficient manufacturing technologies, is slowly coming to an inevitable halt [8].

The problems that arise when electronics components become so small that quantum effects from single electrons start to play a role are of a more fundamental nature and may require a shift toward more energy-efficient technology. Due to the coulombic interactions between electrons at room temperature, the thermal noise in nanoscale electronics components can become of comparable strength to the signal contrast and it is difficult to get rid of the excessive heat. An important goal for advancing information processing technology is, therefore, to develop logic elements (e.g., transistors and memory bits) that do not heavily rely on electric currents.

1.2 The electron spin

As an alternative to conventional semiconductor-based microelectronics, the central technological motivation behind the field of *spintronics* is to carry information via the *spin* of the electrons rather than their *charge*. Although the intrinsic spin of the electron is a property that arises from the quantum mechanical Dirac equation [9], it is useful to apply a quasi-classical view of the electron as a rigid sphere rotating around its own axis, see Fig. 1.1. According to classical electrodynamics [10], a rotating charge density with total charge -*e* creates a magnetic dipole with the magnetic dipole moment

$$\boldsymbol{\mu} = -\frac{ge}{2m}\mathbf{L}\,, \tag{1.1}$$

where g is known as the g-factor, m is the rotating mass[1], and $\mathbf{L}$ is the vector of angular momentum. Applied to the quantum mechanical intrinsic spin angular momentum

[1] Note that the magnetic dipole moment is inversely proportional to the rotating particle's mass. As a result, the electron dipole moment is orders of magnitude larger than the dipole moment of the nuclei. However, the nuclear dipole moment also has important technological applications, e.g., within *magnetic resonance imaging* (MRI)

Figure 1.1: The quasi-classical picture of a free-electron spin arising from the rigid spherical electron with total charge $-e$ spinning around its own axis. The intrinsic spin is $\mathbf{S}_e$ with magnitude $|\mathbf{S}_e| = \hbar/2$. Although modern physics views the electron as a "point-like" particle, the classical picture is still popular and widely used due to its intuitive form.

of the electron, $\mathbf{S}_e$, the equation for the electron spin magnetic dipole moment is

$$\boldsymbol{\mu}_s = -\gamma \mathbf{S}_e \,, \tag{1.2}$$

where $\gamma = g_e \mu_\mathrm{B}/\hbar$ is the gyromagnetic ratio, $g_e \approx 2$ is the electron g-factor, μ_B is the Bohr magneton, and $\hbar$ is Planck's constant. The intrinsic spin of a free electron is a vector quantity with a direction and a magnitude $|\mathbf{S}_e| = \hbar/2$. Accordingly, the magnetic dipole moment has dimensions JT^{-1}.

All chemical elements consist of a finite number of electrons, which often minimize their energy by arranging themselves in pairs of spin-"up" and spin-"down" electrons due to the Pauli exclusion principle [11]. As a result, the total intrinsic spin of the electron cloud around the atomic nucleus vanishes for many elements. However, some materials (typically transition metals) have an unpaired electron in their outermost (valence) shell. The total spin magnetic moment of such materials is finite, and they are, for historical reasons, called *magnetic materials*.

The electrons in magnetic materials can influence neighboring valence electrons through their spins. This interaction is called the *exchange* interaction, see Fig. 1.2. The two dominant types of exchange interactions are the ferromagnetic and the antiferromagnetic couplings. In the former, it is energetically favorable for an electron to align its spin axis along the spin axes of its neighboring electrons. The antiferromagnetic coupling, on the other hand, favors antiparallel alignment of neighboring spins.

There exists several different types of magnetic materials. In paramagnets and diamagnets, the electron spins align parallel and antiparallel, respectively, to an applied external magnetic field. The spin alignment enhances (paramagnets) or diminishes (diamagnets) the magnetic field strength inside the material, but the effect vanishes as soon as the external magnetic field is turned off and the spins randomly diffuse. In *ferromagnets* (FMs) and *antiferromagnets* (AFMs), on the other hand, the mutual exchange interaction between neighboring electrons is so strong that magnetic ordering is upheld even without the influence of an external magnetic field.

The ordering of magnetic materials is lost when the material is heated above a certain critical temperature, called the Curie[2] temperature (T_C) for FMs and the Néel[3] tem-

[2] after Pierre Curie.
[3] after Louis Néel [12].

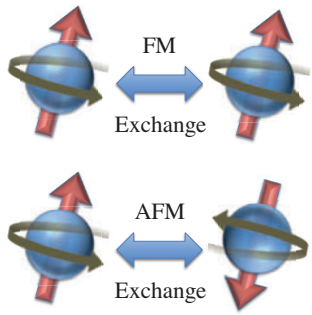

Figure 1.2: Neighboring valence electrons influence each other through the spin-spin exchange interaction. Materials with ordered spin states at equilibrium typically minimize their energy by aligning neighboring spin axes in a parallel (**top**) or antiparallel (**bottom**) configuration. These exchange couplings are called *ferromagnetic* and *antiferromagnetic*, respectively.

perature (T_N) for AFMs. Above these temperatures, most magnetic materials become paramagnetic. Below T_C, FMs exhibit macroscopic *magnetization* from the statistical average of the electron spins. This magnetization has been well known and exploited for thousands of years, e.g., in compasses that couple to Earth's magnetic field. Because the magnetization direction of FMs can be easily measured and manipulated, they are exciting candidates for basic logic elements and have been extensively studied in the last decades. The field of spintronics is mainly focused on the interplay between the ferromagnetic magnetization and charges, currents, and magnetic fields.

One of the most successful discoveries within this field is the *giant magnetoresistance* (GMR) effect [13, 14], which describes that the electrical resistance of magnetic multilayers depends on the magnetization direction of each layer. This discovery was awarded the Nobel Prize in Physics in 2007 and has later generated widespread industrial importance as a fundamental part of magnetic random access memory (MRAM) cells. Another prominent result of spintronics is the *spin transfer torque* (STT) effect [15], which describes how a spin-polarized current can modify the ordered state of a ferromagnetic layer by exerting a torque on the magnetization.

An intriguing possibility in spintronics is to reduce the thermal noise in logic elements by using insulating materials instead of metals or semiconductor. In insulators, information can be carried between stationary spins via the exchange interaction (e.g. spin waves) rather than by moving electrons in charge currents.

1.3 Antiferromagnetic spintronics

In contrast to ferromagnetic materials, neighboring electron spins in AFMs cancel each other out and the statistical average of the magnetic moments vanishes. As a result, AFMs do not exhibit macroscopic magnetization and are harder to detect than FMs. In fact, the antiferromagnetic phase was first discussed in the mid-20$^{\text{th}}$ century after the discovery of the intrinsic spin of the electron. Despite their different macroscopic

behaviors, FMs and AFMs are both types of materials with a strong magnetic ordering on the microscopic level. Reminiscent of the magnetization in FMs, the magnetic order of AFMs can also be measured and manipulated. However, the interactions between the antiferromagnetic order and external forces can be very different from analogous interactions in FMs.

Although they do not (yet) generate the same amount of scientific interest as FMs, antiferromagnetic materials have played important roles as passive components in conventional spintronics circuits for several decades. Most notable is the exploitation of the *exchange bias* effect [16], which describes the extraordinary strong exchange coupling across the interface between a ferromagnetic layer and an antiferromagnetic layer. This effect can been used to "pin" the magnetization direction of ferromagnetic layers in multilayered stacks used for GMR [7].

The field of *antiferromagnetic spintronics* studies the possibility of using AFMs as active information carriers in spintronics circuits [17–19]. AFMs have many properties that make them attractive alternatives to FMs for playing active roles in spintronics components. One of their most important properties is the lack of magnetic stray fields, which allows closer packing of antiferromagnetic elements that do not interfere with the magnetic order of neighboring components. However, the vanishing stray field of AFMs is a double-edged sword: it makes the detection and manipulation of the antiferromagnetic order more challenging than detecting the magnetization in FMs, but it can also lead to stable components that show strong resilience against external perturbations like magnetic fields. Furthermore, the antiparallel exchange interaction between neighboring spins in AFMs leads to very fast dynamics. The order parameter of AFMs can be switched optically on ultrafast time scales [20] and antiferromagnetic spin waves operate coherently at THz frequencies [21], which is much faster than their ferromagnetic counterparts.

1.4 Outline

In the following introductory chapters, I present some of the most important concepts that motivate the main results in Papers [1–5]. The idea is for the reader to have a better understanding of the theoretical and conceptual formalism before embarking on the discussion of the scientific results presented in the subsequent papers. At the end of each chapter, I provide a short summary of the present and potential implications of the presented concepts. For a full discussion of the scientific results, I refer the reader to the papers appended after these introductory chapters.

Chapter 2

The antiferromagnetic order

The concepts presented in this chapter are mainly related to the discussion of the discrete-to-continuous transition for AFMs developed in Paper [5]. The work leading up to this paper was motivated by a series of seemingly contradictory results in the literature concerning one-dimensional antiferromagnetic domain walls: Refs. [22–24] predict that textures in the order parameter are associated with a finite magnetization density, whereas other studies [25–28] do not mention the same connection. Although this discrepancy had been noted in some of the earlier studies, the explanations for the deviating results were rather vague: "[...] some of the finer details of such a reduction [to a continuum model] have been mistreated" [23] and "[...] Haldane [in Ref. [26]] used a different procedure of passing to the continuum limit which did not conserve the total number of degrees of freedom" [22]. The main motivation behind Paper [5] was, therefore, to clear up this confusion using a systematic approach.

In this chapter, Sec. 2.1 presents the transition from the discrete classical Heisenberg Hamiltonian to the continuum model in the exchange approximation. This procedure establishes that antiferromagnetic textures are, indeed, associated with a finite magnetization density. In Sec. 2.2, I discuss typical antiferromagnetic domain wall structures and their properties. I further identify the seemingly contradictory results in the literature as arising from different definitions of the continuum fields in Sec. 2.3, where I compare the discrete-to-continuous *Hamiltonian approach* (applied in Sec. 2.1) with an alternative parametrization procedure called *Haldane's mapping*. Surprisingly, this comparison shows that the two procedures define continuum fields that have critically different physical interpretations. This discrepancy seems so far to have eluded parts of the community. In Sec. 2.4, I include a brief discussion of some of the implications of the presented theory.

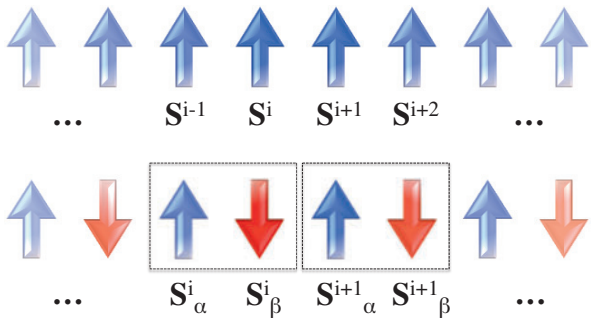

Figure 2.1: (**Top**) Sketch of a one-dimensional spin chain with ferromagnetic nearest-neighbor exchange coupling. In the following, we use arrows to represent single spins, meaning implicitly that each spin is carried by a single electron. For a total of N spins in the spin chain, where S is the magnitude of each spin, the total magnetic moment of the ferromagnetic chain is $M = -\gamma NS$. (**Bottom**) Sketch of a one-dimensional spin chain with antiferromagnetic nearest-neighbor exchange coupling. For an even number of spins in the chain, the total magnetic moment M of a (homogeneous) antiferromagnetic spin chain vanishes.

2.1 From discrete spins to the continuum limit

Our goal is to describe the antiferromagnetic order and (later) its dynamics via classical continuum fields. Naturally, such a representation breaks down if the spin systems that are modeled consist of only a few (e.g., < 10) spins. In such systems, one should expect that the quantum nature of the individual spins plays a relatively more important role and that a classical continuum model is insufficient to describe the spin states. However, because most spin systems of technological importance, at least in 3D, still consist of a large number of spins (e.g., > 100), we expect continuum models to be important descriptive tools for both ferromagnetic and antiferromagnetic systems.

Our starting point is the Heisenberg Hamiltonian due to the exchange coupling between classical spin vectors on a lattice [29]:

$$H = J \sum_{\langle \boldsymbol{\alpha}, \boldsymbol{\beta} \rangle} \mathbf{S}_{\boldsymbol{\alpha}} \cdot \mathbf{S}_{\boldsymbol{\beta}} \,, \tag{2.1}$$

where the positive exchange energy, $J > 0$, describes an antiferromagnetic ground state.[1] See Fig. 2.1 for a schematic comparison between a one-dimensional spin chain with ferromagnetic and antiferromagnetic exchange coupling. In Eq. (2.1), $\langle \boldsymbol{\alpha}, \boldsymbol{\beta} \rangle$ denotes a sum over all nearest-neighbor lattice sites described by the two sublattice indices $\boldsymbol{\alpha}$ and $\boldsymbol{\beta}$, where each spin at an $\boldsymbol{\alpha}$-site has N_D nearest neighbors of type $\boldsymbol{\beta}$, and vice versa. $\boldsymbol{\alpha}$ and $\boldsymbol{\beta}$ must in general be interpreted as D-dimensional vectors, where D is the dimensionality of the AFM. We proceed by describing the simplest model, the

[1] Note that this Hamiltonian describes the ferromagnetic state when $J < 0$. In this state, the spins $\mathbf{S}_{\boldsymbol{\alpha}}$ and $\mathbf{S}_{\boldsymbol{\beta}}$ are equivalent and indistinguishable.

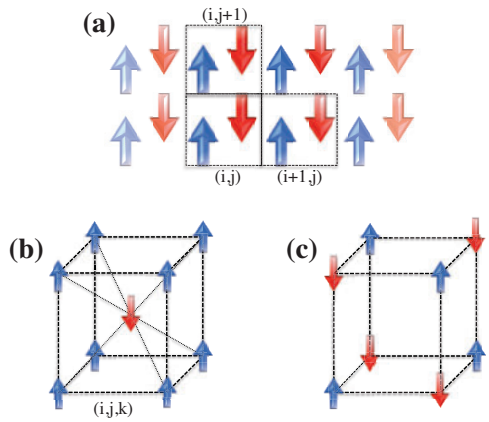

Figure 2.2: For higher-dimensional systems, identifying the antiferromagnetic unit cell becomes increasingly more complicated. **(a)** In 2D, the antiferromagnetic centered squared unit cell can be identified at a 45° angle to the array of spin chains. In 3D, one possibility is the **(b)** body-centered cubic unit cell, which is symmetrically different from the **(c)** simple cubic antiferromagnetic configuration. There exists several different compensated and uncompensated antiferromagnetic spin configurations that can give different dynamics, see, e.g., Ref. [30]. In Paper [5], we study the linear lattice in 1D, the centered squared lattice in 2D, and the body-centered cubic lattice in 3D.

$D = 1$ antiferromagnetic linear spin chain with easy-axis anisotropy. In Paper [5], we show that the following results generalize to the centered squared lattice in 2D and the body-centered cubic lattice in 3D, see Fig. 2.2.

Let us consider a linear spin chain with $2N$ atomic lattice sites, where the spins on half of the lattice sites, indexed by α, minimize their energy by aligning their spins antiparallel to the spin axes of their $N_1 = 2$ nearest neighbor lattice sites, indexed by β, and vice versa. We impose the boundary conditions that the spin on the left end of the spin chain is of type α, whereas the right end of the chain is occupied by a β site. Therefore, in the ground state, the AFM is fully compensated and the total spin vanishes. We define the z axis as the magnetic easy axis. The classical Heisenberg Hamiltonian including the easy-axis anisotropy is

$$H_{1D} = J \sum_{\langle \alpha,\beta \rangle}^{2N-1} \mathbf{S}_\alpha \cdot \mathbf{S}_\beta - K \left(\sum_{\alpha}^{N} S_{\alpha z}^2 + \sum_{\beta}^{N} S_{\beta z}^2 \right) , \tag{2.2}$$

where K is the anisotropy energy. The classical ground state of the Hamiltonian (2.2) is degenerate, $(\mathbf{S}_\alpha, \mathbf{S}_\beta)_0 \rightarrow \pm(S\hat{z}, -S\hat{z})$, where S (in units of $\hbar$) is the spin angular momentum on a single atomic lattice site.

We proceed by introducing the standard definitions[2] of the magnetic and staggered

[2]See Sec. 2.3 for a comparison with an alternative definition that is occasionally mistaken to be equivalent to the present model.

order parameters, $\mathbf{m}_i$ and $\mathbf{l}_i$, on a two-sublattice linear lattice indexed by i [25]:

$$\mathbf{m}_i = \frac{\mathbf{S}^i_\alpha + \mathbf{S}^i_\beta}{2S}, \tag{2.3a}$$

$$\mathbf{l}_i = \frac{\mathbf{S}^i_\alpha - \mathbf{S}^i_\beta}{2S}, \tag{2.3b}$$

where we have paired the sublattice spins $\mathbf{S}^i_\alpha$ and $\mathbf{S}^i_\beta$ in each unit cell running over a total of N antiferromagnetic unit cells. In this convention, $\mathbf{m}_i^2 + \mathbf{l}_i^2 = 1$ and $\mathbf{m}_i \cdot \mathbf{l}_i = 0$. Accordingly, the two spin vectors in unit cell i can be expressed as

$$\mathbf{S}^i_\alpha = S(\mathbf{m}_i + \mathbf{l}_i), \tag{2.4a}$$

$$\mathbf{S}^i_\beta = S(\mathbf{m}_i - \mathbf{l}_i). \tag{2.4b}$$

After inserting the above definition of the sublattice spins in the Heisenberg Hamiltonian, Eq. (2.2) reduces to a sum over antiferromagnetic lattice points:

$$\begin{aligned} H_{1\mathrm{D}} =& JS^2 \sum_i^{N-1} (\mathbf{m}_i - \mathbf{l}_i)[(\mathbf{m}_i + \mathbf{l}_i) + (\mathbf{m}_{i+1} + \mathbf{l}_{i+1})] + JS^2(\mathbf{m}_N^2 - \mathbf{l}_N^2) \\ & - KS^2 \sum_i^N \left[(\mathbf{m}_i + \mathbf{l}_i)_z^2 + (\mathbf{m}_i - \mathbf{l}_i)_z^2 \right]. \end{aligned} \tag{2.5}$$

We continue by using the identities $2\mathbf{m}_i\mathbf{m}_{i+1} = \mathbf{m}_i^2 + \mathbf{m}_{i+1}^2 - (\mathbf{m}_{i+1} - \mathbf{m}_i)^2$ and $(\mathbf{l}_i\mathbf{m}_{i+1} - \mathbf{m}_i\mathbf{l}_{i+1}) = \mathbf{l}_i(\mathbf{m}_{i+1} - \mathbf{m}_i) - \mathbf{m}_i(\mathbf{l}_{i+1} - \mathbf{l}_i)$ to rewrite the bulk part of Eq. (2.5) to

$$\begin{aligned} H_{1\mathrm{D}} \approx & 2JS^2 \sum_i^N (\mathbf{m}_i^2 - \mathbf{l}_i^2) + \frac{JS^2}{2} \sum_i^{N-1} \left[(\mathbf{l}_{i+1} - \mathbf{l}_i)^2 - (\mathbf{m}_{i+1} - \mathbf{m}_i)^2 \right] \\ & + JS^2 \sum_i^{N-1} \left[\mathbf{m}_i(\mathbf{l}_{i+1} - \mathbf{l}_i) - \mathbf{l}_i(\mathbf{m}_{i+1} - \mathbf{m}_i) \right] - 2KS^2 \sum_i^N (m_{i,z}^2 + l_{i,z}^2), \end{aligned} \tag{2.6}$$

where we have disregarded the vanishingly small energy contribution $-JS^2(\mathbf{m}_1^2 + \mathbf{m}_N^2 - \mathbf{n}_1^2 - \mathbf{n}_N^2)/2$ from the edge spins.

In the large-N limit, we may take the continuum approximation, $\Delta \sum_i \to \int dz$ [31], allowing us to write the above Hamiltonian as

$$H_{1\mathrm{D}} \approx \int (dx/\Delta) \mathcal{H}_{1\mathrm{D}}(\mathbf{l}, \mathbf{l}', \mathbf{m}, \mathbf{m}'), \tag{2.7}$$

where $\Delta = 2d$ is the length of the linear antiferromagnetic unit cell and d is the nearest-neighbor distance. dz is an infinitesimal length element along the spin chain axis (chosen to be the z axis), and $\mathbf{l}'$ and $\mathbf{m}'$ are the (dimensionless) spatial derivatives of the staggered field and the magnetization field, respectively. After neglecting a constant contribution, the energy density (in units of energy) is

$$\begin{aligned} \mathcal{H}_{1\mathrm{D}}(\mathbf{l}, \mathbf{l}', \mathbf{m}, \mathbf{m}') =& JS^2 \left[4|\mathbf{m}|^2 + |\mathbf{l}'|^2 - |\mathbf{m}'|^2 + (\mathbf{m} \cdot \mathbf{l}' - \mathbf{l} \cdot \mathbf{m}') \right] \\ & - KS^2 \left[(\mathbf{l} \cdot \hat{z})^2 + (\mathbf{m} \cdot \hat{z})^2 \right]. \end{aligned} \tag{2.8}$$

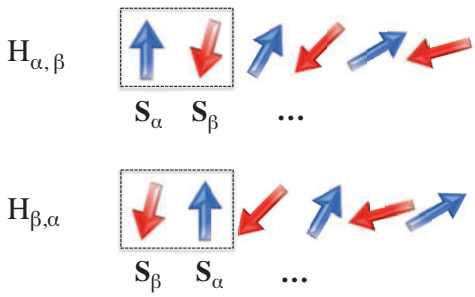

Figure 2.3: For a linear spin chain with antiferromagnetic exchange coupling, the Heisenberg Hamiltonian is not invariant under sublattice exchange ($\mathbf{S}_\alpha \leftrightarrow \mathbf{S}_\beta$) if the order parameter is spatially inhomogeneous, e.g., $H_{\alpha,\beta} \neq H_{\beta,\alpha}$. This property can be visualized by a simplified sketch of a linear spin chain with spatially varying antiferromagnetic order, pictured before (**top**) and after (**bottom**) the permutation of the sublattices. Whereas the internal exchange energy within each unit cell is invariant under such a permutation of the sublattices, the increased deviation from the antiparallel configuration between the unit cells creates a more disordered phase that costs additional exchange energy. In the continuum limit, the energy penalty of the sublattice permutation is captured by the parity-breaking term in the energy functional.

We see that the fourth term in Eq. (2.8) has an unusual parity-breaking form [32, 33] because it is an odd function of the order parameter $\mathbf{l}$.[3] This term results from the procedure of breaking the lattice into pairs [22], and its symmetry properties destroy the energy invariance under sublattice exchange ($\alpha \leftrightarrow \beta$), which is occasionally formulated as a symmetry requirement for continuum models in AFMs [10]. Fig. 2.3 conceptually demonstrates that the energy of an inhomogeneous antiferromagnetic linear spin chain is not invariant under exchange of the two sublattices. The permutation of the sublattices creates a more disordered phase that costs additional exchange energy.

To describe domain wall dynamics in AFMs, it is useful to work in the exchange approximation [10], $|J| \gg |K|$, and consider slowly varying antiferromagnetic textures. In this case, $|\mathbf{m}|^2 \ll |\mathbf{l}|^2$, and we can disregard terms that are of higher order than $|\mathbf{m}|^2$, such as the magnetic anisotropy energy and the magnetic stiffness terms in Eq. (2.8). We also introduce the normalized staggered vector field $\mathbf{n}(z) \equiv \mathbf{l}(z)/|\mathbf{l}(z)|$ and, consequently, write the energy density (2.8) as a function of the deviations $\partial_z\mathbf{n}$ ($\equiv \partial\mathbf{n}/\partial z$) and $\mathbf{m}$ from the homogeneous ground state, in which $\mathbf{m}$ and $\partial_z\mathbf{n}$ vanish. After integrating by parts, we arrive at the free energy density for the linear antiferromagnetic spin chain to the lowest order in the deviations from the homogeneous state [34]:

$$\mathcal{H}_{1D}(\mathbf{n}, \partial_z\mathbf{n}, \mathbf{m}) = \frac{a}{2}|\mathbf{m}|^2 + \frac{A}{2}|\partial_z\mathbf{n}|^2 + L(\mathbf{m}\cdot\partial_z\mathbf{n}) - \frac{K_z}{2}(\mathbf{n}\cdot\hat{z})^2 . \tag{2.9}$$

[3] Note that this term is not identical to the similar-looking exchange term introduced by Lifshitz and Pitaevskii [10] that lead to an anisotropic spin-wave dispersion relation. See the discussion in Paper [5].

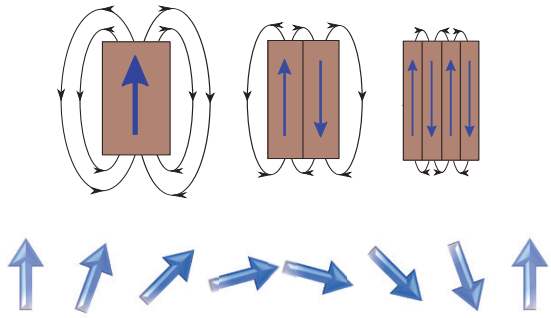

Figure 2.4: (Top) Domains in FMs form to lower the stray-field energy, popularly visualized as magnetic field lines around a magnetic dipole. **(Bottom)** The boundary regions between two domains are called domain walls. These regions exhibit locally increased exchange energy penalties because the spin states deviate from the parallel configuration.

This equation has the following parameters: the homogeneous exchange energy $a = 8JS^2$, the exchange stiffness terms $A = \Delta^2 JS^2$ and $L = 2\Delta JS^2$, and the anisotropy energy $K_z = 2KS^2$. Here, L parametrizes the parity-breaking term in the energy functional.

2.2 Antiferromagnetic domain walls

In bulk FMs, the formation of domain structures can be intuitively understood as resulting from energy minimization: A large number of electrons with their spin axes aligned in the same direction create a strong magnetic dipole with stray fields that can extend to and influence neighboring magnetic materials. Consequently, it is energetically favorable for FMs to lower their stray-field energy by forming domains of magnetic order with magnetization pointing in different directions [11]. See Fig. 2.4 for a schematic presentation of domains and domain wall formation in FMs.

The formation of magnetic domains come at the cost of an increased exchange energy penalty in the boundary regions between the domains. These regions, in which the direction of the magnetization changes from one domain into the other, are called *domain walls*. The distribution of domain sizes is determined by a competition between the "macroscopic" dipole energy and the "microscopic" exchange energy. The former favors smaller domains and the latter favors alignment of all neighboring spins.

It is not obvious that antiferromagnetic materials should exhibit similar domain structures as those observed in FMs. Homogeneous AFMs have no stray fields because the total magnetic moment vanishes at equilibrium. Consequently, other mechanisms than a competition between the dipole energy and the microscopic spin exchange must be responsible for the formation of domains in the antiferromagnetic order. One suggested mechanism for the spontaneous formation of domains in AFMs is via crystal imperfections such as dislocations, grain boundaries or crystallographic twins [35].

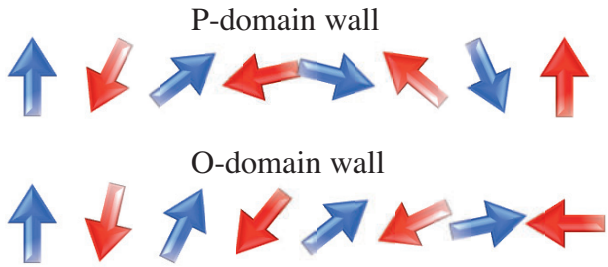

Figure 2.5: One-dimensional antiferromagnetic domain walls can be categorized into two groups, the 180° *phase* domain walls and the 90° *orientational* domain walls [43]. The former is more prominent in antiferromagnetic materials with substantial easy-axis anisotropy energy. The latter may prove to become more technologically important because of the optical (XMLD) and electrical (AMR) contrast between perpendicularly directed domains.

One can also argue that domains of antiferromagnetic order arise spontaneously at finite temperatures below T_N due to entropy considerations: There are many different ways to combine domains, but only one state that is homogeneous. Additionally, at temperatures slightly above T_N, many antiferromagnetic materials exhibit a *ferrimagnetic* precursor phase, in which the magnitudes of the magnetic moments are different for the two sublattices. Ferrimagnets have a macroscopic magnetization and can form magnetic domains that survive into the antiferromagnetic state after slowly cooling below T_N [36]. Yet another way to *design* domain structures in AFMs is via the strong exchange coupling to FMs. An antiferromagnetic layer grown on top of a ferromagnetic layer will typically align its spins along the domain configuration of the FM due to the exchange bias effect [37].

Some decades ago, experimental information about antiferromagnetic domains were hard to obtain and mostly restricted to neutron diffraction studies [38]. Recently, infomation about domains in AFMs has become more experimentally accessible, e.g., via the experimental technique *X-ray magnetic linear dichroism* (XMLD) [39–41]. This technique is based on the different absorption coefficients for X-rays in AFMs depending on the direction of the antiferromagnetic order parameter. Domain walls in AFMs are observed to be as different (if not more so) as their ferromagnetic counterparts. Domain walls in the antiferromagnetic insulator NiO have been observed to be approximately 100 nm wide [42]. On the other hand, using spin-polarized scanning tunneling microscopy, domain walls in monolayers of antiferromagnetic Fe on W(001) have been reported to be only a few lattice spacings wide [43]. Signatures of domains in the elemental AFM Cr also suggest short domain wall widths [44].

In this thesis, we study two types of short one-dimensional antiferromagnetic domain walls [43]: the 90° *orientational* domain walls in Paper [1] and the 180° *phase* domain walls in Papers [2, 5]. Fig. 2.5 presents a schematic comparison between these types of antiferromagnetic domain walls. Studies of domain wall motion in FMs almost exclusively focus on the most common 180° domain walls. In AFMs, there is also

the possibility that 90° domain walls form in systems with low anisotropy. One of the potentially technologically important properties of the antiferromagnetic order parameter is the presence of anisotropic magnetoresistance (AMR) [45–47]. Because the magnetoresistance effects arise from the spin-orbit coupling [48], the AMR in AFMs can be as prominent as in FMs. The AMR contrast is obtained for domains that are rotated 90° (perpendicular) to each other.

The tailoring of 90° orientational antiferromagnetic domain walls would typically require some pinning at the boundaries, e.g., via the exchange bias effect with FMs [1]. In such systems, the domain wall shape must be determined from the boundary conditions. For 180° phase domain walls, on the other hand, the equilibrium shape of domain walls (solitons) can be calculated by minimizing the energy functional (2.9). At equilibrium, the continuum field configuration that minimizes the energy can be found from the variation of the free energy with respect to the staggered field $\mathbf{n}(z)$ and the magnetization field $\mathbf{m}(z)$. The functional derivative of $U[f(x), f'(x)]$ with respect to an arbitrary function $f(x)$ is defined as

$$\frac{\delta U}{\delta f(x)} = \frac{\partial u}{\partial f} - \frac{d}{dx}\frac{\partial u}{\partial f'}, \tag{2.10}$$

where $u[f(x), f'(x)]$ is a density of the functional such that $U = \int u dx$. The functional variations $\delta H_{1D}/\delta \mathbf{n}_0 = 0$ and $\delta H_{1D}/\delta \mathbf{m}_0 = 0$, where we enforce the constraints $|\mathbf{n}_0|^2 = 1$ and $\mathbf{m}_0 \cdot \mathbf{n}_0 = 0$ by adding Lagrange multipliers, lead to the coupled equations for the equilibrium configurations $\mathbf{n}_0$ and $\mathbf{m}_0$ of the staggered field and the magnetization, respectively:

$$\mathbf{n}_0 \times \left[A\partial_z^2 \mathbf{n}_0 + L\partial_z \mathbf{m}_0 + K_z(\mathbf{n}_0 \cdot \hat{z})\hat{z}\right] = 0\,, \tag{2.11a}$$

$$a\mathbf{m}_0 + L\partial_z \mathbf{n}_0 = 0\,. \tag{2.11b}$$

The above result is important because Eq. (2.11b) establishes that textures in the staggered field $\mathbf{n}_0$ induce a finite magnetization density $\mathbf{m}_0 = -(L/a)\partial_z \mathbf{n}_0$ even at equilibrium. This relation arises from the parity-breaking exchange term in Eq. (2.9). The validity of this continuum representation and the presence of such an *intrinsic magnetization* of antiferromagnetic textures was numerically tested and verified in Ref. [23]. Nevertheless, this intrinsic contribution to the total spin of textured AFMs is commonly overlooked in theories describing antiferromagnetic domain wall dynamics. We discuss the probable cause for these oversights by comparing our procedure to a different model that does not include the intrinsic magnetization in Sec. 2.3.

Taking the spatial derivative of Eq. (2.11b) and eliminating $\mathbf{m}_0$ from Eq. (2.11a), lead to a closed equation for the equilibrium staggered field

$$\mathbf{n}_0 \times \left[A^*\partial_z^2 \mathbf{n}_0 + K_z(\mathbf{n}_0 \cdot \hat{z})\hat{z}\right] = 0\,, \tag{2.12}$$

where $A^* = A - L^2/a$ is a renormalized exchange stiffness. To find solutions for

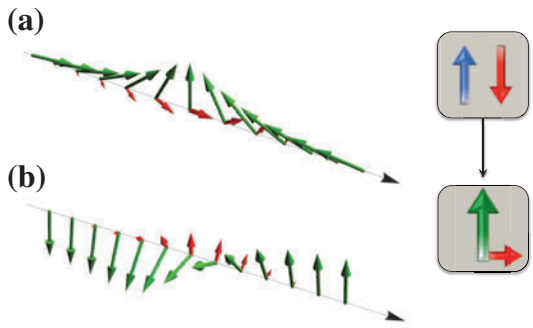

Figure 2.6: (**a**) Sketch of an antiferromagnetic head-to-head Néel (in-plane) domain wall in the discrete staggered field (green arrows), including the intrinsic magnetization (red arrows, not to scale) associated with the textured order parameter. (**b**) A Bloch (out-of-plane) domain wall in the discrete staggered field including the associated intrinsic magnetization.

Eq. (2.12), we introduce the spherical coordinate system with the unit vectors

$$\hat{r} = [\sin\theta\cos\phi, \sin\theta\sin\phi, \cos\theta] \,, \tag{2.13a}$$

$$\hat{\theta} = [\cos\theta\cos\phi, \cos\theta\sin\phi, -\sin\theta] \,, \tag{2.13b}$$

$$\hat{\phi} = [-\sin\phi, \cos\phi, 0] \,, \tag{2.13c}$$

where, by definition, $\mathbf{n}_0 = [\sin\theta_0\cos\phi_0, \sin\theta_0\sin\phi_0, \cos\theta_0]$. After rewriting in the spherical coordinates, a series of solutions for Eq. (2.12) can be found from

$$\partial_z\phi_0 = 0 \,, \tag{2.14a}$$

$$\partial_z^2\theta_0 = \frac{1}{\lambda^2}\sin\theta_0\cos\theta_0 \,, \tag{2.14b}$$

where $\lambda = \sqrt{A^*/K_z}$ is the effective exchange length. Inserted the exchange stiffness and the anisotropy parameter, $\lambda = d\sqrt{J/K}$ is given by a competition between the exchange energy and the anisotropy energy scales, as expected. A trivial solution to the above equations is $\phi_0 = 0$ and $\theta_0 = 0$, which corresponds to a homogeneous AFM with all spins polarized along the positive or negative z axis. The excited state can be found by introducing the substitutions $\sin\theta_0 \to \pm\mathrm{sech}(z/\lambda)$ and $\cos\theta_0 \to \pm\tanh(z/\lambda)$ so that $\theta_0 \to 2\arctan[\exp(z/\lambda)]$. These solutions describe 180° Walker domain walls [49] in the Néel (in-plane) configuration, where λ is the domain wall half-width.

There exists also other possible solutions to Eq. (2.12), depending on the boundary conditions, e.g., the Bloch domain wall or spin spirals. See Fig. 2.6[4] for a sketch of a Néel and a Bloch domain wall, including the intrinsic magnetization. In the following, we always mean the Néel configuration when considering 180° domain walls in AFMs.

[4]Note that the discrete representation of the continuum fields $\mathbf{n}_i$ and $\mathbf{m}_i$ in Fig. 2.6 is nice for visual representation of domain wall structures, but it can also be misleading because the arrows do not represent classical spin vectors in this case.

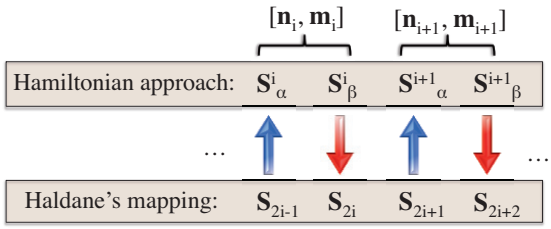

Figure 2.7: (**Top**) In the Hamiltonian approach, Eqs. (2.3) define discrete values for the staggered field $\mathbf{n}_i$ and the magnetization field $\mathbf{m}_i$ at the center point of all antiferromagnetic unit cells indexed by i. The continuum fields are defined from linear combinations of the sublattice spins $\mathbf{S}^i_\alpha$ and $\mathbf{S}^i_\beta$. (**Bottom**) In Haldane's mapping, every single spin $\mathbf{S}_i$ is mapped onto two continuum fields, the Néel field $\tilde{\mathbf{n}}_i$ and the "canting" field $\tilde{\mathbf{m}}_i$.

2.3 The Hamiltonian approach vs. Haldane's mapping

The procedure (described in Sec. 2.1) of breaking the antiferromagnetic lattice into spin pairs before transitioning to the continuum limit is called the Hamiltonian approach [31]. A recurring source of confusion while working on the details of Paper [5], were the existence of different parametrization procedures for the continuum fields that we originally assumed were conceptually equivalent to our approach. It turns out that the nonequivalence of these different parametrization procedures is the key for clarifying the seemingly contradictory results in the literature concerning the intrinsic magnetization. To shed light on this issue, we include a direct comparison between the Hamiltonian approach and Haldane's mapping [26, 50, 31] of the antiferromagnetic order parameter.

In contrast to the spin pairing described by Eqs. (2.3) and (2.4), Haldane's parametrization maps each spin in the linear spin chain onto two continuum fields such that

$$\mathbf{S}_i/S = (-1)^i \tilde{\mathbf{n}}_i \sqrt{1-|\tilde{\mathbf{m}}_i|^2} + \tilde{\mathbf{m}}_i\,, \tag{2.15}$$

where $\tilde{\mathbf{n}}$ is the unitary Néel field and $\tilde{\mathbf{m}}$ is the "canting" field.[5] Fig. 2.7 compares the spin indexing in the Hamiltonian approach with that of Haldane's mapping. By equating the expressions for $\mathbf{S}^i_\alpha$ and $\mathbf{S}^i_\beta$ in Eqs. (2.4) and their corresponding expressions in Haldane's parametrization, we find the relationship

$$\mathbf{m}_i + \mathbf{n}_i\sqrt{1-|\mathbf{m}_i|^2} = -\,\tilde{\mathbf{n}}_{2i-1}\sqrt{1-|\tilde{\mathbf{m}}_{2i-1}|^2} + \tilde{\mathbf{m}}_{2i-1}\,, \tag{2.16a}$$

$$\mathbf{m}_i - \mathbf{n}_i\sqrt{1-|\mathbf{m}_i|^2} = \tilde{\mathbf{n}}_{2i}\sqrt{1-|\tilde{\mathbf{m}}_{2i}|^2} + \tilde{\mathbf{m}}_{2i}\,. \tag{2.16b}$$

In the exchange approximation, $\mathbf{m} \ll \mathbf{n}$ and $\tilde{\mathbf{m}} \ll \tilde{\mathbf{n}}$, and we can safely disregard the

[5] Note that this mapping introduces extra degrees of freedom, which must subsequently be reduced by limiting the Fourier components of the fields $\tilde{\mathbf{n}}$ and $\tilde{\mathbf{m}}$ to include only long-wavelength excitations [50]. Without this reduction, the continuum fields are not unambiguously defined.

square roots in the above expression. It follows that

$$\mathbf{n}_i \approx -\frac{1}{2}(\tilde{\mathbf{n}}_{2i-1} + \tilde{\mathbf{n}}_{2i}) + \frac{1}{2}(\tilde{\mathbf{m}}_{2i-1} - \tilde{\mathbf{m}}_{2i})\,, \tag{2.17a}$$

$$\mathbf{m}_i \approx -\frac{1}{2}(\tilde{\mathbf{n}}_{2i-1} - \tilde{\mathbf{n}}_{2i}) + \frac{1}{2}(\tilde{\mathbf{m}}_{2i-1} + \tilde{\mathbf{m}}_{2i})\,. \tag{2.17b}$$

We proceed by assuming that there are only small-angled spatial variations in the continuum fields. For such a situation, we may apply the gradient approximation $\tilde{\mathbf{n}}_{i+1} \approx \tilde{\mathbf{n}}_i + (\Delta/2)\partial_z\tilde{\mathbf{n}}$ (and similar for the canting field), where $\Delta/2 = d$ is the nearest neighbor distance. In particular, to directly compare the two parametrization procedures, we define continuum field values for $\tilde{\mathbf{n}}$ and $\tilde{\mathbf{m}}$ at the center point of each unit cell: $\tilde{\mathbf{n}}_{i+1/2} \approx \tilde{\mathbf{n}}_i + (\Delta/4)\partial_z\tilde{\mathbf{n}}_i$ (and similar for $\tilde{\mathbf{m}}$). Inserting these lowest order gradient approximations into Eqs. (2.17), results in a one-to-one mapping between the continuum fields of the Hamiltonian approach and Haldane's parametrization:

$$\mathbf{n} \to -\tilde{\mathbf{n}} + (\Delta/4)\partial_z\tilde{\mathbf{m}} + \mathcal{O}(|\tilde{\mathbf{m}}|^2)\,, \tag{2.18a}$$

$$\mathbf{m} \to \tilde{\mathbf{m}} - (\Delta/4)\partial_z\tilde{\mathbf{n}} + \mathcal{O}(|\tilde{\mathbf{m}}|^2)\,. \tag{2.18b}$$

This important result establishes that the continuum fields $\tilde{\mathbf{n}}$ and $\tilde{\mathbf{m}}$ of Haldane's mapping are not identical to the staggered and magnetization fields $\mathbf{n}$ and $\mathbf{m}$ of the Hamiltonian approach. By inserting this mapping into the energy functional (2.9) and keeping only terms of the order $|\tilde{\mathbf{m}}|^2$ in the exchange approximation, we find the continuum limit energy functional of Haldane's mapping:

$$\mathcal{H}_{\text{Hal}}(\tilde{\mathbf{n}}, \partial_z\tilde{\mathbf{n}}, \tilde{\mathbf{m}}) = \frac{a}{2}|\tilde{\mathbf{m}}|^2 + \frac{A}{2}|\partial_z\tilde{\mathbf{n}}|^2 - \frac{K_z}{2}(\tilde{\mathbf{n}}\cdot\hat{z})^2\,. \tag{2.19}$$

The above result has two obvious implications: (1) The parity-breaking exchange term in Eq. (2.9), which leads to the intrinsic magnetization, vanishes after a transformation of the continuum fields, e.g., $\mathbf{m} \to \tilde{\mathbf{m}} - (\Delta/4)\partial_z\tilde{\mathbf{n}}$. (2) The physical interpretations of the magnetization field $\mathbf{m}$ and Haldane's canting field $\tilde{\mathbf{m}}$ are critically different. The magnetization field $\mathbf{m}$ can be interpreted as a magnetization density in the sense that the total spin (both intrinsic and dynamic) of the AFM can be found from integration, $\mathbf{M}/S = \int \mathbf{m}\, dV$. The canting field $\tilde{\mathbf{m}}$, on the other hand, represents only the dynamic magnetization induced by temporal variations of the Néel field $\tilde{\mathbf{n}}$ and not the total magnetization.

An overall requirement, however, is that the physics remains the same for the two procedures, including the existence of the intrinsic magnetization. Although the canting field $\tilde{\mathbf{m}}$ in Haldane's mapping does not include the intrinsic contribution to the magnetization density, the total spin can be found from $\mathbf{M}/S \approx \sum_{i=1}^{2N}[(-1)^i\tilde{\mathbf{n}}(z_i) + \tilde{\mathbf{m}}(z_i)]$. The intrinsic magnetization can be identified as arising from the first terms in the sum. For a slowly varying $\tilde{\mathbf{n}}$ in, e.g., the $\hat{z}$ direction, $\sum_{i=1}^{2N}(-1)^i\tilde{\mathbf{n}}(z_i)\cdot\hat{z} \approx [\tilde{n}_z(z_1) - \tilde{n}_z(z_{2N})]/2$ [51], which is generally nonzero for textured order parameters.

2.4 Outlook

In Paper [5], we demonstrate with analytical results and supporting numerical analysis that the intrinsic magnetization of antiferromagnetic textures can alter the dynamics of collective modes that are under the influence of external forces that couple directly to the intrinsic magnetization. In particular, we show that an inhomogeneous but static magnetic field creates a potential energy landscape for a one-dimensional domain wall. This effect can possibly be used to accurately pin the position of antiferromagnetic domain walls.

The results presented in this chapter are the most recent in this thesis. Although the earlier papers on antiferromagnetic domain wall motion do not take the intrinsic magnetization into account, the retroactive effects on the earlier publications are not dramatic: Paper [1] studies the current-induced dynamics of a 90° orientational domain wall. Although (spin-polarized) currents also couple to the intrinsic magnetization, the dynamic effects of this coupling are indirect and of higher order in the small parameter $\sqrt{K/J}$ than the direct coupling identified in Ref. [52]. Therefore, these corrections can safely be assumed to be small or negligible. In Paper [2], only internal (spin-wave-induced) forces act on the 180° domain wall. In such a situation, the magnetization field $\mathbf{m}$ is a slave variable that can be eliminated from the equations of motion and the intrinsic magnetization plays no role in the dynamics. In Paper [4], we describe expansions around a homogeneous antiferromagnetic state without any macroscopic textures. Consequently, the results are not affected by the intrinsic magnetization.

Chapter 3

Dynamics in antiferromagnets

The previous chapter developed tools for describing textures in the antiferromagnetic order via spatially varying continuum vector fields. In this chapter, we progress to describe the dynamics of these continuum fields. The concepts presented in the following sections come mainly from Papers [1, 2], which study two different scenarios of antiferromagnetic *domain wall motion*. The motivation behind Paper [1] was to express the phenomenological theory of current-induced torques in AFMs [27] via the conceptually much simpler *collective coordinate description* [53]. Paper [2] was motivated by the theory of *magnon-driven spin transfer torque* (STT) on a ferromagnetic domain wall [54]. The magnon-driven STT effect originates from a phase shift of the spin waves when traversing the ferromagnetic domain wall. A notable result from the numerical analysis of the magnon-domain wall interaction is the complicated excitation frequency dependence of the domain wall velocity. We were interested in describing the analogous problem of spin waves interacting with domain walls in AFMs.

In Sec. 3.1, I present the equations of motion for the magnetization in FMs and describe ferromagnetic spin waves for later comparison with the theory for AFMs. Sec. 3.2 develops the coupled equations of motion for the antiferromagnetic continuum fields. The collective coordinate approach is presented in Sec. 3.3. In Sec. 3.4, I introduce the concept of antiferromagnetic spin waves, and later, in Sec. 3.5, demonstrate that the spin-wave amplitude depends crucially on the spatial distribution and frequency of the excitation source. Sec. 3.6 describes the interaction between spin waves and domain walls in AFMs. This interaction results from transfer of linear momentum rather than angular momentum. In Sec 3.7, I compare the radically different properties of linearly polarized and circularly polarized spin waves in AFMs.

Note that this chapter follows the notation of Papers [1, 2] and uses Haldane's unitary Néel field $\tilde{\mathbf{n}}$ and the dimensionfull canting field $\tilde{\mathbf{m}}$ (in units of Am^{-1}), for which I suppress the tilde notation such that $\tilde{\mathbf{n}} \to \mathbf{n}$ and $\tilde{\mathbf{m}} \to \mathbf{m}$.

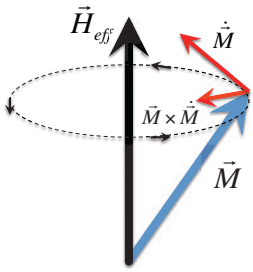

Figure 3.1: The precession of a macroscopic magnetization $\mathbf{M}$ around the direction of an effective magnetic field $\mathbf{H}_{\text{eff}}$, described by the LLG equation (3.1). A finite Gilbert constant α damps the precession such that, in time, the magnetization aligns with the effective field.

3.1 Ferromagnetic spin wave theory

Before describing spin wave excitations in AFMs, let us repeat the analogous problem in FMs as a reference for the subsequent discussion. Consider a one-dimensional ferromagnetic spin chain with easy-axis anisotropy so that all spins point along the positive z direction at equilibrium. The local magnetization can be described by the continuum vector field $\mathbf{M}(z,t)$. The ferromagnetic dynamics are described by the Landau-Lifshitz-Gilbert (LLG) [55, 56] equation

$$\dot{\mathbf{M}} = -\gamma \mathbf{M} \times \mathbf{H}_{\text{eff}} + \frac{\alpha}{M_s} \mathbf{M} \times \dot{\mathbf{M}}\,, \tag{3.1}$$

where γ is the gyromagnetic ratio, α is the dimensionless Gilbert damping parameter, $\mathbf{H}_{\text{eff}}$ is the effective magnetic field, and M_s is the saturation magnetization. Eq. (3.1) describes the precession of the magnetization around an axis defined by the direction of the effective field, where a finite damping relaxes the precession angle such that, in time, the magnetization aligns with the effective field, see Fig. 3.1.

The effective magnetic field is defined as the (negative) functional derivative of the energy functional $U_{\text{F}}(\mathbf{M})$ of the FM: $\mathbf{H}_{\text{eff}} \equiv -\delta U_{\text{F}}(\mathbf{M})/\delta \mathbf{M}$. We consider here a simple uni-axial and one-dimensional FM with easy axis along the z direction. The energy functional is

$$U_{\text{F}}(\mathbf{M}) = \int dz \left[\frac{A}{2} \left| \frac{\partial \mathbf{M}}{\partial z} \right|^2 - \frac{K_z}{2} (\mathbf{M} \cdot \hat{z})^2 \right], \tag{3.2}$$

where A and K_z (in the appropriate dimensions) parametrize the exchange stiffness and the anisotropy energy, respectively. The first term in Eq. (3.2) represents the energy cost of an inhomogeneous magnetization and the second term represents the energy gain from aligning the magnetization along the easy z direction. From the definition of the functional derivative (2.10), we calculate the effective magnetic field as $\mathbf{H}_{\text{eff}} = A\partial_z^2 \mathbf{M} + K_z M_z \hat{z}$.

To describe spin-wave excitations on top of the homogeneous FM, we apply the *an-*

satz that the magnetization field can be described by $\mathbf{M}(z,t)/M_s = \hat{z} + hm_x(z,t)\hat{x} + hm_y(z,t)\hat{y}$, where m_x and m_y are small perpendicular excitations around the homogeneous ferromagnetic state. Inserting this ansatz into the LLG equation (3.1) and expanding to first order in the small excitation parameter h, give

$$\frac{1}{\gamma}\left[\dot{m}_x(z,t) + \alpha\dot{m}_y(z,t)\right] = A\partial_z^2 m_y(z,t) - K_z m_y(z,t)\,, \tag{3.3a}$$

$$\frac{1}{\gamma}\left[\dot{m}_y(z,t) - \alpha\dot{m}_y(z,t)\right] = -A\partial_z^2 m_x(z,t) + K_z m_x(z,t)\,. \tag{3.3b}$$

We further assume that the magnetic excitations are harmonic oscillations in space and time, $m_{x(y)} = m_0 \exp\left[i(kz - \omega t)\right]$, where k and ω are the wave vector and frequency of the spin waves, respectively. After introducing the left-circularly and right-circularly polarized modes $m_\pm = m_x \pm i m_y$, we can combine Eqs. (3.3a) and (3.3b) to give the familiar quadratic dispersion relation for spin waves in FMs [10]:

$$\omega(1 + i\alpha) = \gamma(Ak^2 + K_z)\,, \tag{3.4}$$

which shows that the spin-wave spectrum is gapped with the collective excitation (or "macrospin") frequency given by $\omega_K = \gamma K_z$.

The LLG equation (3.1), inserted the effective field but without damping, can be rewritten as [54]

$$\dot{\mathbf{M}} = -\gamma K_z M_z \mathbf{M} \times \hat{z} - \partial_z \mathbf{J}\,, \tag{3.5}$$

where $\mathbf{J} = \gamma A(\mathbf{M} \times \partial_z \mathbf{M})$ defines the *spin-wave spin current* [57]. From Eq. (3.5), we can construct a continuity equation for the spin angular momentum along the z direction as

$$\dot{M}_z + \partial_z J_z = 0\,, \tag{3.6}$$

where J_z is the z component of $\mathbf{J}$. For the right-circularly polarized and left-circularly polarized harmonic oscillations $m_\pm = \rho_m \exp\left[i(kz - \omega t)\right]$, where ρ_m is the complex spin wave amplitude, $J_z = \pm\gamma|\rho_m|^2 Ak$ [54]. The sign of the spin current is determined by the spin-wave helicity. When passing through a ferromagnetic domain wall, the spin waves change their phase, causing the spin-wave spin current to change sign. This transfer of spin angular momentum between passing spin waves and the domain wall is the driving force for the magnon-induced domain wall motion. In the following sections, we develop a similar formalism for antiferromagnetic spin waves and describe the coupling between travelling spin waves and antiferromagnetic domain walls.

3.2 The Landau-Lifshitz equations of motion for AFMs

Let us return to antiferromagnetic dynamics, which is described via the dynamic equations of the unitary Néel field $\mathbf{n}$ and the canting field $\mathbf{m}$. The coupled equations of motion for $\mathbf{n}$ and $\mathbf{m}$ that are analogous to the ferromagnetic LLG equation (3.1) can be found from several different approaches. A popular procedure is to develop

linear combinations of the two LLG equations for the sublattice magnetic moments $\mathbf{M}_\alpha$ and $\mathbf{M}_\beta$ [23, 58, 24]. We used a similar method to compute the antiferromagnetic coupled equations of motion in Paper [4], which is further discussed in Chapter 4. Yet another approach was used by Hals *et al.* [27], who phenomenologically constructed the equations of motion for $\mathbf{n}$ and $\mathbf{m}$ from symmetry relations [59].

Here, we apply a somewhat different, but fundamentally equivalent, approach, following the presentation in Paper [5]. We construct the Lagrangian density and directly compute the dynamic equations for $\mathbf{n}$ and $\mathbf{m}$ from the principle of least action and the Euler-Lagrange equations. The Lagrangian density is defined as $\mathcal{L} = \mathcal{K} - \mathcal{U}$, where $\mathcal{K}$ is the kinetic energy and $\mathcal{U}$ is the potential energy. In FMs, the kinetic term for a single spin is constructed from the spin Berry phase, resulting in $\mathcal{K}_\mathrm{F} = \rho_\mathrm{F}\dot{\phi}(\cos\theta - 1)$ [60, 61], where ρ_F is the magnitude of the spin per lattice point, θ is the polar angle and ϕ is the azimuthal angle in the spherical coordinate system.

Analogous to the procedure for constructing the kinetic term for a single spin in a ferromagnet, $\mathcal{K}$ for AFMs can be defined from the Berry phase of the spin *pair* $\mathbf{S}_\alpha + \mathbf{S}_\beta$ that constitutes the antiferromagnetic unit cell:

$$\int \mathcal{K} d\mathbf{r} = -\frac{\rho_\mathrm{AF}}{2}\left[\sum_\alpha \mathbf{A}_\alpha \cdot \dot{\mathbf{S}}_\alpha + \sum_\beta \mathbf{A}_\beta \cdot \dot{\mathbf{S}}_\beta\right], \tag{3.7}$$

where $\rho_\mathrm{AF} = 2S\hbar$ is the magnitude of the staggered spin angular momentum per unit cell and $\mathbf{A}_{\alpha(\beta)}$ is a gauge potential for the kinetic energy of the sublattice spins.

Several different gauges may lead to the correct equations of motion. For AFMs, it is convenient to choose the gauge potential such that the spin pair Berry phase (3.7) vanishes in the strictly antiparallel configuration, $\mathbf{S}_\alpha = -\mathbf{S}_\beta$. One such choice of gauge is $\mathbf{A}_{\alpha(\beta)} = -\hat{\phi}_{\alpha(\beta)}\cos\theta_{\alpha(\beta)}/\sin\theta_{\alpha(\beta)}$, which is identical to that which is normally used to describe the kinetic energy of a single spin in FMs [61], but generalized here to include both spins in the antiferromagnetic unit cell.

By expanding the spin-pair Berry phase in small deviations from the antiparallel configuration, $\theta_\beta \to \pi - (\theta_\alpha + \delta\theta)$ and $\phi_\beta \to \pi + (\phi_\alpha + \delta\phi)$, and transferring back to the $[\mathbf{n}, \mathbf{m}]$ basis, disregarding terms of the order $|\mathbf{m}|^4$ and higher to be able to describe the kinetic term via the unitary Néel field $\mathbf{n}$, the antiferromagnetic Lagrangian density in the exchange approximation is given by [26, 22]

$$\mathcal{L} = \frac{1}{\gamma}\mathbf{m}(\dot{\mathbf{n}} \times \mathbf{n}) - \mathcal{U}\,. \tag{3.8}$$

We continue by varying this Lagrangian with respect to the Néel field $\mathbf{n}$ and the canting field $\mathbf{m}$, $\delta L/\delta\mathbf{n} = 0$ and $\delta L/\delta\mathbf{m} = 0$. The resulting coupled equations of motion are

$$(\dot{\mathbf{n}} \times \mathbf{n}) = \gamma\frac{\delta U}{\delta \mathbf{m}}\,, \tag{3.9a}$$

$$2(\mathbf{m} \times \dot{\mathbf{n}}) + (\dot{\mathbf{m}} \times \mathbf{n}) = \gamma\frac{\delta U}{\delta \mathbf{n}}\,, \tag{3.9b}$$

where $U(\mathbf{n}, \mathbf{m})$ is the antiferromagnetic free-energy functional.

After taking the cross product with $\mathbf{n}$, and using the constraints $|\mathbf{n}|^2 = 1$ and $\mathbf{m} \cdot \mathbf{n} = 0$ (which transforms to $\dot{\mathbf{m}} \cdot \mathbf{n} = -\mathbf{m} \cdot \dot{\mathbf{n}}$ after taking the time derivative), we arrive at the same equations of motion that were developed from a phenomenological approach in Ref. [27] based on the interrelated symmetries of the continuum fields:

$$\dot{\mathbf{n}} = \gamma \mathbf{f}_{\mathbf{m}} \times \mathbf{n}\,, \tag{3.10a}$$

$$\dot{\mathbf{m}} = \gamma \mathbf{f}_{\mathbf{n}} \times \mathbf{n} + \gamma \mathbf{f}_{\mathbf{m}} \times \mathbf{m}\,, \tag{3.10b}$$

where $\mathbf{f}_{\mathbf{n}} = -\delta U/\delta \mathbf{n}$ and $\mathbf{f}_{\mathbf{m}} = -\delta U/\delta \mathbf{m}$ are effective Néel and canting fields, respectively. These Landau-Lifshitz type equations for the antiferromagnetic continuum fields are used as starting points for developing the collective coordinate equations of motion in Paper [1] and to describe the interaction between antiferromagnetic spin waves and domain walls in Paper [2].

In Sec. 2.1, following the derivation in Paper [5], we show that the antiferromagnetic energy functional (2.9) that follows from the one-dimensional Heisenberg Hamiltonian includes a parity-breaking term that is responsible for the intrinsic magnetization of antiferromagnetic textures. Because Paper [5] is the most recent work in this thesis, the preceding Papers [1, 2, 4] on antiferromagnetic dynamics do not include such a parity-breaking term in the energy functional. However, as discussed in Sec. 2.3, energy functionals without this parity-breaking term are still valid continuum representations of AFMs, provided that the continuum field $\mathbf{m}$ is interpreted as Haldane's nonequilibrium *canting* field.

To calculate the effective Néel and canting fields, we use the energy functional

$$U = \int d\mathbf{r} \left[\frac{a}{2}|\mathbf{m}|^2 + \frac{A}{2} \sum_{i=x,y,z} |\partial_i \mathbf{n}|^2 - \frac{K_z}{2}(\mathbf{n} \cdot \hat{z})^2 - \mathbf{H} \cdot \mathbf{m} \right], \tag{3.11}$$

where a is the homogeneous exchange constant, A is the exchange stiffness, K_z is the anisotropy energy, and $\mathbf{H}$ represents the external magnetic field. This energy functional describes an easy axis model, in which it is energetically favorable for the spins in the AFM to align along the positive or negative z axis. Taking the functional derivatives of Eq. (3.11) results in the effective fields

$$\mathbf{f}_{\mathbf{n}} = -\frac{\delta U}{\delta \mathbf{n}} = A\nabla^2 \mathbf{n} + K_z(\mathbf{n} \cdot \hat{z})\hat{z}\,, \tag{3.12a}$$

$$\mathbf{f}_{\mathbf{m}} = -\frac{\delta U}{\delta \mathbf{m}} = -a\mathbf{m} + \mathbf{H}\,. \tag{3.12b}$$

However, this procedure does not take into account that the Néel field $\mathbf{n}$ and the canting field $\mathbf{m}$ are dependent quantities and follow the constraints $\mathbf{n} \cdot \mathbf{m} = 1$ and $|\mathbf{n}|^2 = 1$. These constraints can be enforced in the variation, e.g., via the method of Langrange multipliers. The resulting effective fields that enforce these constraints are [27]

$$\mathbf{f}^*_{\mathbf{n}} = A\mathbf{n} \times (\nabla^2 \mathbf{n} \times \mathbf{n}) + K_z(\mathbf{n} \cdot \hat{z})\mathbf{n} \times (\hat{z} \times \mathbf{n}) - (\mathbf{H} \cdot \mathbf{n})\mathbf{m}\,, \tag{3.13a}$$

$$\mathbf{f}^*_{\mathbf{m}} = -a\mathbf{m} + \mathbf{n} \times (\mathbf{H} \times \mathbf{n})\,. \tag{3.13b}$$

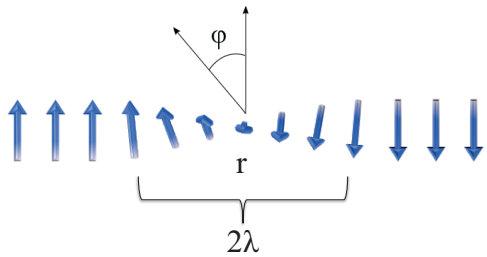

Figure 3.2: Instead of calculating the full dynamics of the order parameter vector field (blue arrows), the collective coordinate approach describes the dynamics of the soft modes while assuming that the texture remains rigid during the dynamics. This figure presents a simple example of three collective coordinates defined for a Bloch domain wall configuration in the order parameter (ferromagnetic or antiferromagnetic). We can define collective coordinates for, e.g., the domain wall center, $r(t)$, the helicity, $\phi(t)$, and the domain wall half-width, $\lambda(t)$.

where both $\mathbf{f}^*_{\mathbf{m}}$ and $\mathbf{f}^*_{\mathbf{n}}$ by definition are perpendicular to $\mathbf{n}$. We note that because the canting field $\mathbf{m}$ is a slave variable that can be eliminated from the equations of motion (3.10), the resulting *effective* dynamic equation for the Néel field $\mathbf{n}$ is invariant with respect to whether the constraints are enforced in the calculation of the effective fields (3.13) or not (3.12).

3.3 The method of collective coordinates

In FMs, the shape of magnetic textures (e.g., domain walls, vortices, or other solitons) is often rigid and does not transform even when they are influenced by external forces. In such situations, only a few, *soft* modes dominate the magnetization dynamics, as described in the seminal work of Schryer and Walker on ferromagnetic domain walls [49]. The temporal evolution of these soft modes can be described by the dynamics of a finite set of *collective coordinates*. This approach greatly simplifies the understanding of complex magnetization dynamics, making it possible to approximately describe the low-energy dynamics by considering only the dynamics of a few soft modes while assuming that the underlying magnetic texture remains rigid. See Fig. 3.2 for an example of how the collective coordinates can be defined for a Bloch domain wall profile.

The collective coordinate approach was recently revived to describe the dynamics of a vortex domain wall in a ferromagnetic nanostrip [53, 62]. This method transforms the LLG equation (3.1) into a series of equations of motion for the collective modes that are simpler and more intuitive for the physical interpretation of the magnetization dynamics. The coupled equations of motion for the antiferromagnetic continuum fields (3.10) are hard to solve exactly for general order parameter textures. Therefore, motivated by the collective coordinate description of ferromagnetic dynamics, we adopted a similar approach in Paper [1] to develop the equations of motion for collective coordinates in AFMs.

First, let us introduce magnetization dissipation to the description of the antiferromagnetic dynamics. In the Lagrangian formalism, dissipation is typically introduced via the Rayleigh dissipation functional [63, 52, 28]. Alternatively, Hals *et al.* [27] introduced dissipation to Eqs. (3.10) by phenomenologically adding the lowest order terms that are allowed by symmetry. The equations of motion including dissipation take the form

$$\dot{\mathbf{n}} = (\gamma \mathbf{f}_{\mathbf{m}} - G_1 \dot{\mathbf{m}}) \times \mathbf{n}\,, \tag{3.14a}$$

$$\dot{\mathbf{m}} = (\gamma \mathbf{f}_{\mathbf{n}} - G_2 \dot{\mathbf{n}}) \times \mathbf{n} + (\gamma \mathbf{f}_{\mathbf{m}} - G_1 \dot{\mathbf{m}}) \times \mathbf{m}\,, \tag{3.14b}$$

where G_1 and G_2 are phenomenological Gilbert damping parameters for the canting field and the Néel field, respectively. Symmetrical two-sublattice models [58, 4] predict that $G_1 l = G_2/l$. However, to the best of the author's knowledge, there is yet no experimental evidence of the strengths of these dissipation terms. Later, we discuss the relative strengths of the G_1 and G_2 dissipative terms based on considerations of the modeled system.

From Eq. (3.14a), inserted Eq. (3.14b) and the effective magnetic field (3.13b), we derive an expression for the canting field

$$\mathbf{m} = -\frac{1}{a}\mathbf{n} \times \left(\frac{1}{\gamma}\dot{\mathbf{n}} + \mathbf{n} \times \mathbf{H} + G_1 \mathbf{f}_{\mathbf{n}}\right), \tag{3.15}$$

where we have disregarded the nonlinear terms in Eq. (3.14b). From this equation, we can conclude that the canting field $\mathbf{m}$ is a slave variable that is fully determined by the dynamics of the Néel field $\mathbf{n}$. As a result, we can eliminate $\mathbf{m}$ and derive a closed equation for $\mathbf{n}$ by taking the time derivative of Eq. (3.14a) and combining with the linear terms in Eq. (3.14b) and Eq. (3.15). The resulting effective equation of motion for the Néel field is

$$\ddot{\mathbf{n}} = a\gamma^2 \mathbf{f}_{\mathbf{n}} - \gamma \mathbf{n} \times \dot{\mathbf{H}} + \gamma G_1 \dot{\mathbf{f}}_{\mathbf{n}} - a\gamma G_2 \dot{\mathbf{n}}\,, \tag{3.16}$$

which is valid in linear response. This equation is a second order differential equation for $\mathbf{n}$ and establishes that the Néel field dynamics in AFMs are fundamentally different from the dynamics of the magnetization in FMs, which is described by the first order differential LLG equation (3.1).

We note that the G_1 dissipative term in Eq. (3.16) scales as $AG_1/(\lambda\tau)$, where λ and τ are characteristic length and time scales of textures in the order parameter. The G_2 dissipative term, on the other hand, scales as aG_2/τ. In analyzing the relative strengths of these two dissipative terms, we use the relation between the inhomogeneous exchange constant and the exchange stiffness, $a \sim A/(l^2 d^2)$ [64, 5], where d is the lattice constant and $l = |\mathbf{l}_0|$ is the length of the antiferromagnetic order parameter, e.g., the staggered magnetic moment per unit cell. Dissipation in metallic FMs arises from the spin-orbit interaction in combination with electron scattering [65]. It is likely that similar mechanisms in AFMs have comparable effects on the Néel field and the canting field such that $G_1 l \approx G_2/l \ll 1$. From this we can conclude that the G_2 dissipative term dominates for textures that are significantly larger than the lattice constant,

$\lambda \gg d$. This is the case for most realistic systems, including the models of domain walls we study in Papers [1, 2, 5] and, therefore, we safely disregard the G_1 dissipative term in the following.

Eq. (3.16) can be transformed by requiring that the time dependence of the textured Néel field is described by a set of collective coordinates $\{b_i(t)\}$ such that $\mathbf{n}(\mathbf{r},t) \equiv \mathbf{n}(\mathbf{r},\{b_i(t)\})$. The time derivative is then $\dot{\mathbf{n}} = \dot{b}_i \partial_{b_i}\mathbf{n}$. Similarly, $\ddot{\mathbf{n}} = \ddot{b}_i \partial_{b_i}\mathbf{n} + \mathcal{O}(\dot{b}_i^2)$, where the second term can be disregarded in a linear response analysis because it is quadratic in the driving forces. We continue by taking the scalar product of Eq. (3.16) with $\partial_{b_j}\mathbf{n}$ and integrate over the space. The resulting equations of motion for the collective modes $\{b_i(t)\}$ can be cast as

$$M^{ij}(\ddot{b}_j + \gamma a G_2 \dot{b}_j) = F^i\,, \tag{3.17}$$

where M^{ij} is an effective mass and F^i are the forces acting on the collective coordinates b_i. This equation implies that rigid antiferromagnetic textures can be interpreted as inertial quasi-particles with an effective mass. Their dynamics are similar to the motion of classical particles subject to dissipation-induced friction and external forces, e.g., Newton's second law. Contrasting the description of external torques acting on FMs [66], antiferromagnetic textures move as a response to external *forces* and not torques.

The effective mass tensor is given by

$$M^{ij} = \frac{1}{a\gamma^2}\int dV \partial_{b_i}\mathbf{n}\cdot\partial_{b_j}\mathbf{n}\,. \tag{3.18}$$

The total force F^i is a sum of several different contributions. In particular, we make the distinction between internal and external forces. The internal forces are

$$F^i_X(b_i) = \int dV \partial_{b_i}\cdot\mathbf{f}_\mathbf{n} = \partial_{b_i}U_X\,, \tag{3.19}$$

where U_X denotes the effective material-specific forces that act on the AFM through the exchange interaction and the magnetic anisotropy. The external force from a magnetic field can be expressed as

$$F^i_H(b_i) = \frac{1}{a\gamma}\int dV \dot{\mathbf{H}}\cdot(\mathbf{n}\times\partial_{b_i}\mathbf{n})\,, \tag{3.20}$$

which shows that only time-varying magnetic fields and not constant magnetic fields exert forces on antiferromagnetic textures. In Paper [5], we identify yet another magnetic field-induced force, proportional to the spatial derivative of an external magnetic field [$\sim (\partial_{b_i}\mathbf{n}\cdot\partial_i\mathbf{H})$]. This force from inhomogeneous magnetic fields should be added to the above equations of motion due to the influence of the intrinsic magnetization of antiferromagnetic textures.

Ref. [27] introduced the current-induced reactive (adiabatic) torque $\boldsymbol{\tau}_\eta = \eta\gamma(\mathbf{J}_c\cdot\nabla)\mathbf{n}$ and the dissipative (non-adiabatic) torque $\boldsymbol{\tau}_\beta = \beta\gamma(\mathbf{J}_c\cdot\nabla)\mathbf{n}\times\mathbf{n}$ to Eqs. (3.14a) and

(3.14b), respectively, where $\mathbf{J}_c$ is the charge current and $\eta(\beta)$ parametrize the adiabatic (nonadiabatic) current-induced torque. In the collective coordinate description, these torques are converted into the current-induced forces

$$F_J^i(b_i) = \int dV \left[\frac{\eta}{a\gamma} \partial_{b_i}\mathbf{n} \cdot (\mathbf{j}_c \cdot \nabla)\mathbf{n} + \beta \partial_{b_i}\mathbf{n} \cdot (\mathbf{J}_c \cdot \nabla)\mathbf{n} \right] , \tag{3.21}$$

where alternating currents (ac) are responsible for adiabatic forces and direct currents (dc) give rise to nonadiabatic forces.[1]

The collective coordinate equation of motion (3.17) is model independent. Therefore, by studying the dynamics of antiferromagnetic textures under the influence of external forces, Eq. (3.17) can be used to decipher experimental values for the inhomogeneous exchange constant a or the damping constant G_2, which can otherwise be difficult to determine experimentally. In Paper [1], we apply the collective coordinate description to the dynamics of a 90° exchange-bias-pinned orientational domain wall (see Fig. 2.5) under the influence of a direct charge current. We show that the dynamics of the domain wall center coordinate follow a harmonic oscillator equation. We also describe how these oscillations could possibly be experimentally detected via the AMR effect.

3.4 Spin waves in AFMs

Antiferromagnetic spin waves can be excited by applying local time-varying external magnetic fields that cause the spins in a confined part of the AFM to resonate at the driving frequency of the external fields. In this section, our goal is to study how spin-wave excitations in the continuum fields $\mathbf{n}$ and $\mathbf{m}$ can be described. The starting point is the energy functional for a homogeneous AFM with easy-axis anisotropy, Eq. (3.11). At equilibrium, all spins point along the positive or negative z axis, $\mathbf{n}_0 = \hat{z}$, and the canting field $\mathbf{m}$ vanishes. A perpendicularly directed external field $\mathbf{H}_{\text{ext}}(z,t) = H_x(z,t)\hat{x} + H_y(z,t)\hat{y}$ leads to a relative canting of the spins in the vicinity of the excitation source.

Spin waves in AFMs can be described as linear deviations of the Néel field $\mathbf{n}$ and the canting field $\mathbf{m}$ around their equilibrium values. We adopt a similar approach as the ferromagnetic definition in Sec. 3.1 to describe the excitation of spin waves in a one-dimensional antiferromagnetic spin chain. We expand $\mathbf{n}(z,t)$ and $\mathbf{m}(z,t)$ for small excitations h around the homogeneous state

$$\mathbf{n}(z,t) = \hat{z} + h\left[n_x(z,t)\hat{x} + n_y(z,t)\hat{y}\right] , \tag{3.22a}$$

$$\mathbf{m}(z,t) = h\left[m_x(z,t)\hat{x} + m_y(z,t)\hat{y}\right] . \tag{3.22b}$$

By inserting this ansatz into the full equations of motion (3.14) and expanding to

[1] Note that in Paper [1], the reactive torque was parametrized by $\eta + \beta G_1$ instead of only by η. However, for most systems, if one considers $\eta \sim \beta l$, the second dissipative contribution to the reactive torque is negligible.

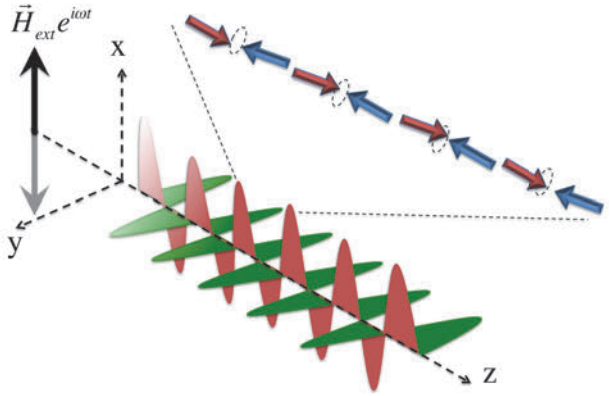

Figure 3.3: A confined harmonically oscillating external field with driving frequency $\omega_0 > \omega_K$ excites parallel canting field oscillations (**red**) and perpendicular Néel field excitations (**green**). This figure shows linearly polarized n_y-waves.

linear order in the small parameter h, we find

$$\dot{n}_x(z,t) = \gamma H_y(z,t) - \gamma a m_y(z,t) - G_1 \dot{m}_y(z,t)\,, \tag{3.23a}$$
$$\dot{n}_y(z,t) = -\gamma H_x(z,t) + \gamma a m_x(z,t) + G_1 \dot{m}_x(z,t)\,, \tag{3.23b}$$
$$\dot{m}_x(z,t) = -\gamma K_z n_y(z,t) + \gamma A \partial_z^2 n_y(z,t) - G_2 n_y(z,t)\,, \tag{3.23c}$$
$$\dot{m}_y(z,t) = \gamma K_z n_x(z,t) - \gamma A \partial_z^2 n_x(z,t) + G_2 n_x(z,t)\,. \tag{3.23d}$$

These equations show that spin-wave excitations in AFMs consists of coupled and phase-shifted excitations in the Néel field and the canting field, see Fig. 3.3 for a sketch of linearly polarized antiferromagnetic spin waves. Note that antiferromagnetic spin waves are good analogs of electromagnetic waves, with the Néel field excitations playing the role of the electric field, polarized perpendicular to the canting field excitations.

We see that we can combine the equations above and eliminate m_x and m_y. After taking the time derivative of Eqs. (3.23a) and (3.23b) and inserting Eqs. (3.23c) and (3.23d), we find the equations

$$\ddot{n}_x(z,t) = \gamma \dot{H}_y(z,t) + a\gamma^2 \left[A\partial_z^2 n_x(z,t) - K_z n_x(z,t)\right] - a G_2 \dot{n}_x(z,t)\,, \tag{3.24a}$$
$$\ddot{n}_y(z,t) = -\gamma \dot{H}_x(z,t) + a\gamma^2 \left[A\partial_z^2 n_y(z,t) - K_z n_y(z,t)\right] - a G_2 \dot{n}_y(z,t)\,, \tag{3.24b}$$

where we have safely disregarded the G_1 dissipative term because the spin waves have wavelengths that are significantly longer than the lattice constant, $\lambda_{\mathrm{sw}} \gg d$ (see Sec. 3.3 for the discussion of the relative strengths of the G_1 and G_2 dissipative terms).

Let us first assume, analogous to ferromagnetic spin waves, that a precessing external magnetic field oscillating at the driving frequency ω, $\mathbf{H}_{\mathrm{ext}} \to h(i\hat{x} \pm \hat{y}) \exp(i\omega t)$, excites circularly polarized travelling harmonic oscillations in the Néel field: $n_\pm \equiv$

$n_x \pm i n_y = n_0 \exp i(kz - \omega t)$. The Néel field excitations are phase shifted with respect to the excitation source because the external field couples to the canting field $\mathbf{m}$. Without dissipation, the combination of Eqs. (3.24) inserted the harmonic excitation source gives the familiar antiferromagnetic spin-wave dispersion [10]

$$(\omega \pm \gamma h)^2 = a\gamma^2(Ak^2 + K_z)\,, \tag{3.25}$$

which, in contrast to the ferromagnetic dispersion relation (3.4), is linear far away from the collective macrospin frequency $\omega_K = \gamma\sqrt{aK_z}$. The frequencies of spin-wave excitations in AFMs are typically larger than for FMs due to their dependence on the large exchange parameter a. Antiferromagnetic spin waves have been shown to operate coherently in the THz regime [21].

Eqs. (3.24) reveal another important property of antiferromagnetic spin waves that is different from the analogous problem (3.3) in FMs. Whereas magnetic excitations in the perpendicular directions $\hat{x}$ and $\hat{y}$ are intrinsically coupled in FMs, these perpendicular modes are decoupled in AFMs. The result is that ferromagnetic spin waves in easy-axis FMs are always circularly polarized. Spin waves in AFMs, on the other hand, can have arbitrary polarizations depending on the excitation source, e.g., an excitation field polarized along the x direction excites Néel field excitations that are polarized along the y direction, and vice versa.

3.5 Calculating the spin-wave amplitude

One prominent feature of the ferromagnetic magnon-driven domain wall motion [54] that, in our view, lacked a proper explanation, was the strong frequency dependence of the resulting domain wall velocity. In the following, we explain this feature by demonstrating that the spin-wave amplitude, and therefore also the spin-wave-mediated forces, depend crucially on the spatial distribution of the excitation field and not only on its strength. Our calculation is done for antiferromagnetic spin waves, but a similar dependence can also be found for ferromagnetic spin waves.

For simplicity, we study linear excitations of the Néel field, but the result generalizes also to circularly polarized spin waves. After inserting the harmonically oscillating excitation field $\mathbf{H}_{\text{ext}} = H_{\text{ext}}(z)\exp(-i\omega_0 t)\hat{x}$ in Eq. (3.24b) and taking the Fourier transform in the spatial (z) and temporal (t) coordinates, we find the relation

$$\tilde{n}_y(k,\omega) = \frac{\sqrt{2\pi}\gamma\omega_0\delta(\omega-\omega_0)\tilde{H}_{\text{ext}}(k)}{\omega^2 - a\gamma^2(Ak^2+K_z) + i\omega a G_2}\,, \tag{3.26}$$

where $\tilde{n}_y(k,\omega) \equiv \mathcal{F}_{z,t}\{n_y(z,t)\}$ is the spatio-temporal Fourier transform of the Néel field excitations, $\delta(\omega)$ is the Dirac delta function and $\tilde{H}_{\text{ext}} = \mathcal{F}_z\{H_{\text{ext}}\}$ is the spatial Fourier transform of the excitation source. The delta function makes the temporal inverse Fourier transform trivial and we directly see that the excited spin waves oscillate at the driving frequency ω_0.

We want to describe the spin-wave amplitude as a function of the spatial distribution of the excitation field $H_{\text{ext}}(z)$, which we assume is placed/centered at $z = 0$. The

inverse Fourier transform of Eq. (3.26) in the spatial coordinate is complicated. However, we note that in the limit of low dissipation ($G_2 \to 0$), the wavelength spectrum is strongly peaked around the resonance condition $k_0 \to \pm[(\omega_0^2 - a\gamma^2 K_z)/(a\gamma^2 A)]^{1/2}$, where we assume that $\omega_0^2 > a\gamma^2 K_z$ so that $\pm k_0$ are real wave numbers. Driving frequencies below the gap frequency ω_K do not excite traveling spin-wave excitations [2].

At resonance, the denominator of Eq. (3.26) has complex poles at $k \to \pm k_0$. We expand the denominator in small deviations from the most resonant wave vectors, $k \approx \pm k_0 + \delta k$, to find the two solutions

$$n_{y\pm}(z,t) \approx e^{i(\pm k_0 z - \omega_0 t)} \gamma \omega_0 \tilde{H}_{\text{ext}}(\pm k_0) \int d(\delta k) \frac{e^{i\delta k z}}{\mp 2aA\gamma^2 k_0 \delta k + i\omega a G_2}, \tag{3.27}$$

where we have shifted the integration variable in the inverse Fourier transform from k to δk. This integral can be solved, giving two solutions for the spin-wave excitations:

$$n_{y\pm}(z,t) \approx \frac{\gamma}{v_g} \tilde{H}_{\text{ext}}(\pm k_0) \Theta(\pm z) e^{i(\pm k_0 z - \omega_0 t + \pi/2) \mp \gamma a G_2 z/(2v_g)}, \tag{3.28}$$

where $v_g \equiv \partial\omega_0/\partial k_0 = \gamma^2 aAk_0/\omega_0$ is the spin-wave group velocity and $\Theta(z)$ is the Heaviside step function. These spin-wave solutions have several properties that are intuitively easy to appreciate: They describe waves traveling in opposite directions out and away from the excitation source centered at $z = 0$. The spin waves are phase shifted by $\pi/2$ with respect to the excitation field because H_{ext} first induces the small canting m_x along the perpendicular direction. A nonzero Gilbert damping parameter G_2 leads to an exponential damping of the amplitude as the spin waves travel. The spin-wave amplitude is highly sensitive to the driving frequency and the spatial Fourier transform of the excitation source.

A typical modeling scheme for the excitation of spin waves in FMs and AFMs is to apply locally oscillating excitation fields at fixed positions along the spin chain. The frequency of the spin waves is subsequently controlled by varying the external field driving frequency [54, 67, 2]. Eq. (3.28) shows that the resulting spin-wave amplitudes depend crucially on the shape of the excitation source and that different amplitudes must be expected for different driving frequencies. This leads to a strong frequency dependence for the spin-wave-induced domain wall motion.

3.6 Spin waves interacting with domain walls in AFMs

In this section, we describe the interaction between spin waves and domain walls in AFMs. In Paper [2], we chose to study a 180° Néel (in-plane) domain wall (see Sec. 2.2) given by the Walker configuration $\mathbf{n}_0(\xi,t) = [\operatorname{sech}\xi\cos\phi_w, \operatorname{sech}\xi\sin\phi_w, \tanh\xi]$, where $\xi = (z - r_w)/\lambda_w$ is the dimensionless spatial coordinate, r_w is the domain wall center coordinate, ϕ_w is the helicity, and λ_w is the domain wall half-width.

Analogous to the description in Sec. 3.4, the spin waves can be described by the ansatz

$$\mathbf{n}(\xi,t) \to \hat{r} + h\left[n_\theta(\xi,t)\hat{\theta} + n_\phi(\xi,t)\hat{\phi}\right], \tag{3.29a}$$

$$\mathbf{m}(\xi,t) \to h\left[m_\theta(\xi,t)\hat{\theta} + m_\phi(\xi,t)\hat{\phi}\right], \tag{3.29b}$$

where the notations $n_{\theta(\phi)}$ and $m_{\theta(\phi)}$ describe linear order excitations of the Néel field and the canting field in the $\hat{\theta}(\hat{\phi})$ directions, perpendicular to the domain wall configuration. Inserting this ansatz into Eqs. (3.10) and expanding the Néel field to the linear order in the small excitation parameter h, lead to the equations of motion for the spin-wave excitations

$$\ddot{n}_{\theta(\phi)} = aK_z\gamma^2[\partial_\xi^2 n_{\theta(\phi)} + (2\mathrm{sech}^2\xi - 1)n_{\theta(\phi)}] - a\gamma G_2\dot{n}_{\theta(\phi)}\,, \tag{3.30}$$

where we have disregarded the G_1 dissipative term as in Sec. 3.4. We note that far to the left and to the right of the domain wall, $\mathrm{sech}\,\xi \to 0$, and the above equations reduce to the homogeneous spin-wave equations (3.24), as expected. We also note that the n_θ and n_ϕ modes are decoupled, which allows arbitrary polarizations for the antiferromagnetic spin waves. By separating the temporal and spatial dependence of the spin waves as $n_{\theta(\phi)}(\xi,t) = n_{\theta(\phi)}(\xi)\exp(-i\omega t)$, Eq. (3.30) can be cast as

$$\hat{H}n_{\theta(\phi)}(\xi) = q^2 n_{\theta(\phi)}(\xi), \tag{3.31}$$

where the operator $\hat{H} = [-\partial_\xi^2 - 2\mathrm{sech}^2(\xi)]$. The eigenvalues $q^2 = [\omega^2/(\gamma^2 aK_z) - 1 + i\omega G_2/(\gamma K_z)]$ define the dispersion relation of the antiferromagnetic spin waves. Eq. (3.31) is a time-independent Schrödinger-type equation with the Pöschl-Teller potential. However, when $G_2 \neq 0$, $\hat{H}$ is non-hermitian and has complex eigenvectors. Without dissipation, a striking property of the Pöschl-Teller potential is that it is reflectionless and offers exact solutions in the form of travelling-wave eigenfunctions [68].

For real ($G_2 \to 0$ and $\omega^2 > \gamma^2 aK_z$) eigenvectors q, the solutions to Eq. (3.31) represent propagating wave excitations that are superimposed on the domain wall texture, see Fig. 3.4. These solutions can be written as

$$n_{\theta(\phi)}(\xi,t) = \rho_q e^{i\Omega}(\tanh\,\xi - iq)\,, \tag{3.32}$$

where ρ_q is the eigenvector-dependent spin-wave amplitude that we later map to the result presented in Sec. 3.5. $\Omega = q\xi - \omega t$, so that $\mathrm{Re}\{\Omega\}$ is the general phase of the wavelike excitations. When $G_2 > 0$, the imaginary part of q leads to the exponential damping of the spin-wave amplitude. We must demand that this imaginary damping term is small to find an approximate expression for the domain wall velocity. However, close to the macrospin resonance frequency, this assumption breaks down because $\mathrm{Re}\{q\} \to 0$. Consequently, we are not able to describe the interaction between ultra-long-wavelength spin waves and domain walls with this description.

Spin waves are *linear* excitations of the Néel field in the small excitation parameter h. Analogous to the magnon-induced spin-transfer torque in FMs [54], capturing the dynamic interactions between spin waves and antiferromagnetic domain walls requires

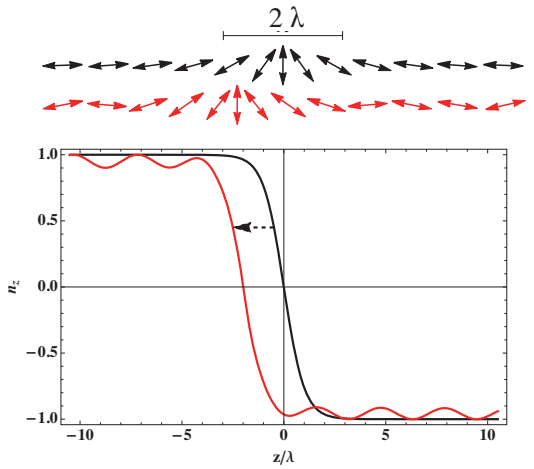

Figure 3.4: Sketch of a spin wave interacting with an antiferromagnetic domain wall. Linearly polarized spin waves incoming from the left attract the domain wall center coordinate, and the domain wall moves to the left.

that we expand $\mathbf{n}(\xi,t)$ and $\mathbf{m}(\xi,t)$ to *quadratic* order in h around the equilibrium texture $\hat{r}$. Accordingly, we propose the extended ansatz

$$\mathbf{n}(\xi,t) \to \left[1-\frac{h^2}{2}(|n_\theta|^2+|n_\phi|^2)\right]\hat{r}+h\left(n_\theta\hat{\theta}+n_\phi\hat{\phi}\right), \tag{3.33a}$$

$$\mathbf{m}(\xi,t) \to h^2 m_r^{(2)}\hat{r}+\left(hm_\theta+h^2m_\theta^{(2)}\right)\hat{\theta}+\left(hm_\phi+h^2m_\phi^{(2)}\right)\hat{\phi}, \tag{3.33b}$$

where we have also included the quadratic-order excitations of the canting field, $m^{(2)}_{\theta(\phi)}$ and $m_r^{(2)} = -(m_\theta n_\theta + m_\phi n_\phi)$, which results from enforcing the constraint $\mathbf{m}\cdot\mathbf{n}=0$ to quadratic order in h. We assume that the spatial coordinate ξ depends on time through the dynamics of the domain wall center coordinate $r_w(t)$. We also treat the out-of-plane angle $\phi_w(t)$ as a collective coordinate in the same manner as $r_w(t)$. This collective coordinate approach is equivalent to assuming that the domain wall moves and rotates as a rigid object, and that any distortion of the domain wall shape is captured by the linear-order excitations n_θ and n_ϕ.

We proceed by inserting the ansatz (3.33) into the full equations of motion (3.14) including the effective fields. We further assume that the domain wall center acceleration $\ddot{r}_w(t)$ and chirality acceleration $\dot{\phi}_w(t)$ are quadratic effects in the parameter h and, therefore, are proportional to the square of the spin-wave amplitudes. In this way, we can distinguish between the linear-order equations that lead to the spin-wave equations (3.30) and the quadratic-order equations that contain the interactions between the spin waves and the domain wall. After eliminating $\mathbf{m}$ and integrating over the

space as in Sec. 3.3, we find to the order h^2 the relations

$$\int_{-\infty}^{\infty} d\xi \operatorname{sech}\xi(\ddot{r}_w + a\gamma G_2 \dot{r}_w) = a\gamma^2 K_z \lambda_w^2 \int_{-\infty}^{\infty} d\xi \operatorname{sech}\xi (n_\phi \partial_\xi n_\phi + \tanh\xi\, |n_\theta|^2)\,, \quad (3.34a)$$

$$\int_{-\infty}^{\infty} d\xi \operatorname{sech}\xi(\ddot{\phi}_w + a\gamma G_2 \dot{\phi}_w) = a\gamma^2 K_z \lambda_w \int_{-\infty}^{\infty} d\xi \operatorname{sech}\xi\, n_\phi (\partial_\xi n_\theta - \tanh\xi\, n_\theta)\,. \quad (3.34b)$$

Although the above equations predict that the interactions between antiferromagnetic spin waves and domain walls can be complicated in the general case, we note that spin waves linearly polarized parallel ($n_\phi = 0$) or perpendicular ($n_\theta = 0$) to the domain wall plane do not lead to an acceleration of the chirality, $\ddot{\phi}_w \to 0$. Therefore, we follow Paper [2] and describe the interactions resulting from linearly polarized n_ϕ-waves transverse to the domain wall plane. For such a simplified system, we find that the above dynamic equations reduce to

$$\ddot{r}_w + a\gamma G_2 \dot{r}_w = \frac{a\gamma^2 K_z \lambda_w}{2\pi} \int_{-\infty}^{\infty} d\xi \operatorname{sech}\xi \tanh\xi\, |n_\phi|^2\,, \quad (3.35a)$$

$$\ddot{\phi}_w + a\gamma G_2 \dot{\phi}_w = 0\,, \quad (3.35b)$$

where we have used integration by parts to express the integral in this form. In Paper [2], we describe the spin wave excitations via real harmonic functions[2] and subsequently take the temporal average of the spin waves to calculate the force on the coordinate r_w. Here, we apply the equivalent procedure of calculating the force on the domain wall from the absolute square of the complex spin waves in Eq. (3.32).

Without dissipation ($G_2 \to 0$), $q \to k\lambda_w = [\omega^2/(a\gamma^2 K_z) - 1]^{1/2}$, where k is the real wave number of the spin waves at the driving frequency ω. In such a situation, the integral on the right-hand side of Eq. (3.35a) vanishes because the integrand is an odd function around the domain wall center coordinate r_w. This does *not* imply, however, that n_ϕ-waves leave the domain wall unaffected, but rather that the domain wall is allowed to move with a constant velocity.[3] However, if we include a finite dissipation ($G_2 > 0$), the spin waves are exponentially damped and the integrand in Eq. (3.35a) acquires an even component. From this component, we can calculate the steady-state velocity $\dot{r}_w$. For small damping, $\mathrm{Re}\{q\} \approx k\lambda_w$ and $\mathrm{Im}\{q\} \approx Q/2 = \gamma a G_2/(2v_g)$, where Q is the spin-wave damping factor.

Far to the left ($\xi \to -\infty$), the domain wall has no influence on the spin waves such that $|n_\phi(-\infty)|^2 \to |n_{y+}|^2$, where n_{y+} is the right-going mode in Eq. (3.28). Applying the small dissipation approximation $Q \ll k\lambda_w$, we find the relation

$$\rho_q^2 = \frac{(\gamma \tilde{H}_{\mathrm{ext}}/\lambda_w)^2}{v_g \omega k} e^{-Q(|z-z_0|)}\,, \quad (3.36)$$

[2]Note that Eq. (7) in Paper [2] misses a factor λ_w to get the correct dimensions. Eq. (8) is a small-G_2 approximation of the real spin-wave solutions. This can be slightly misleading, because the small damping limit that leads to the main result, Eq. (9), is ultimately taken to solve the integral in Eq. (7).

[3]In this case, the acceleration phase of the domain wall is caused by the transient spin-wave fronts, which we cannot describe by this quasi-equilibrium approach.

where z_0 is the position of the spin-wave excitation source. Plugging this relation back into the integral on the right-hand side of Eq. (3.35a), and solving for the steady state, $\ddot{r}_w \to 0$, the domain wall drift velocity becomes

$$\dot{r}_w = -\frac{1+3(k\lambda_w)^2}{6v_g}\left(\frac{\gamma\tilde{H}_{\text{ext}}}{k\lambda_w}\right)^2 e^{-Q|\xi_0|}\,, \tag{3.37}$$

where $|\xi_0| = |r_w - z_0|/\lambda_w$ represents the (dimensionless) distance from the excitation source to the domain wall. Contrasting Eq. (9) in Paper [2], the above result expresses the domain wall velocity directly as a function of the spatial Fourier transform of the excitation field $\tilde{H}_{\text{ext}}$.

Eq. (3.37) predicts that the domain wall is attracted toward the excitation source and that the velocity depends quadratically on the excitation field strength, as expected. The velocity also depends crucially on the spatial distribution of the excitation source. The group velocity of antiferromagnetic spin waves vanishes for extreme long-wavelength spin waves. Accordingly, Eq. (3.37) predicts that low frequency excitations just above the macrospin frequency ω_K are most effective for attracting antiferromagnetic domain walls with linearly polarized spin waves. However, the expansion in terms of a small damping factor Q breaks down in this limit, and the spin-wave group velocity v_g sets a physical upper limit on the domain wall velocity.

3.7 Circularly polarized spin waves interacting with domain walls

In Paper [2], we demonstrate that the interactions between circularly polarized spin waves and domain walls are qualitatively very different from the interactions with linearly polarized spin waves described in the previous section. Instead of attracting the domain wall, circularly polarized spin waves scatter off and push the domain wall away from the excitation source with a resulting velocity that is an order of magnitude larger than for the attractive motion caused by linearly polarized waves. The domain wall also acquires a net angular velocity $\dot{\phi}_w$.

In this section, we briefly discuss this critical dependence of the domain wall dynamics on the spin-wave polarization. The spin-wave equations (3.30) allow arbitrary polarization angles because the oscillations in the perpendicular $\hat{\theta}$ and $\hat{\phi}$ directions are decoupled. We can construct right- and left-circularly polarized spin waves by phase shifting one of the components with respect to the other:

$$\chi_\pm(\xi,t) = n_\theta(\xi,t)\hat{\theta} \pm i n_\phi(\xi,t)\hat{\phi}\,. \tag{3.38}$$

There is an important difference between linearly polarized and circularly polarized antiferromagnetic spin waves. The latter carry spin angular momentum whereas the former do not. To elucidate this phenomenon, let us consider the equation of motion for the canting field (3.14a) without dissipation but inserted the effective fields (3.13).

Analogous to Eq. (3.5) for FMs, the equation of motion for $\mathbf{m}$ can be cast as

$$\dot{\mathbf{m}} = -\gamma K_z n_z \mathbf{n} \times \hat{z} - \partial_z \mathbf{J}_{\mathbf{m}} , \tag{3.39}$$

where $\mathbf{J}_{\mathbf{m}} = \gamma A(\mathbf{n} \times \partial_z \mathbf{n})$ is the spin-wave-mediated spin current through the AFM. Analogous to the similar expression for FMs [57, 54], the z component of Eq. (3.39) has the form of a conservation law for spin angular momentum: $\dot{m}_z + \partial_z J_{m_z} = 0$. In the coordinate system of the domain wall, we find that the spin-wave-mediated spin current in the z direction is

$$J_{m_z}(\xi) = \frac{\gamma A}{\lambda_w}(n_\theta \partial_{\tilde{\xi}} n_\phi - n_\phi \partial_{\tilde{\xi}} n_\theta)\tanh\xi = \frac{\gamma A}{2i\lambda_w}(\chi_\pm \partial_{\tilde{\xi}} \chi_\pm^* - \chi_\pm^* \partial_{\tilde{\xi}} \chi_\pm)\tanh\xi , \tag{3.40}$$

from which we can conclude that J_{m_z} vanishes for linearly polarized spin waves and that circularly polarized spin waves are associated with the spin current $J_{m_z} = \pm\gamma A k \rho_q^2$, where the sign depends on the helicity. Furthermore, the spin current changes its sign when passing through the domain wall. Because angular momentum is conserved, the traveling spin waves deposit their spins on the domain wall. In contrast to the situation for FMs, where this transfer of angular momentum is responsible for the domain wall motion, the strong exchange interaction in the AFM counteracts the buildup of an increasing local magnetic moment.

The result of the spin transfer from circularly polarized spin waves passing through a domain wall is that the domain wall starts to precess and that the reflectionless Pöschl-Teller potential is destroyed. The spin waves transfer linear momentum to the domain wall on reflection, and the domain wall is propelled away from the excitation source.

3.8 Outlook

The collective coordinate approach of Paper [1] (presented in Sec. 3.3) has a wide range of applicability because of its model independence. Variations of the concepts presented in this paper have recently been applied to describe the thermophoresis of antiferromagnetic solitons [69], antiferromagnetic magnonic crystals [70], and the dynamics and formation of antiferromagnetic skyrmions [71]. Following the publication of Paper [2], Kim *et al.* [28] provided an extensive study of the interactions between circularly polarized spin waves and antiferromagnetic domain walls. They found that the domain wall motion in this case results not only from spin-wave reflection, but also has a component due to the redshift of the spin-wave frequency on transmission through the domain wall. By considering the large precession frequency of the domain wall and the associated Doppler shift, they calculated a more general expression for the resulting domain wall velocity than Eq. (12) in Paper [2].

Chapter 4

Including temperature effects

In the preceding chapters, I have described the antiferromagnetic order parameter and its dynamics well below the ordering temperature T_N. In this regime, the temperature-induced spin fluctuations in magnetic materials are typically negligible compared to the external forces induced by currents or magnetic fields. The subfield of *spin caloritronics* [72], on the other hand, deals with the intermediate-temperature regime and describes the interactions between magnetic materials and heat gradients, both in the bulk and across interfaces in magnetic heterostructures.

One of the central concepts in spin caloritronics is the *spin Seebeck effect* (SSE) [73], which describes how a temperature gradient induces a spin current in FMs. The reciprocal effect, that a spin accumulation can induce a heat current, is called the *spin Peltier effect* (SPE). Spin caloritronics effects in AFMs are not so well known, but a recent study predicts that the SSE vanishes in AFMs [74]. In Paper [4], we challenge this prediction and demonstrate that the thermal coupling between an antiferromagnetic insulator (AFI) and a normal metal (N) is relatively strong despite a vanishing SSE. The heat current across the interface is carried by a *staggered* spin current, and not a regular spin current. The staggered SSE can, therefore, be substantial in such systems.

In this chapter, Sec 4.1 describes how temperature fluctuations can be included into the equations of motion for the antiferromagnetic order parameter and the magnetization via the *fluctuation-dissipation theorem*. In Sec. 4.2, I discuss the interfacial heat current between an antiferromagnetic insulator and an adjacent normal metal and describe how the result differs from the analogous problem in FMs. Sec. 4.3 presents a short discussion of the consequences of the theory and preludes the next chapter.

Note that Paper [4] uses the notation $\mathbf{n}$ and $\mathbf{m}$ for the dimensionless antiferromagnetic order parameter and the magnetization field, respectively. To avoid further confusion with the unitary Néel field in the preceding chapters, I continue using $\mathbf{l}$ for the order parameter in this chapter, following the notation in Chapter 2.

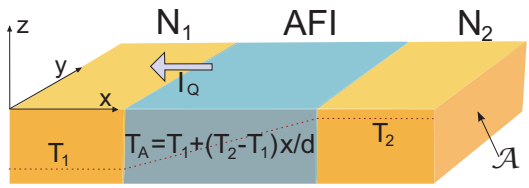

Figure 4.1: An antiferromagnetic insulator (AFI) sandwiched between two normal metals N_1 and N_2. A temperature gradient between the two normal metals, $\Delta T = T_2 - T_1$, induces a heat current I_Q that flows along the heat gradient in the AFI and across the AFI | N_1 interface. We assume that N_1 (to the left) is a good spin sink, whereas the interface coupling between AFI and N_2 (to the right) is weak. $\mathcal{A}$ and d are the cross section and the thickness of the heterostructure, respectively.

4.1 The fluctuation-dissipation theorem

The coupled antiferromagnetic Landau-Lifshitz-type equations (3.10) do not include temperature effects and describe staggered dynamics well below the Néel temperature. However, dissipation in magnetic materials is intrinsically coupled to temperature fluctuations and normally increases with higher temperature. For FMs, this coupling to the temperature can be included in the LLG phenomenology via the fluctuation-dissipation theorem [75, 65], which adds temperature-induced fluctuations to the LLG equation in the form of stochastic torques that give random kicks to the magnetization depending on the local temperature. We aim to add such torques to the dynamic equations for AFMs.

Let us consider an (initially homogeneous) antiferromagnetic insulator (AFI) sandwiched between two normal metals N_1 and N_2, see Fig. 4.1 for a sketch of the model. The equations of motion[1] for the staggered order parameter and the magnetization are

$$\dot{\mathbf{l}} = \boldsymbol{\omega}_m \times \mathbf{l} + \boldsymbol{\omega}_l \times \mathbf{m} + \boldsymbol{\tau}_l \,, \tag{4.1a}$$

$$\dot{\mathbf{m}} = \boldsymbol{\omega}_l \times \mathbf{l} + \boldsymbol{\omega}_m \times \mathbf{m} + \boldsymbol{\tau}_m \,, \tag{4.1b}$$

where the effective staggered field (in units of s^{-1}) $\boldsymbol{\omega}_l = -(\gamma/l)\delta U/\delta \mathbf{l}$ and effective magnetic field $\boldsymbol{\omega}_m = -(\gamma/l)\delta U/\delta \mathbf{m}$ are functional derivatives of the energy functional U. $l = |\mathbf{l}_0|$ is the magnitude of the staggered magnetic moment at equilibrium, and $\boldsymbol{\tau}_l$ and $\boldsymbol{\tau}_m$ are fluctuation-dissipation torques that act on the staggered order and

[1] Note that Eqs. (4.1) are defined for the order parameter $\mathbf{l}$ and not the unitary Néel field $\mathbf{n} = \mathbf{l}/|\mathbf{l}|$. The resulting equations of motion have a symmetrical form that is useful for describing homogeneous AFMs or expansions around the homogeneous state. The unitary Néel field description in Eqs. (3.10) is, in turn, more useful for describing textures such as domain walls.

the magnetization, respectively. The energy functional is

$$U = \frac{l}{2\gamma}\int d\mathbf{r}\left[\omega_E(\mathbf{l}^2-\mathbf{m}^2)-\omega_A(l_z^2+m_z^2)+\omega_A\sum_{i=x,y,z}\left[(\lambda_l\partial_i\mathbf{l})^2+(\lambda_m\partial_i\mathbf{m})^2\right]\right], \quad (4.2)$$

where ω_E and ω_A (in units of s^{-1}) are exchange and anisotropy energies, respectively. λ_l and λ_m denote exchange lengths associated with $\mathbf{l}$ and $\mathbf{m}$. The resulting effective fields from the functional derivatives are

$$\boldsymbol{\omega}_l = \omega_E\mathbf{l}+\omega_A(\mathbf{l}\cdot\hat{z})\hat{z}+\omega_A(\lambda_l\nabla)^2\mathbf{l}, \quad (4.3a)$$

$$\boldsymbol{\omega}_m = -\omega_E\mathbf{m}+\omega_A(\mathbf{m}\cdot\hat{z})\hat{z}+\omega_A(\lambda_l\nabla)^2\mathbf{m}. \quad (4.3b)$$

Following the phenomenological introduction of the dissipative terms in Ref. [27], we write the fluctuation-dissipation torques as

$$\boldsymbol{\tau}_l = (\mathbf{h}_m-\alpha\dot{\mathbf{m}})\times\mathbf{l}+(\mathbf{h}_l-\alpha\dot{\mathbf{l}})\times\mathbf{m}, \quad (4.4a)$$

$$\boldsymbol{\tau}_m = (\mathbf{h}_l-\alpha\dot{\mathbf{l}})\times\mathbf{l}+(\mathbf{h}_m-\alpha\dot{\mathbf{m}})\times\mathbf{m}, \quad (4.4b)$$

where $\mathbf{h}_l$ and $\mathbf{h}_m$ are fluctuating stochastic fields and α is the damping parameter. Importantly, we note that the stochastic fields and the damping parameter have contributions both from the bulk and from the interface scattering. For homogeneous macrospin excitations, $\alpha^{(b)}$ describes the bulk Gilbert damping, whereas $\alpha^{(b)}+\alpha^{(p)}/d$ is the damping at the interface, where $\alpha^{(p)}$ is the enhanced dissipation due to spin pumping [76]. To distinguish between the bulk and interfacial effects of the fluctuating forces, we decompose the coordinate $\mathbf{r} = (x,\boldsymbol{\rho})$ into a longitudinal coordinate $x\in[0,d]$ and the two-dimensional in-plane coordinate $\boldsymbol{\rho}$, see Fig. 4.1. The fluctuation-dissipation torques can then be represented as $\tau_\nu(\mathbf{r}) \to \tau_\nu^{(b)}(\mathbf{r})+\delta(x-x_0)\tau_\nu^{(p)}(\boldsymbol{\rho})$, where $x_0 = 0^+$ is infinitesimally close to the AFI | N_1 interface, and the index ν denotes l_i or m_i, where i is one of the cartesian components x, y, and z.

Although the averages and cross correlations of all the stochastic fields vanish, the fluctuation-dissipation theorem implies that there is a connection between the variance of $\mathbf{h}_l$ and $\mathbf{h}_m$ and the damping constants in the bulk AFI and at the AFI | N_1 interface:

$$\langle h_\nu^{(p)}(\boldsymbol{\rho},t)h_\nu^{(p)}(\boldsymbol{\rho}',t')\rangle = \frac{\gamma\alpha^{(p)}R(t-t',T_1)}{l\pi}\delta(\boldsymbol{\rho}-\boldsymbol{\rho}'), \quad (4.5a)$$

$$\langle h_\nu^{(b)}(\mathbf{r}',t)h_\nu^{(b)}(\mathbf{r}',t')\rangle = \frac{\gamma\alpha^{(b)}R(t-t',T_A)}{l\pi}\delta(\mathbf{r}-\mathbf{r}'), \quad (4.5b)$$

where the correlation function $R(t,T)$ depends on the local temperature profile, $T_A(x)$. In Eq. (4.5a), we assume that the spin-current fluctuations at the AFI | N_1 interface depend on the temperature T_1 of N_1, analogous to the situation for FMs [77].

4.2 Heat current

Because the external forces in this system do not change, the heat current can be found from the continuity equation for the energy

$$\langle \dot{U} \rangle + \nabla \mathbf{j}_{\mathrm{U}} = 0\,, \tag{4.6}$$

where $\mathbf{j}_{\mathrm{U}}$ can be identified as the heat current density. Furthermore, the total heat current across the AFI | N_1 interface can be integrated up as $I_Q = \int d\boldsymbol{\rho}(-\hat{x}\cdot \mathbf{j}_{\mathrm{U}})$. Using the continuity equation (4.6) and the equations of motion for the continuum fields (4.1), the interfacial heat current can be expressed as

$$I_Q = \frac{L}{\gamma}\langle \omega_A \lambda_l \partial_x \mathbf{l}\cdot\dot{\mathbf{l}} + \omega_A \lambda_m \partial_x \mathbf{m}\cdot\dot{\mathbf{m}}\rangle|_{x=0}\,, \tag{4.7}$$

where $\langle\rangle$ denotes a temporal average. I_Q can be calculated in the linear response by assuming that the stochastic fields $\mathbf{h}_m$ and $\mathbf{h}_l$ induce the small perturbations $m_{x(y)}$ and $l_{x(y)}$ on top of the equilibrium configuration $\mathbf{l} = \hat{z}$ and $\mathbf{m} = 0$. For the full calculation of the heat current I_Q in terms of the stochastic fields $\mathbf{h}_l$ and $\mathbf{h}_m$ and the correlation function $R(t,T)$, we refer to the treatment in Paper [4]. However, as a prelude to the next chapter, we consider the final result for the heat current

$$I_Q = \sum_{N=0}^{\infty} \frac{1}{t_N^{(p)}} \int_0^{\infty} d\omega \mathcal{D}_N(\omega)\hbar\omega \left\{ f(\omega,T_2)\left[1-f(\omega,T_1)\right] - f(\omega,T_1)\left[1-f(\omega,T_2)\right]\right\}\,, \tag{4.8}$$

where we have included that the continuum field perturbations can be viewed as an ensemble of excited *magnons*. The magnons in the AFI and the electron-hole pairs in N_1 and N_2 follow quantum statistics and is distributed according to the Bose-Einstein distribution function $f(\omega,T)$. $\mathcal{D}_N(\omega)$ is the mode-dependent density of magnon states. The heat current that flows across the AFI | N_1 interface is inversely proportional to the spin-pumping-induced spin-wave (magnon) relaxation time

$$1/t_0^{(p)} = \frac{\alpha^{(p)}}{d}\omega_E\,, \tag{4.9a}$$

$$1/t_{N\neq 0}^{(p)} = \frac{2\alpha^{(p)}}{d}\omega_E\,, \tag{4.9b}$$

which shows that the heat current is proportional to the exchange energy ω_E. This result differs from analogous expressions for spin-wave relaxation rates in FMs, which are proportional to the much smaller magnon energy ω.

The heat current (4.8) has an intuitive form because it describes the difference in magnon scattering probabilities at the two interfaces AFI | N_1 and AFI | N_2. These probabilities depend on the distribution of magnons in the AFI and the distribution of empty states in the normal metals, given the temperatures at the interfaces. Because the scattering probabilities are, in general, different for the two interfaces, a magnonic current flows from N_2 to N_1 across the AFI. The total heat current is then given by a sum over all staggered-spin-carrying longitudinal magnon modes N integrated over all frequencies ω.

4.3 Outlook

A similar procedure as the one presented in the preceding chapters, including the fluctuation-dissipation theorem, was used in Ref. [69] to describe the thermally induced dynamics (thermophoresis) of an antiferromagnetic soliton via the collective coordinate approach.

By considering the heat current (4.8) as resulting from interfacial electron-magnon scattering, where the magnons follow quantum statistics and are distributed according to the quantum mechanical Bose-Einstein distribution, we have made the important classical-to-quantum crossover. In the next section, we complete the transition from classical models of magnetic materials to the quantum description of collective spin excitations and describe the ultrafast spin currents in a ferromagnetic metal induced by rapid heating with a femtosecond laser pulse.

Chapter 5

Transition to the ultrafast regime

In the previous chapter, I described how to add temperature effects to the Landau-Lifshitz phenomenology for AFMs via the fluctuation-dissipation theorem. This theorem expresses a fundamental link between stochastic temperature-induced spin fluctuations and the magnetization dissipation, both in the bulk and at the interfaces between magnetic materials and adjacent normal metals. However, this procedure is limited to stochastic forces that are relatively weak compared to the exchange forces that are responsible for sustaining the magnetic order. In the opposite high-energy limit, we find the subfield of *ultrafast magnetization dynamics* [78, 79], which studies the rapid demagnetization resulting from ultrafast excitation of a magnetic material by a femtosecond laser pulse.

One of the main motivations behind Paper [3] was a range of recent observations [80–82] showing that ultrafast demagnetization in magnetic heterostructures lead to secondary effects such as the generation of ultrafast spin currents in normal metals adjacent to the magnetic materials. Our idea was that these effects may be related to intermediate-temperature spin caloritronics phenomena such as the spin Seebeck effect [83, 72]. However, no theoretical formalism existed that united the description of the ultrafast demagnetization in the bulk and across interfaces in magnetic heterostructures with the phenomena taking place at lower energies.

Sec. 5.1 describes the subfield of ultrafast magnetization dynamics and some of its challenges from a spintronics point of view. I proceed by presenting our model for ultrafast demagnetization in a ferromagnetic metal, including the important concept of splitting the electrons into itinerant s states and localized d states. In Sec. 5.2, I present the calculation of the s-d spin current following Fermi's Golden Rule. A key concept is the nonthermalized magnon distribution function. Sec. 5.3 expresses the out-of-equilibrium spin accumulation among the itinerant electrons and the accompanying equations of motion for the spin accumulation and the magnon distribution function. In the last section (Sec. 5.4), I discuss how the ideas of Paper [3] can be extended to treat interface scattering and multi-sublattice materials.

5.1 Modelling ultrafast magnetization dynamics

The field of ultrafast magnetization dynamics [84, 78, 79] studies the dynamic reaction of magnetic materials after rapid excitation by femtosecond laser pulses. These laser-induced perturbations are so fast and violent that they challenge the highest energy scale associated with magnetic order: The microscopic exchange energy that governs the ordering temperature T_C. Several different mechanisms and scenarios have been proposed to explain the rapid quenching of the magnetic moment observed after laser excitation. Some theories propose that the demagnetization results from direct spin transfer from the laser field to the magnetic material via the inverse Faraday effect [85] or other effective magnetic fields induced by the irradiating laser light [86]. Although such laser-induced effective magnetic fields may play a role in magnetization switching close to the Curie point T_C [87], we adopt the view that ultrafast laser-induced demagnetization is predominantly a result of incoherent heat transfer from the laser pulse to the electron system [88, 89].

The magnetization dynamics resulting from rapid laser heating are predominantly longitudinal, contrasting the low-frequency ferromagnetic resonance (FMR) [90], in which only the direction of the magnetization varies and not its magnitude. FMR effects in FMs are well described by the transverse LLG phenomenology [Eq. (3.1)] [10, 56]. For finite temperatures below T_C, the Landau-Lifshitz equation can be extended to include temperature-dependent longitudinal magnetization relaxation via stochastic Langevin terms [75] [similar to Eqs. (4.5)]. The resulting longitudinal Landau-Lifshitz-Bloch (LLB) equation [91] has been shown to accurately describe the temperature-dependent average magnetization of FMs up to the phase transition at T_C.

In ultrafast magnetization experiments, however, the temperature of the itinerant electrons in magnetic metals increases to $T_s \geq T_C$ on a time scale typically less than 100 fs. This regime is beyond the validity of the LLG phenomenology, which is designed to address low-energy magnetization dynamics. Relaxation terms based on the LLB treatment [92] should also be treated with scepticism because the Langevin correlation terms of such models are based on a simple Markovian environment without any feedback or internal dynamics. For high-energy perturbations such as femtosecond laser pulses, no subsystem can be viewed as a featureless reservoir for energy and angular momentum. Consequently, we assume that the statistical average of the transverse magnetization during ultrafast demagnetization vanishes for all practical purposes. The remaining dynamics can be described via rate equations for longitudinal spin transfer between the electronic subsystems.

One of the main assumptions of our model of ultrafast magnetization dynamics, is the distinction between two different groups of electrons [93]: the itinerant *s* electrons that are loosely bound to the atomic nuclei, and the localised *d* electrons that are responsible for the macroscopic magnetization. See Fig. 5.1 for a simplified sketch of the electron energy levels. We note that such a clear distinction may not be realistic for all ferromagnetic metals, where the continuum of electron states below the Fermi energy ϵ_F are typically well described by Stoner-like models [94]. Accordingly, the

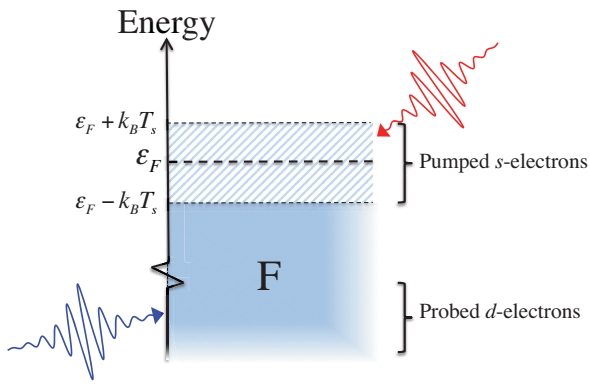

Figure 5.1: For a typical pump-probe experiment of laser-induced ultrafast magnetization dynamics [95], it is useful to distinguish between two types of electrons based on the energy level on which they interact with the laser pulse. The "pump" laser pulse (red) excites itinerant s electrons in an energy region $\pm k_B T_s$ around the Fermi level ϵ_F. The magnetization of the magnetic material, however, is typically "probed" (blue) at a higher laser frequency, e.g., at a deeper energy level, where the spin-carrying d electrons can be assumed to be localized.

grouping of the electrons as "itinerant" or "localized" is somewhat semantic.

However, the distinction is justified when the electrons operate and interact at different energy scales. This is typically the situation in pump-probe experiments used for studying ultrafast magnetization dynamics, in which the pump laser pulse excites (itinerant) electrons in a small energy region in the vicinity of the Fermi level. On the other hand, the experimental methods for optically probing magnetization are usually tuned to the absorption edge of (localized) electron orbitals buried deeply *below* the Fermi level [96, 95], and may, therefore, be largely insensitive to the spin density of the s-electrons, which is deposited close to the Fermi energy, see Fig. 5.1.

Our model is based on the assumption that the primary interaction channel between the laser-excited s electrons and the magnetic d electrons can be described via the electron-magnon scattering. Central to this description, is the assumption that the energy of the itinerant s electrons thermalize rapidly due to Coulombic scattering and can be described by a Fermi-Dirac distribution. The same quasi-equilibrium assumption cannot be made for the localized spins, which thermalize via the much slower magnon-magnon interactions.

We have now presented the basic concepts and ideas behind our theory and proceed to formalize the model. Let us consider a ferromagnetic metal (F) in which the electronic continuum can be grouped into itinerant s-electron states and localized d-electron states. The Hamiltonian that describes F is $\hat{H} = \hat{H}_0 + \hat{H}_{sd}$, where $\hat{H}_0$ consists of decoupled s- and d-electron energies, including the kinetic energy of the itinerant electrons, the d-d exchange energy, the dipole interactions, and the crystalline and Zeeman fields. We are interested in describing the s-d exchange interaction, which

can be formulated via the Hamiltonian

$$\hat{H}_{sd} = J_{sd} \sum_j \mathbf{S}_j^d \cdot \mathbf{s}(\mathbf{r}_j)\,, \tag{5.1}$$

where J_{sd} is the exchange energy and $\mathbf{S}_j^d$ $[\mathbf{s}(\mathbf{r}_j)]$ is the d-electron (s-electron) spin vector (spin density) at lattice point j. We conveniently rewrite the d-electron spin vectors $\mathbf{S}_j^d$ via the following Holstein-Primakoff transformations [97]:

$$S_j^+ = S_j^x + iS_j^y = \sqrt{2S} a_j^\dagger \sqrt{1 - \frac{a_j^\dagger a_j}{2S}}\,, \tag{5.2a}$$

$$S_j^- = S_j^x - iS_j^y = \sqrt{2S} \sqrt{1 - \frac{a_j^\dagger a_j}{2S}} a_j\,, \tag{5.2b}$$

$$S_j^z = a_j^\dagger a_j - S_j\,, \tag{5.2c}$$

where S is the saturation value of the spin density (in units of $\hbar$), and the Fourier transforms $a_q^\dagger(a_q) = \sum_j \exp(-i\mathbf{q}\cdot\mathbf{r}_j) a_j^\dagger(a_j)$ are bosonic creation (annihilation) operators for magnons with wave number $q = |\mathbf{q}|$. These operators satisfy the commutation relation $[a_q^\dagger, a_{q'}] = \delta_{qq'}$. Following Refs. [98, 99], we keep only the first order contributions in the Holstein-Primakoff transformations (5.2) and express the s-electron spin density via electronic field operators. The s-d Hamiltonian (5.1) becomes

$$\hat{H}_{sd} = \sum_{q,k,k'} V_{qkk'} a_q c_{k\uparrow}^\dagger c_{k'\downarrow} + \text{H.c.}\,, \tag{5.3}$$

where $c_{k\sigma}^\dagger$ ($c_{k\sigma}$) is the creation (annihilation) operator for s electrons with momentum k and spin σ. $\hat{H}_{sd}$ describes the electron-magnon interaction, in which an s electron with momentum k flips its spin while creating or annihilating a magnon with momentum q and spin $\hbar$. The scattering strength is determined by the matrix element $V_{qkk'}$.

5.2 s-d spin current following Fermi's Golden Rule

This section presents the derivation of the s-d spin current starting from Eq. (5.3). We assume that the dephasing effects are large enough for the system to be described by the density matrix $\hat{\rho}_{sd} = \hat{\rho}_s \otimes \hat{\rho}_d$, and that all the energy scales in the system (E_q, E_k, and $E_{k'}$) are smaller than the Fermi energy ϵ_F. As described in the previous section, we assume that the kinetic energy of the hot s electrons quickly thermalize due to Coulombic scattering and we can define

$$\left\langle c_{k\sigma}^\dagger c_{k'\sigma'} \right\rangle = \text{Tr}\left[\hat{\rho}_s c_{k\sigma}^\dagger c_{k'\sigma'}\right] = n_{\text{FD}}(E_k - \mu_\sigma)\delta_{kk'}\delta_{\sigma\sigma'}\,, \tag{5.4a}$$

$$\left\langle a_q^\dagger a_{q'} \right\rangle = \text{Tr}\left[\hat{\rho}_s a_q^\dagger a_{q'}\right] = n(E_q)\delta_{qq'}\,, \tag{5.4b}$$

where $n_{\text{FD}}(E_k - \mu_\sigma)$ is the quasi-equilibrated (thermalized) Fermi-Dirac distribution function at the chemical potential μ_σ and the s-electron temperature $T_s \ll T_F$, where

$T_F = \epsilon_F/k_B$ is the Fermi temperature. There are initially no restrictions on the form of the magnon distribution function $n(E_q)$. It thermalizes toward the Bose-Einstein distribution via magnon-magnon interactions if the system is allowed to relax. The thermalization rate, $\tau_{\text{th}}^{-1} \sim \hbar^{-1}\epsilon_m[\epsilon_m/(k_B T_C)]^3$ [100], where ϵ_m is a characteristic energy of the thermal magnon cloud, is typically much lower than the demagnetization rates after laser pulse excitation. Consequently, the magnon distribution should be treated as nonthermalized on the relevant time scales of the demagnetization process.

When $\hat{H}_{sd}$ is not the dominant part of the Hamiltonian, it can be treated as a perturbation. Following a mean-field approach, we apply Fermi's Golden Rule to the lowest order in the *s-d* interaction $\hat{H}_{sd}$. Fermi's Golden Rule states that the transition rate between two states can be calculated from the matrix elements of the perturbing potential between the final and the initial states [101]. Accordingly, the spin transfer from *s* to *d* states can be expressed as

$$\begin{aligned} I_{sd} =& \frac{2\pi}{V}\sum_{q,k,k'}\Big[\text{Tr}\left\{V^*_{qkk'}a^\dagger_q c^\dagger_{\downarrow k}c_{\uparrow k'}\hat{\rho}_{sd}V_{qkk'}a_q c^\dagger_{\uparrow k}c_{\downarrow k'}\right\} \\ &- \text{Tr}\left\{V_{qkk'}a_q c^\dagger_{\uparrow k}c_{\downarrow k'}\hat{\rho}_{sd}V^*_{qkk'}a^\dagger_q c^\dagger_{\downarrow k}c_{\uparrow k'}\right\}\Big]\delta(E_q + E_{k'} - E_k)\,, \end{aligned} \tag{5.5}$$

where V is the volume of the ferromagnet and the total spin current is given by the imbalance between the creation and annihilation of magnons due to spin-flip scattering of s-electrons. The delta function ensures energy conservation. Using the above definitions of the electron and magnon distribution functions (5.4), I_{sd} simplifies to

$$\begin{aligned} I_{sd} =& \frac{2\pi}{V}\sum_{q,k,k'}|V_{qkk'}|^2\delta(E_q + E_{k'} - E_k) \\ &\times\Big\{[n_{\text{FD}}(E_k - \mu_\uparrow)][1 - n_{\text{FD}}(E_{k'} - \mu_\downarrow)][1 + n(E_q)] \\ &- [n_{\text{FD}}(E_{k'} - \mu_\downarrow)][n_{\text{FD}}(E_k - \mu_\uparrow)][n(E_q)]\Big\}. \end{aligned} \tag{5.6}$$

Next, we apply the identities $n_{\text{FD}}(x)[1 - n_F(y)] = n_{\text{BE}}(x - y)[n_{\text{FD}}(y) - n_{\text{FD}}(x)]$ and $1 + n_{\text{BE}}(x) = -n_{\text{BE}}(-x)$ [101], where n_{BE} is the Bose-Einstein distribution function.[1] After rearranging, the spin current becomes

$$\begin{aligned} I_{sd} =& \frac{2\pi}{V}\sum_{q,k,k'}|V_{qkk'}|^2\delta(E_q + E_{k'} - E_k) \\ &\times[n_{\text{FD}}(E_k - \mu_\uparrow) - n_{\text{FD}}(E_{k'} - \mu_\downarrow)][n_{\text{BE}}(E_q - \mu_s) - n(E_q)]\,, \end{aligned} \tag{5.7}$$

where we have defined the out-of-equilibrium spin accumulation $\mu_s = \mu_\uparrow - \mu_\downarrow$ as the difference in the chemical potential of spin-up and spin-down itinerant electrons.

[1] Note that these manipulations are applied only to the *s*-electron distribution function, whereas the form of the magnon distribution function $n(E_q)$ remains arbitrary at this point.

Because the *s*-electron-hole pairs are all distributed in close to the Fermi level ϵ_F, we can safely assume that their densities of state are approximately described by the density of state at the Fermi level, $D_\uparrow(\epsilon) \approx D_\downarrow(\epsilon) \approx D_s(\epsilon_F)$. Next, we insert $1 = \int d\epsilon_q \int d\epsilon \int d\epsilon' \delta(\epsilon_q - E_q)\delta(\epsilon - E_k)\delta(\epsilon' - E_{k'})$. After integration over ϵ and ϵ' and using the identity $\int dx[n_F(x) - n_F(x+y)] = y$, we find that the spin current can be expressed as

$$I_{sd} = \int d\epsilon_q \Gamma(\epsilon_q)\mathcal{D}(\epsilon_q)(\epsilon_q - \mu_s)[n_{\mathrm{BE}}(\epsilon_q - \mu_s) - n(\epsilon_q)]\,, \tag{5.8}$$

where $\mathcal{D}(\epsilon_q)$ is the magnon density of states. The form of Eq. (5.8) reveals that the *s*-*d* spin transfer depends on the distribution of magnons and electron-hole pairs (empty scattering states) among the excited *s* electrons. Naturally, the electron-magnon scattering is quenched by a large spin accumulation μ_s, which serves as a feedback effect that limits the number of available scattering states. The scattering rate is defined as [99]

$$\Gamma(\epsilon_q) = \frac{2\pi V^2}{\mathcal{D}(\epsilon_q)} \int \frac{d^3k}{(2\pi)^3}\frac{d^3k'}{(2\pi)^3}\frac{d^3q}{(2\pi)^3}|V_{qkk'}|^2\delta(\epsilon - \epsilon_F)\delta(\epsilon' - \epsilon_F)\delta(E_q - \epsilon_q). \tag{5.9}$$

We do not directly calculate the scattering rate $\Gamma(\epsilon_q)$, but posit that the *s*-*d* scattering rate increases for high-energy magnons according to the transverse spin diffusion [98]. Accordingly, we can write $\Gamma(\epsilon_q) = \Gamma_0 + \chi A q^2$, where χ parametrizes the enhanced scattering of high-energy magnons, and A is the stiffness of F. This energy dependence is different in the bulk than for scattering across interfaces. For low-temperature scattering across the interface between a FM and a normal metal, the interfacial scattering rate $\Gamma^i(\epsilon_q)$ is relatively weakly energy-dependent [99].

In Paper [3], we show that for the low-energy coherent magnetic precession of FMR, $\Gamma_0 \to 2\alpha$, where α is the Gilbert damping constant that is accessible through FMR experiments. This provides the link between the macrospin description at low energies and the high-energy scattering. In the ultrafast regime, however, the demagnetization rate $\Gamma(\epsilon_q)$ is predominantly governed by the *effective* Gilbert damping $\alpha^* \approx \chi\epsilon_b$, where ϵ_b is the magnon energy at the edge of the Brillouin zone.[2]

5.3 The out-of-equibrium spin accumulation

We orient the coordinate system such that the local spin density points in the negative z direction at equilibrium. The total spin density in the z direction becomes $S_z = n_d - S$, where we have defined the out-of-equilibrium magnon density n_d. We assume that the magnons follow a quadratic dispersion, $\epsilon_q = \epsilon_0 + Aq^2$, where ϵ_0 is the magnon gap. The total spin density in the z direction is determined by a thermal average over the excited magnon states. It follows that $\langle a_q^\dagger a_{q'}\rangle = n(\epsilon_q)\delta_{qq'}$ defines the magnon

[2]Note that it is necessary to introduce a high-energy cut-off in the *s*-*d* scattering integral (5.8) at the bandwidth ϵ_b because of the nonexistence of magnons with wavelengths shorter than the lattice spacing.

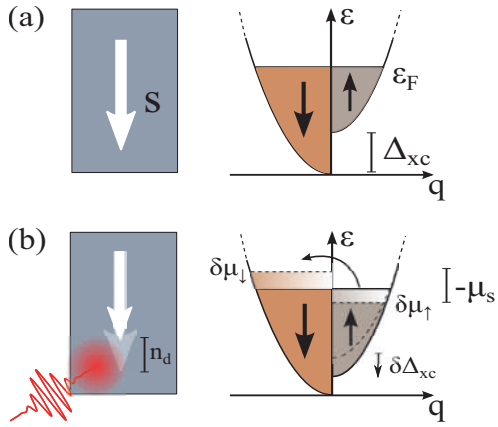

Figure 5.2: (**a**) For metallic ferromagnets with macroscopic spin density vector **S**, the itinerant electrons are spin polarized due to the mean-field exchange interaction mediated by the localized d electrons. The electron bands are, therefore, shifted by the exchange gap Δ_{xc}. (**b**) After a laser pulse rapidly heats the itinerant electrons, two effects lead to a change in the out-of-equilibrium spin accumulation μ_s: electron-magnon scattering and a lowering of the exchange gap by $\delta\Delta_{xc}$ because the total spin density of the d electrons is reduced by a finite magnon density n_d.

distribution function $n(\epsilon_q)$, which is related to the total magnon density through $n_d = \int_{\epsilon_0}^{\epsilon_b} d\epsilon_q \mathcal{D}(\epsilon_q) n(\epsilon_q)$, where the density of magnon states $\mathcal{D} = \sqrt{\epsilon_q - \epsilon_0}/(4\pi A^{3/2})$.

In an ultrafast demagnetization scenario, the out-of-equilibrium spin accumulation among the s electrons has two contributions: one from the change in the density of states and one from the temperature-induced variations in the distribution function, see Fig. 5.2 for a sketch of the electronic bands. We proceed by developing an expression for the spin accumulation. The density (in units of $\hbar$) of spin-up(down) electrons is defined as

$$n_{\uparrow(\downarrow)} = \int d\epsilon D_{\uparrow(\downarrow)}(\epsilon - \Delta_{\uparrow(\downarrow)}) f(\epsilon - \mu_{\uparrow(\downarrow)}) \,, \tag{5.10}$$

where $D_{\uparrow(\downarrow)}(\epsilon - \Delta_{\uparrow(\downarrow)})$ is the density of states for spin-up(down) electrons given the band edge $\Delta_{\uparrow(\downarrow)}$, and $f(\epsilon - \mu_{\uparrow(\downarrow)})$ is the electron distribution function given the chemical potential $\mu_{\uparrow(\downarrow)}$. To find an expression for the *out-of-equilibrium* spin density, we expand $n_{\uparrow(\downarrow)} = n^0_{\uparrow(\downarrow)} + \Delta n_{\uparrow(\downarrow)}$, where $n^0_{\uparrow(\downarrow)}$ is the spin-up(down) electron density at equilibrium. The resulting out-of-equilibrium spin density for spin-up(down) electrons is

$$\begin{aligned} \Delta n_{\uparrow(\downarrow)} =& -\delta\Delta_{\uparrow(\downarrow)} \int d\epsilon \frac{\partial}{\partial\epsilon} D_{\uparrow(\downarrow)}(\epsilon - \Delta_{\uparrow(\downarrow)}) f(\epsilon - \epsilon_F) \\ & - \delta\mu_{\uparrow(\downarrow)} \int d\epsilon D_{\uparrow(\downarrow)}(\epsilon - \Delta_{\uparrow(\downarrow)}) \frac{\partial}{\partial\epsilon} f(\epsilon - \epsilon_F) \\ \approx& -\delta\Delta_{\uparrow(\downarrow)} D^{\epsilon_F}_{\uparrow(\downarrow)} - \delta\mu_{\uparrow(\downarrow)} D^{\epsilon_F}_{\uparrow(\downarrow)} \,, \end{aligned} \tag{5.11}$$

where $\delta\Delta_{\uparrow(\downarrow)}$ is a small change in the band edge, $\delta\mu_{\uparrow(\downarrow)}$ is a small change in the chemical potential, and $D^{\epsilon_F}_{\uparrow(\downarrow)}$ is the density of states at the Fermi level. In the last transition in Eq. (5.11), we have used integration by parts and assumed that all electronic excitations are close to the Fermi level, so that the derivative of the distribution function can be approximated to a delta function. From the above relation and assuming charge conservation, $\Delta n_\uparrow = -\Delta n_\downarrow$, we calculate an expression for the out-of-equilibrium spin accumulation

$$\mu_s = \delta\mu_\uparrow - \delta\mu_\downarrow = \frac{\delta n_s}{D} + \delta\Delta_{xc}\,, \tag{5.12}$$

where δn_s is the out-of-equilibrium spin density, $D = 2D^{\epsilon_F}_\uparrow D^{\epsilon_F}_\downarrow / (D^{\epsilon_F}_\uparrow + D^{\epsilon_F}_\downarrow)$, and $\delta\Delta_{xc} = \delta\Delta_\uparrow - \delta\Delta_\downarrow$ is the dynamics-induced out-of-equilibrium change in the exchange splitting [102].

We can now formulate the equations of motion for the spin accumulation μ_s and the magnon density n_d. We neglect the contribution from all other relaxation channels of the d-electron spin than the s-d interaction. Therefore, $\partial_t n_d = I_{sd}/\hbar$ and the equations of motion are given as

$$\frac{\partial}{\partial t}\mu_s = \frac{\mu_s}{\tau_s} + \frac{\rho}{\hbar} I_{sd}\,, \tag{5.13a}$$

$$\frac{\partial}{\partial t} n(\epsilon_q) = \frac{\Gamma(\epsilon_q)}{\hbar}(\epsilon_q - \mu_s)\left[n_{\mathrm{BE}}(\epsilon_q - \mu_s) - n(\epsilon_q)\right]\,, \tag{5.13b}$$

where $\rho = -1/D - \Delta_{xc}/S$. τ_s describes the spin-orbit relaxation time of the s-electron spin density to the lattice, and is typically of the order of picoseconds [103]. τ_s represents the only channel for dissipation of spin angular momentum out of the combined electron system.

The equations of motion (5.13) describe the coupled dynamics of the hot s electrons and the excited magnons via the spin accumulation μ_s and the distribution function $n(\epsilon_q)$. Initially after rapid heating of the s-electron bath to $T_s \geq T_C$, the magnon distribution function is empty. In this stage of the demagnetization process, the s-d scattering mainly excites magnons close to the Brillioun zone edge ϵ_b because high-energy states are populated much faster than are low-energy states. We have written Eq. (5.13b) as an energy-resolved equation to emphasize the nonthermalized state of the excited magnons.

Ref. [104] presents a bulk demagnetization theory that is conceptually similar to ours, but where the magnons are treated as thermalized, following a Bose-Einstein energy distribution at the magnon temperature T_m. The itinerant electrons are assumed to have a vanishing out-of-equilibrium spin density. In our view, the nonthermalized state of the excited magnons and the out-of-equilibrium spin accumulation are central ingredients in the description of ultrafast magnetization dynamics. Atomistic modelling of thermally induced switching in ferrimagnetic GdFeCo supports the notion that the excited magnons are distributed in nonequilibrium states [105]. In particular, retaining a finite out-of-equilibrium spin accumulation is important to describe the laser-induced ultrafast spin currents that arise in magnetic heterostructures [81, 82].

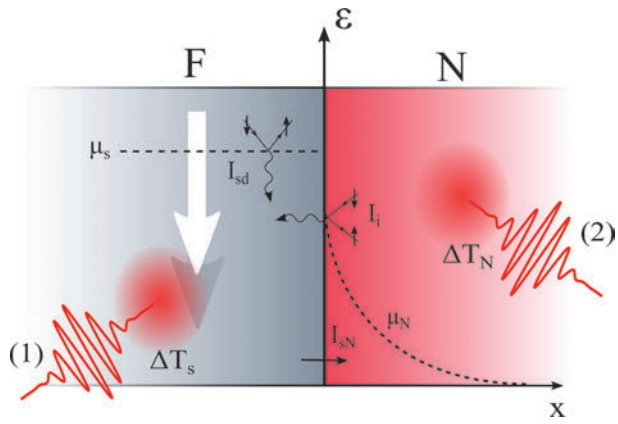

Figure 5.3: The high-energy electron-magnon scattering describes two different ultrafast heating scenarios: **(1)** F is directly heated by a femtosecond laser pulse. The temperature of the *s* electrons rapidly increases by ΔT_s. This temperature jump induces a finite magnon density n_d via the *s-d* spin current I_{sd} (5.8) and a finite spin accumulation μ_s in F. **(2)** F can be demagnetized indirectly via the interfacial spin current I_i after rapid laser heating of the electrons in N. I_i leads to a finite spin accumulation μ_N that subsequently diffuses into N as an ultrafast spin current. In addition to I_{sd} and I_i, we must also include the interfacial spin current I_{sN}, which describes the spin-dependent transport between itinerant electrons in F and N.

5.4 Outlook

In Paper [3], we have presented the basic building blocks of a theory of ultrafast demagnetization in a bulk ferromagnetic metal via the *s-d* electron-magnon interaction. One of the main strengths of our theory is that the formalism can also be used to describe interfacial scattering between magnetic materials and adjacent normal metals in magnetic heterostructures, see Fig. 5.3. In such a scenario, the interfacial scattering between the spin-carrying *d* electrons in F and the itinerant electrons in *N* can be described by a similar rate equation as Eq. (5.8), but with a different *interfacial* scattering rate $\Gamma^i(\epsilon_q)$. For long-wavelength magnons, the interfacial spin current can be described in the language of *spin pumping*, and the low-energy scattering rate can be identified as $\Gamma_0^i = g_{\uparrow\downarrow}/(\pi S)$, where $g_{\uparrow\downarrow}$ is the *spin-mixing conductance* (per unit area) [106, 107]. This identification demonstrates that our procedure can be used to unify the description of ultrafast spin-current generation at the interfaces in magnetic heterostructures with the low- and intermediate-temperature phenomena, which are all parametrized by the spin-mixing conductance [108].

Fig. 5.3 presents two possible scenarios for ultrafast magnetization dynamics in magnetic heterostructures that both can be described by our model. One can either rapidly heat the *s* electrons in F or the itinerant electrons in the adjacent normal metal N. Both scenarios lead to the demagnetization of F through electron-magnon scattering in the bulk or at the F | N interface. Varying the magnetic layer thickness (and other material-specific parameters) results in different demagnetization rates because the

bulk scattering rate is governed by the effective Gilbert damping parameter whereas the interfacial scattering rate is governed by the effective spin-mixing conductance.

In contrast to the other papers in this thesis, which focus on dynamics in AFMs, Paper [3] describes ultrafast magnetization dynamics in a FM. However, the connection between this paper and AFMs is clarified by considering the natural next step of the theory of high-energy electron-magnon scattering. In the field of ultrafast magnetization dynamics, multi-sublattice ferrimagnetic materials such as GdFe have long been studied because their magnetic states can be switched using only ultrafast laser pulses [79, 109]. This behavior is normally explained as a combination of two effects: Heat-induced demagnetization and a strong antiferromagnetic exchange interaction between the two magnetic sublattices [92]. In the high-energy limit, the clear distinction between antiferromagnetic and ferrimagnetic materials is somewhat erased because the response to ultrafast excitation may differ for the different sublattices. Consequently, there is a possibility that AFMs also induce (transient) ultrafast spin currents as well as ultrafast staggered spin currents after rapid heating by femtosecond laser pulses. To model such a system would be an interesting and natural next step from the theory presented in Paper [3].

Bibliography

[1] E. G. Tveten, A. Qaiumzadeh, O. A. Tretiakov, and A. Brataas, Phys. Rev. Lett., **110**, 127208 (2013).

[2] E. G. Tveten, A. Qaiumzadeh, and A. Brataas, Phys. Rev. Lett., **112**, 147204 (2014).

[3] E. G. Tveten, A. Brataas, and Y. Tserkovnyak, Phys. Rev. B, **92**, 180412 (2015).

[4] A. Brataas, H. Skarsvåg, E. G. Tveten, and E. Løhaugen Fjærbu, Phys. Rev. B, **92**, 180414 (2015).

[5] E. G. Tveten, T. Müller, J. Linder, and A. Brataas, Phys. Rev. B, **93**, 104408 (2016).

[6] G. Moore, Proceedings of the IEEE, **86**, 82 (1998).

[7] R. Waser, *Nanoelectronics and information technology* (John Wiley & Sons, 2012).

[8] D. Clark, Wall Street Journal Digits Tech News and Analysis (2015).

[9] P. A. Dirac, in *Proceedings of the Royal Society of London A: Mathematical, Physical and Engineering Sciences*, Vol. 117 (The Royal Society, 1928) pp. 610–624.

[10] E. M. Lifshitz and L. P. Pitaevskii, *Statistical Physics, Course of Theoretical Physics*, Vol. 9 (Pergamon, Oxford, 1980).

[11] C. Kittel, *Introduction to solid state physics*, 8th ed. (Wiley, 2005).

[12] L. Néel, in *Annales de Physique*, Vol. 3 (1948) pp. 137–198.

[13] M. N. Baibich, J. M. Broto, A. Fert, F. N. Van Dau, F. Petroff, P. Etienne, G. Creuzet, A. Friederich, and J. Chazelas, Phys. Rev. Lett., **61**, 2472 (1988).

[14] G. Binasch, P. Grünberg, F. Saurenbach, and W. Zinn, Phys. Rev. B, **39**, 4828 (1989).

[15] D. Ralph and M. Stiles, J. Magn. Magn. Mat., **320**, 1190 (2008).

[16] F. Radu and H. Zabel, in *Magnetic Heterostructures*, Springer Tracts in Modern Physics, Vol. 227, edited by H. Zabel and S. D. Bader (Springer Berlin Heidelberg, 2008) pp. 97–184.

[17] A. H. MacDonald and M. Tsoi, Phil. Trans. R. Soc. A, **369**, 3098 (2011).

[18] R. Duine, Nat. Mater., **10**, 344 (2011).

[19] E. V. Gomonay and V. M. Loktev, Low Temperature Physics, **40**, 17 (2014).

[20] S. Wienholdt, D. Hinzke, and U. Nowak, Phys. Rev. Lett., **108**, 247207 (2012).

[21] T. Kampfrath, A. Sell, G. Klatt, A. Pashkin, S. Mahrlein, T. Dekorsy, M. Wolf, M. Fiebig, A. Leitenstorfer, and R. Huber, Nat. Photon., **5**, 31 (2011).

[22] B. A. Ivanov and A. K. Kolezhuk, Phys. Rev. Lett., **74**, 1859 (1995).

[23] N. Papanicolaou, Phys. Rev. B, **51**, 15062 (1995).

[24] A. C. Swaving and R. A. Duine, Phys. Rev. B, **83**, 054428 (2011).

[25] I. V. Bar'yakhtar and B. A. Ivanov, Solid State Communications, **34**, 545 (1980).

[26] F. D. M. Haldane, Phys. Rev. Lett., **50**, 1153 (1983).

[27] K. M. D. Hals, Y. Tserkovnyak, and A. Brataas, Phys. Rev. Lett., **106**, 107206 (2011).

[28] S. K. Kim, Y. Tserkovnyak, and O. Tchernyshyov, Phys. Rev. B, **90**, 104406 (2014).

[29] P. W. Anderson, Phys. Rev., **86**, 694 (1952).

[30] O. Gomonay, Phys. Rev. B, **91**, 144421 (2015).

[31] D. Cabra and P. Pujol, in *Quantum Magnetism*, Lecture Notes in Physics, Vol. 645, edited by U. Schollwöck, J. Richter, D. Farnell, and R. Bishop (Springer Berlin Heidelberg, 2004) pp. 253–305.

[32] I. Affleck, Nuclear Physics B, **257**, 397 (1985).

[33] I. Affleck, Journal of Physics: Condensed Matter, **1**, 3047 (1989).

[34] B. A. Ivanov and A. K. Kolezhuk, Fiz. Niz. Temp, **21**, 355 (1995).

[35] D. I. Paul, Phys. Rev., **126**, 78 (1962).

[36] O. Bezencenet, D. Bonamy, R. Belkhou, P. Ohresser, and A. Barbier, Phys. Rev. Lett., **106**, 107201 (2011).

[37] F. Nolting, A. Scholl, J. Stohr, J. W. Seo, J. Fompeyrine, H. Siegwart, J. P. Locquet, S. Anders, J. Luning, E. E. Fullerton, M. F. Toney, M. R. Scheinfein, and H. A. Padmore, Nature, **405**, 767 (2000).

[38] W. L. Roth, Journal of Applied Physics, **31**, 2000 (1960).

[39] A. Scholl, J. Stöhr, J. Lüning, J. W. Seo, J. Fompeyrine, H. Siegwart, J.-P. Locquet, F. Nolting, S. Anders, E. E. Fullerton, M. R. Scheinfein, and H. A. Padmore, Science, **287**, 1014 (2000).

[40] S. Czekaj, F. Nolting, L. J. Heyderman, P. R. Willmott, and G. van der Laan, Phys. Rev. B, **73**, 020401 (2006).

[41] E. Folven, T. Tybell, A. Scholl, A. Young, S. T. Retterer, Y. Takamura, and J. K. Grepstad, Nano Letters, **10**, 4578 (2010).

[42] N. B. Weber, H. Ohldag, H. Gomonaj, and F. U. Hillebrecht, Phys. Rev. Lett., **91**, 237205 (2003).

[43] M. Bode, E. Y. Vedmedenko, K. von Bergmann, A. Kubetzka, P. Ferriani, S. Heinze, and R. Wiesendanger, Nat. Mater., **5**, 477 (2006).

[44] R. Jaramillo, T. F. Rosenbaum, E. D. Isaacs, O. G. Shpyrko, P. G. Evans, G. Aeppli, and Z. Cai, Phys. Rev. Lett., **98**, 117206 (2007).

[45] B. G. Park, J. Wunderlich, X. Martí, V. Holý, Y. Kurosaki, M. Yamada, H. Yamamoto, A. Nishide, J. Hayakawa, H. Takahashi, A. B. Shick, and T. Jungwirth, Nat. Mater., **10**, 347 (2011).

[46] X. Martí, B. G. Park, J. Wunderlich, H. Reichlová, Y. Kurosaki, M. Yamada, H. Yamamoto, A. Nishide, J. Hayakawa, H. Takahashi, and T. Jungwirth, Phys. Rev. Lett., **108**, 017201 (2012).

[47] D. Herranz, R. Guerrero, R. Villar, F. G. Aliev, A. C. Swaving, R. A. Duine, C. van Haesendonck, and I. Vavra, Phys. Rev. B, **79**, 134423 (2009).

[48] A. B. Shick, S. Khmelevskyi, O. N. Mryasov, J. Wunderlich, and T. Jungwirth, Phys. Rev. B, **81**, 212409 (2010).

[49] N. L. Schryer and L. R. Walker, J. Appl. Phys., **45**, 5406 (1974).

[50] A. Auerbach, *Interacting electrons and quantum magnetism* (Springer Science & Business Media, 2012).

[51] E. Fradkin and M. Stone, Phys. Rev. B, **38**, 7215 (1988).

[52] R. Cheng and Q. Niu, Phys. Rev. B, **89**, 081105 (2014).

[53] O. A. Tretiakov, D. Clarke, G.-W. Chern, Y. B. Bazaliy, and O. Tchernyshyov, Phys. Rev. Lett., **100**, 127204 (2008).

[54] P. Yan, X. S. Wang, and X. R. Wang, Phys. Rev. Lett., **107**, 177207 (2011).

[55] E. M. Lifshitz and L. P. Pitaevskii, *Statistical Physics, Part 2*, 3rd ed., Course of Theoretical Physics, Vol. 9 (Pergamon, Oxford, 1980).

[56] T. Gilbert, Magnetics, IEEE Transactions on, **40**, 3443 (2004).

[57] Y. Kajiwara, K. Harii, S. Takahashi, J. Ohe, K. Uchida, M. Mizuguchi, H. Umezawa, H. Kawai, K. Ando, K. Takanashi, S. Maekawa, and E. Saitoh, Nature, **464**, 262 (2010).

[58] H. V. Gomonay and V. M. Loktev, Phys. Rev. B, **81**, 144427 (2010).

[59] A. Andreev and V. I. Marchenko, Sov. Phys. Usp, **23** (1980).

[60] H.-B. Braun and D. Loss, Phys. Rev. B, **53**, 3237 (1996).

[61] G. Tatara, H. Kohno, and J. Shibata, Phys. Rep., **468**, 213 (2008).

[62] D. J. Clarke, O. A. Tretiakov, G.-W. Chern, Y. B. Bazaliy, and O. Tchernyshyov, Phys. Rev. B, **78**, 134412 (2008).

[63] H. V. Gomonay, R. V. Kunitsyn, and V. M. Loktev, Phys. Rev. B, **85**, 134446 (2012).

[64] V. G. Bar'yakhtar, B. A. Ivanov, and M. V. Chetkin, Sov. Phys. Usp, **28**, 563 (1985).

[65] A. Brataas, Y. Tserkovnyak, and G. E. W. Bauer, Phys. Rev. B, **84**, 054416 (2011).

[66] A. Brataas, A. D. Kent, and H. Ohno, Nat. Mater., **11**, 372 (2012).

[67] J. Linder, Phys. Rev. B, **86**, 054444 (2012).

[68] J. Lekner, American Journal of Physics, **75**, 1151 (2007).

[69] S. K. Kim, O. Tchernyshyov, and Y. Tserkovnyak, Phys. Rev. B, **92**, 020402 (2015).

[70] R. E. Troncoso, C. Ulloa, F. Pesce, and A. S. Nunez, Phys. Rev. B, **92**, 224424 (2015).

[71] J. Barker and O. A. Tretiakov, Phys. Rev. Lett., **116**, 147203 (2016).

[72] G. E. W. Bauer, E. Saitoh, and B. J. van Wees, Nat. Mater., **11**, 391 (2012).

[73] K. Uchida, S. Takahashi, K. Harii, J. Ieda, W. Koshibae, K. Ando, S. Maekawa, and E. Saitoh, Nature, **455**, 778 (2008).

[74] Y. Ohnuma, H. Adachi, E. Saitoh, and S. Maekawa, Phys. Rev. B, **87**, 014423 (2013).

[75] W. F. Brown, Phys. Rev., **130**, 1677 (1963).

[76] Y. Tserkovnyak, A. Brataas, G. E. W. Bauer, and B. I. Halperin, Rev. Mod. Phys., **77**, 1375 (2005).

[77] J. Foros, A. Brataas, Y. Tserkovnyak, and G. E. W. Bauer, Phys. Rev. Lett., **95**, 016601 (2005).

[78] A. Kirilyuk, A. V. Kimel, and T. Rasing, Rev. Mod. Phys., **82**, 2731 (2010).

[79] A. Kirilyuk, A. V. Kimel, and T. Rasing, Reports on Progress in Physics, **76**, 026501 (2013).

[80] A. Melnikov, I. Razdolski, T. O. Wehling, E. T. Papaioannou, V. Roddatis, P. Fumagalli, O. Aktsipetrov, A. I. Lichtenstein, and U. Bovensiepen, Phys. Rev. Lett., **107**, 076601 (2011).

[81] E. Turgut, C. La-o vorakiat, J. M. Shaw, P. Grychtol, H. T. Nembach, D. Rudolf, R. Adam, M. Aeschlimann, C. M. Schneider, T. J. Silva, M. M. Murnane, H. C. Kapteyn, and S. Mathias, Phys. Rev. Lett., **110**, 197201 (2013).

[82] G.-M. Choi, B.-C. Min, K.-J. Lee, and D. G. Cahill, Nat. Commun., **5** (2014).

[83] J. Xiao, G. E. W. Bauer, K.-c. Uchida, E. Saitoh, and S. Maekawa, Phys. Rev. B, **81**, 214418 (2010).

[84] E. Beaurepaire, J.-C. Merle, A. Daunois, and J.-Y. Bigot, Phys. Rev. Lett., **76**, 4250 (1996).

[85] J. P. van der Ziel, P. S. Pershan, and L. D. Malmstrom, Phys. Rev. Lett., **15**, 190 (1965).

[86] G. P. Zhang and W. Hübner, Phys. Rev. Lett., **85**, 3025 (2000).

[87] C. D. Stanciu, F. Hansteen, A. V. Kimel, A. Kirilyuk, A. Tsukamoto, A. Itoh, and T. Rasing, Phys. Rev. Lett., **99**, 047601 (2007).

[88] B. Koopmans, G. Malinowski, F. Dalla Longa, D. Steiauf, M. Fahnle, T. Roth, M. Cinchetti, and M. Aeschlimann, Nat. Mater., **9**, 259 (2010).

[89] A. J. Schellekens and B. Koopmans, Phys. Rev. B, **87**, 020407 (2013).

[90] C. Kittel, Phys. Rev., **73**, 155 (1948).

[91] D. A. Garanin, Phys. Rev. B, **55**, 3050 (1997).

[92] J. H. Mentink, J. Hellsvik, D. V. Afanasiev, B. A. Ivanov, A. Kirilyuk, A. V. Kimel, O. Eriksson, M. I. Katsnelson, and T. Rasing, Phys. Rev. Lett., **108**, 057202 (2012).

[93] A. J. Schellekens and B. Koopmans, Phys. Rev. Lett., **110**, 217204 (2013).

[94] E. C. Stoner, Proceedings of the Royal Society of London. Series A, **165**, 372 (1938).

[95] I. Radu, K. Vahaplar, C. Stamm, T. Kachel, N. Pontius, H. A. Durr, T. A. Ostler, J. Barker, R. F. L. Evans, R. W. Chantrell, A. Tsukamoto, A. Itoh, A. Kirilyuk, T. Rasing, and A. V. Kimel, Nature, **472**, 205 (2011).

[96] C. La-O-Vorakiat, E. Turgut, C. A. Teale, H. C. Kapteyn, M. M. Murnane, S. Mathias, M. Aeschlimann, C. M. Schneider, J. M. Shaw, H. T. Nembach, and T. J. Silva, Phys. Rev. X, **2**, 011005 (2012).

[97] T. Holstein and H. Primakoff, Phys. Rev., **58**, 1098 (1940).

[98] Y. Tserkovnyak, E. M. Hankiewicz, and G. Vignale, Phys. Rev. B, **79**, 094415 (2009).

[99] S. A. Bender, R. A. Duine, and Y. Tserkovnyak, Phys. Rev. Lett., **108**, 246601 (2012).

[100] S. A. Bender, R. A. Duine, A. Brataas, and Y. Tserkovnyak, Phys. Rev. B, **90**, 094409 (2014).

[101] H. Bruus and K. Flensberg, *Many-Body Quantum Theory in Condensed Matter Physics*, 2nd ed. (Oxford University Press, Oxford, 2002).

[102] B. Y. Mueller, A. Baral, S. Vollmar, M. Cinchetti, M. Aeschlimann, H. C. Schneider, and B. Rethfeld, Phys. Rev. Lett., **111**, 167204 (2013).

[103] R. Meservey and P. M. Tedrow, Phys. Rev. Lett., **41**, 805 (1978).

[104] A. Manchon, Q. Li, L. Xu, and S. Zhang, Phys. Rev. B, **85**, 064408 (2012).

[105] J. Barker, U. Atxitia, T. A. Ostler, O. Hovorka, O. Chubykalo-Fesenko, and R. W. Chantrell, Sci. Rep., **3**, 3262 (2013).

[106] A. Brataas, Y. V. Nazarov, and G. E. W. Bauer, Phys. Rev. Lett., **84**, 2481 (2000).

[107] Y. Tserkovnyak, A. Brataas, and G. E. W. Bauer, Phys. Rev. Lett., **88**, 117601 (2002).

[108] S. A. Bender and Y. Tserkovnyak, Phys. Rev. B, **91**, 140402 (2015).

[109] T. A. Ostler, J. Barker, R. F. L. Evans, R. W. Chantrell, U. Atxitia, O. Chubykalo-Fesenko, S. El Moussaoui, L. Le Guyader, E. Mengotti, L. J. Heyderman, F. Nolting, A. Tsukamoto, A. Itoh, D. Afanasiev, B. A. Ivanov, A. M. Kalashnikova, K. Vahaplar, J. Mentink, A. Kirilyuk, T. Rasing, and A. V. Kimel, Nat. Commun., **3** (2012).

Paper I

"Staggered Dynamics in Antiferromagnets by Collective Coordinates"

Erlend G. Tveten, Alireza Qaiumzadeh, Oleg A. Tretiakov, and Arne Brataas.

Physical Review Letters **110**, 127208 (2013).

Staggered Dynamics in Antiferromagnets by Collective Coordinates

Erlend G. Tveten,[1] Alireza Qaiumzadeh,[1] O. A. Tretiakov,[2,3] and Arne Brataas[1]

[1]*Department of Physics, Norwegian University of Science and Technology, NO-7491 Trondheim, Norway*
[2]*Institute for Materials Research, Tohoku University, Sendai 980-8577, Japan*
[3]*Department of Physics and Astronomy, Texas A&M University, College Station, Texas 77843-4242, USA*

(Received 1 October 2012; published 21 March 2013)

Antiferromagnets can be used to store and manipulate spin information, but the coupled dynamics of the staggered field and the magnetization are very complex. We present a theory which is conceptually much simpler and which uses collective coordinates to describe staggered field dynamics in antiferromagnetic textures. The theory includes effects from dissipation, external magnetic fields, as well as reactive and dissipative current-induced torques. We conclude that, at low frequencies and amplitudes, currents induce collective motion by means of dissipative rather than reactive torques. The dynamics of a one-dimensional domain wall, pinned at 90° at its ends, are described as a driven harmonic oscillator with a natural frequency inversely proportional to the length of the texture.

DOI: 10.1103/PhysRevLett.110.127208 PACS numbers: 85.75.−d, 75.50.Ee, 75.78.Fg

New developments have created opportunities for using antiferromagnets (AFMs) as active components in spintronics devices [1]. AFMs are ordered spin systems which lack a macroscopic magnetization in equilibrium because neighboring spins compensate each other. Analogous to ferromagnets, in AFMs domain walls can be engineered [2], the anisotropic tunneling magnetoresistance (AMR) is substantial [3], spin-wave logic gates can be useful [4], and the order parameter can be switched ultrafast by light [5]. Additionally, AFMs have no stray fields, and high-temperature antiferromagnetic semiconductors can be realized [6], enabling control of the carrier concentration governing all transport properties.

In magnetic materials, currents induce torques on the magnetic moments [7]. In ferromagnets, these torques can be used to switch the magnetization, induce steady state precession in magnetic oscillator circuits, or move domain walls. Theoretical [8] and experimental [9] results indicate that current-induced torque effects are present in AFMs as well, and that these effects are of the same order of magnitude as in ferromagnets. However, several aspects are fundamentally different. For instance, the dynamics in AFMs are described by coupled equations of the staggered field and the (out-of-equilibrium) magnetization. Current-induced torques affect these variables differently.

In AFMs, the staggered field may spatially vary and is influenced by external magnetic fields and currents. Traditionally, understanding the complex behavior of the temporal- and spatial-dependent order parameter requires solving a set of coupled equations with many degrees of freedom. In this Letter, we formulate a conceptually simpler theory of how external forces influence the staggered field and magnetization dynamics in AFMs in terms of a few collective coordinates. Our description is based on the phenomenological theory of insulating AFMs [10], extended to account for charge current flow [11], making the theory valid also for metallic and semiconducting AFMs. It includes the effects of dissipation, external magnetic fields, and both reactive (adiabatic) and dissipative (nonadiabatic) current-induced torques in slowly varying inhomogeneous antiferromagnetic textures.

Consider a basic AFM lattice consisting of two magnetic sublattices, with magnetic moments $\mathbf{m}_1(\mathbf{r}, t)$ and $\mathbf{m}_2(\mathbf{r}, t)$, so that the total magnetization is $\mathbf{m}(\mathbf{r}, t) = \mathbf{m}_1(\mathbf{r}, t) + \mathbf{m}_2(\mathbf{r}, t)$, and the antiferromagnetic order parameter is $\mathbf{l}(\mathbf{r}, t) \equiv \mathbf{m}_1(\mathbf{r}, t) - \mathbf{m}_2(\mathbf{r}, t)$. In the absence of magnetic fields and textures, the equilibrium magnetization vanishes and $\mathbf{l}(\mathbf{r}, t)$ is finite and homogeneous. Below, we consider the dynamics of the magnetization vector and the unit Néel vector $\mathbf{n}(\mathbf{r}, t) = \mathbf{l}(\mathbf{r}, t)/l(\mathbf{r}, t)$.

To the lowest order in textures and magnetizations, the AFM free energy reads [10,11]

$$U = \int d\mathbf{r}\left[\frac{a}{2}\mathbf{m}^2 + \frac{A}{2}\sum_{i=x,y,z}(\partial_i \mathbf{n})^2 - \mathbf{H}\cdot\mathbf{m}\right], \quad (1)$$

where a and A are the homogeneous and inhomogeneous exchange constants, respectively. $\mathbf{H}$ represents the external magnetic field. From the free energy [Eq. (1)] and the constraints $|\mathbf{n}| = 1$ and $\mathbf{m}\cdot\mathbf{n} = 0$, which are valid for temperatures well below the Néel temperature, we can construct the effective fields $\mathbf{f}_n = -\delta U/\delta\mathbf{n} = A\mathbf{n}\times(\nabla^2\mathbf{n}\times\mathbf{n}) - \mathbf{m}(\mathbf{H}\cdot\mathbf{n})$ and $\mathbf{f}_m = -\delta U/\delta\mathbf{m} = -a\mathbf{m} + \mathbf{n}\times(\mathbf{H}\times\mathbf{n})$. In all our results, we may generalize the free energy [Eq. (1)] by adding anisotropy terms, e.g., the easy-axis anisotropy $K_z n_z^2/2$.

Hals *et al.* [11] introduced phenomenological reactive (adiabatic) and dissipative (nonadiabatic) current-induced torque terms, as well as dissipation. With these additional terms, the equations of motion are

$$\dot{\mathbf{n}} = (\gamma \mathbf{f}_m - G_1 \dot{\mathbf{m}}) \times \mathbf{n} + \eta\gamma(\mathbf{J}\cdot\nabla)\mathbf{n}, \quad (2)$$

$$\dot{\mathbf{m}} = [\gamma \mathbf{f}_n - G_2 \dot{\mathbf{n}} + \beta\gamma(\mathbf{J}\cdot\nabla)\mathbf{n}] \times \mathbf{n} + T_{nl}, \quad (3)$$

where γ is the gyromagnetic ratio, G_1 and G_2 are phenomenological Gilbert damping parameters, and η (β) parametrize the adiabatic (nonadiabatic) current-induced torque terms. Throughout this Letter, we disregard all nonlinear terms that are contained in T_{nl} [11]. Equations (2) and (3) are the AFM analogs to the Landau-Lifshitz-Gilbert-Slonczewski equation for ferromagnets. By combining these equations, the magnetization can be expressed in terms of the antiferromagnetic order parameter, giving a closed equation for the staggered field vector $\mathbf{n}$ to the linear order in the out-of-equilibrium deviations $\mathbf{m}$, $\partial_t\mathbf{n}$, $\mathbf{J}$, and $\mathbf{H}$:

$$\frac{\ddot{\mathbf{n}}}{\tilde{\gamma}} = -\mathbf{n}\times\dot{\mathbf{H}} + G_1\dot{\mathbf{f}}_n + (\eta + G_1\beta)(\dot{\mathbf{J}}\cdot\nabla)\mathbf{n} + a[\gamma\mathbf{f}_n - G_2\dot{\mathbf{n}} + \gamma\beta(\mathbf{J}\cdot\nabla)\mathbf{n}]. \quad (4)$$

Here $\tilde{\gamma} \equiv \gamma/(1 + G_1G_2)$ is a modified effective gyromagnetic ratio in the presence of dissipation. Equation (4) is the starting point for deriving the collective coordinate equations of motion for AFMs.

In ferromagnets, magnetic textures are often rigid, so that only a few, soft modes dominate the magnetization dynamics, as in the seminal work of Schryer and Walker on domain wall motion [12]. The evolution of these soft modes can be described by a finite set of collective coordinates. This approach greatly simplifies the understanding of complex magnetization dynamics, making it possible to approximately describe the dynamics at low energies by considering only a few soft modes.

The collective coordinate approach has recently been applied to magnetization dynamics in ferromagnets [13]. We now present how the equations of motion for the collective coordinates can be constructed for AFMs. We transform Eq. (4) by requiring the time dependence of the Néel field to be described by a set of collective coordinates $\{b_i(t)\}$: $\mathbf{n}(\mathbf{r}, t) \equiv \mathbf{n}(\mathbf{r}, \{b_i(t)\})$. The time derivative of the staggered field is then $\dot{\mathbf{n}} = \dot{b}_i\partial_{b_i}\mathbf{n}$. Similarly, $\ddot{\mathbf{n}} = \ddot{b}_i\partial_{b_i}\mathbf{n} + \mathcal{O}(\dot{b}_i^2)$, where the second term is disregarded in our linear response analysis since it is quadratic in the driving forces.

The dissipation is described in Eq. (4) via the terms $G_1\dot{\mathbf{f}}_n$ and $aG_2\dot{\mathbf{n}}$. The first term scales as $G_1A/(\lambda^2\tau)$, where λ and τ are characteristic length and time scales of the staggered field texture. The second term scales as aG_2/τ. In analyzing the relative strengths of these dissipative terms, we use the fact that the homogeneous and the inhomogeneous exchange constants are related through $a \sim A/(l^2d^2)$ [14], where d is the lattice constant and we have introduced the antiferromagnetic order parameter $\mathbf{l}$ above. Dissipation in metallic ferromagnets is small since it arises from the spin-orbit interaction in combination with electron scattering [15]. It is likely that similar mechanisms in AFMs are also weak, and that they have comparable effects on the staggered field and the magnetization: $G_1l \approx G_2/l \ll 1$. From this we can conclude that $\tilde{\gamma} \approx \gamma$ and that the second dissipative term $aG_2\dot{\mathbf{n}}$ dominates in realistic systems, where the typical size of the texture λ is such that $\lambda \gg d$. Hence $G_1\dot{\mathbf{f}}_n$ can be safely disregarded in the equation of motion [Eq. (4)].

Our main result is the equations of motion for the soft modes:

$$M^{ij}(\ddot{b}_j + \gamma a G_2 \dot{b}_j) = F^i. \quad (5)$$

This equation is derived by introducing the collective coordinates to Eq. (4), taking the scalar product with $\partial_{b_j}\mathbf{n}$, and integrating over the space. The dynamics are equivalent to the classical motion of a massive particle subject to dissipation-induced friction and external forces. This equation is model independent and can be used to determine the parameters of AFMs, e.g., the Gilbert damping G_2 and the homogeneous exchange constant a, which are usually difficult to identify in experiments.

In Eq. (5), M^{ij} is the effective mass arising from the exchange interaction between the spins. The total force inducing motion of the collective coordinates, $F^i = F^i_X + F^i_J + F^i_H$, is a sum of the exchange force, the current-induced force, and the external field force:

$$M^{ij}(\mathbf{b}) = \frac{1}{a\gamma^2}\int dV \partial_{b_i}\mathbf{n}\cdot\partial_{b_j}\mathbf{n}, \quad (6a)$$

$$F^i_X(\mathbf{b}) = \int dV \partial_{b_i}\mathbf{n}\cdot\mathbf{f}_n, \quad (6b)$$

$$F^i_J(\mathbf{b}) = \int dV\Big[\beta\partial_{b_i}\mathbf{n}\cdot(\mathbf{J}\cdot\nabla)\mathbf{n} + \frac{\eta + G_1\beta}{a\gamma}\partial_{b_i}\mathbf{n}\cdot(\dot{\mathbf{J}}\cdot\nabla)\mathbf{n}\Big], \quad (6c)$$

$$F^i_H(\mathbf{b}) = \frac{1}{a\gamma}\int dV \dot{\mathbf{H}}\cdot(\mathbf{n}\times\partial_{b_i}\mathbf{n}). \quad (6d)$$

More generally, Eq. (6b) can also be expressed as $F^i_X = \partial_{b_i}U$, to include the effective material-specific forces which act on the AFM through the exchange interaction and magnetic anisotropy. Equation (6c) includes the reactive and dissipative current-induced forces, both of which are important for the dynamics of the collective coordinates b_i. Equation (6d) represents the response to an external magnetic field. Note that in the linear response regime, only time varying external magnetic fields affect the dynamics of the collective coordinates in AFMs, in contrast to the situation for ferromagnets [13], making the collective motion in AFMs more resistant to stray fields.

We now apply the general collective coordinate description Eq. (5) to an isotropic one-dimensional antiferromagnetic texture, an orientational domain wall [16], in which the antiferromagnet is pinned in the x and z directions at $z = 0$ and $z = \lambda$, respectively. The staggered field $\mathbf{n}(z, t)$ varies slowly in the z direction (see Fig. 1). The pinning

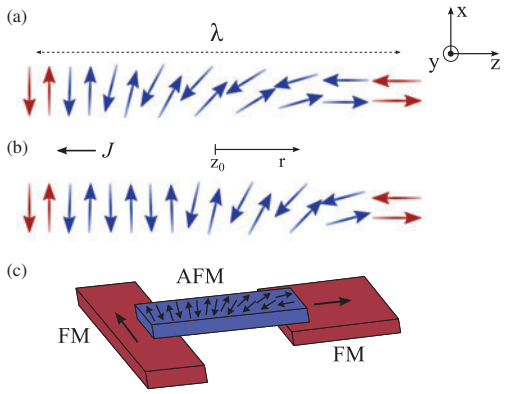

FIG. 1 (color online). A one-dimensional antiferromagnetic texture pinned at a relative angle of 90° in the left and right reservoirs. (a) shows the equilibrium orientation of the staggered field, (b) depicts how a current J exerts a torque on the staggered field vector, forcing the center coordinate z_0 to be displaced by r, and (c) shows schematically a setup of an AFM between two pinning ferromagnets.

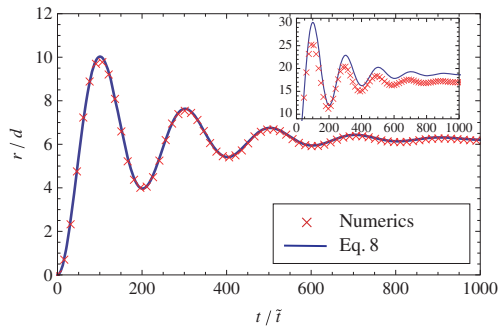

FIG. 2 (color online). Transient response of the deviation r from the equilibrium position $z_0 = \lambda/2$, after a constant current has been applied at time $t = 0$. The antiferromagnetic texture shows damped oscillations around a new perturbed position. The magnitude of the perturbation depends on the system length and the current density. The inset shows the response when the current density is tripled.

can be achieved by placing the antiferromagnet in contact with ferromagnets, as schematically shown in Fig. 1(c). In general, the staggered field can be expressed in terms of two angles θ and ϕ: $\mathbf{n}(z, t) = \{\cos\theta\cos\phi, \cos\theta\sin\phi, \sin\theta\}$. In equilibrium $\theta = \theta_{\mathrm{eq}}$ and $\phi = 0$, with $\theta_{\mathrm{eq}}(z) = \pi z/(2\lambda)$. Without loss of generality, we assume that the out-of-plane angle ϕ remains zero when a current passes through the system, which gives an antiferromagnetic texture varying in the x-z plane only.

In the steady state regime with a constant current along the z direction $\mathbf{J} = J\hat{z}$ the solution of Eq. (4) is $\theta_s(z) = \frac{\pi}{2}(1 - e^{Qz})/(1 - e^{Q\lambda})$, where $Q = \beta J/A$. As a collective coordinate representing the softest mode, we use the deviation of the texture center r from its equilibrium position z_0, which is the point where the x component of the staggered field vector equals the z component, $\theta(r) = \pi/4$. In equilibrium, when there are neither applied currents nor external fields, the center coordinate is $z_0 = \lambda/2$. Motivated by the steady state solution θ_s, expanding for small Q in the low current regime to the linear order in the deviation r from equilibrium, we use Eq. (5) with the ansatz that the staggered field can be fully described by the sine and cosine of a function $\theta(z, r)$:

$$\theta(z, r) = \frac{\pi z}{2\lambda}\left[1 + \frac{4(z - \lambda)r}{\lambda^2}\right]. \tag{7}$$

Using this ansatz and the equation of motion Eq. (5), we find that the deviation from equilibrium r obeys

$$M\ddot{r} + \Gamma\dot{r} + M\omega_0^2 r = F_J + F_H, \tag{8}$$

where $M = \lambda/(a\gamma^2)$ is the effective mass, $\omega_0 = \gamma(10Aa)^{1/2}/\lambda$ is the natural frequency of the system, and $\Gamma = \lambda G_2/\gamma$ is the damping coefficient. There are two contributions to the external forces: one from the current, $F_J = -5\lambda[\beta J + (\eta + \beta G_1)\dot{J}/(a\gamma)]/4$, and the other from time-varying external fields, $F_H = 5\lambda^2\dot{H}_y/(2\pi a\gamma)$. For dc currents, the reactive (adiabatic) force parametrized by η plays no role, and only the dissipative (nonadiabatic) force parametrized by β is important for the texture dynamics. When the driving forces are independent of time, Eq. (8) describes damped harmonic oscillations about a new perturbed position $r_{\mathrm{new}} = -\beta J\lambda^2/(8A)$. This solution is valid as long as $r_{\mathrm{new}} \ll \lambda/2$. Hence, using $\beta^* = \beta Jd/A = -0.005$, the approach works well for systems with lengths up to several hundred lattice constants.

Numerical values for the natural frequency can be estimated for antiferromagnetic metals. For example, in FeMn, the inhomogeneous exchange constant is $A = 0.94 \times 10^{-14}$ J/m [17], the lattice constant is $d_{\mathrm{FeMn}} = 3.6$ Å [18], and the magnetic moment per sublattice is $1.65\mu_B$, with μ_B being the Bohr magneton, giving a natural frequency of approximately 1 GHz for a FeMn texture with a length of 100 lattice constants.

In Fig. 2, the solution of the time-dependent equation of motion Eq. (8) for r has been compared to numerical results of a micromagnetic simulation of the coupled equations Eqs. (2) and (3), with the boundary conditions described in Fig. 1. The equations were first written in dimensionless form by scaling the z axis with the lattice constant d, and the time axis with $\tilde{t} = (\gamma al)^{-1}$. Other dimensionless quantities, as well as the numerical values used in the simulation presented in Fig. 2, are summarized in Table I.

Figure 2 shows that the complex spatiotemporal dynamics of the antiferromagnetic texture can be described by the motion of the single soft mode r. Fitting the simple equation of motion Eq. (8) to experimental data, e.g., from

TABLE I. Dimensionless numerical constants.

Constant	Composition	Value
a^*	al^2d^2/A	1
α_1	$G_1 l$	0.01
α_2	G_2/l	0.01
β^*	$\beta J d/A$	-0.005
η^*	$\eta J d/(Al)$	-0.005
λ^*	λ/d	100

AMR measurements, can provide good estimates of the phenomenological parameters in AFMs. The generality of Eq. (5) also makes the collective coordinate approach a powerful tool for investigating the dynamics of more complex antiferromagnetic textures with more than a single soft mode.

The staggered dynamics represented by the center coordinate r can be measured via the AMR effect. The magnitude of the AMR in bulk AFMs is not known, but since the tunneling AMR [3] is significant, we believe its bulk value will be too. A plausible assumption is that the simplest possible phenomenological model of AFM AMR is similar to the AMR in ferromagnets, but with the AMR depending on the orientation of the staggered field rather than the magnetization: $\rho(\mathbf{n}) = \rho_0 + \rho_{\mathrm{ani}}(\mathbf{n}\cdot\hat{z})^2$, where ρ_0 is the isotropic resistivity and ρ_{ani} is the anisotropic resistivity. Integrating the resistivity over the system, using the ansatz in Eq. (7), and expanding to linear order in r, gives the effect of the antiferromagnetic texture on the resistance as $R(t) = R_0 + \rho_{\mathrm{ani}}[\lambda/2 - 8r(t)/\pi^2]$. Therefore, it should be possible to observe the effects of both dc and ac currents. For dc currents, the total resistance $R(t)$ will be enhanced or reduced depending on the current direction. For ac currents, by sweeping the frequency, one should observe enhanced deviations of the resistance when the frequency equals the natural frequency of the texture. This setup offers the possibility of measuring the effect of the current-induced torque on the staggered field, a phenomenon which is, in general, difficult to observe experimentally.

We can also apply our collective coordinate approach to an AFM domain wall described by the Walker ansatz: $\tan(\theta_w) = e^{(z-r_w)/\lambda_w}$. Here we introduce the easy axis anisotropy K_z, defining the domain wall width as $\lambda_w = \sqrt{A/K_z}$. To the best of our knowledge, the experimental values of K_z for antiferromagnetic materials are still not available. However, anisotropy energies in AFMs can be comparable to, or even stronger than, those in ferromagnets since they often involve heavy elements with a strong spin-orbit interaction [19]. We also reintroduce the out-of-plane tilt angle ϕ_w, and use the center of the domain wall r_w, ϕ_w, and the domain wall width λ_w as the three collective coordinates. In agreement with the simplified treatment in Refs. [11,20], by applying a constant current, the domain wall motion gradually relaxes to a steady state, where the wall moves with the constant velocity $\dot{r}_w \approx -\gamma\beta J/G_2$. Our approach shows that the out-of-plane tilt angle is a hard mode, which can only be excited by a time varying external magnetic field. This is very different from the motion of domain walls in ferromagnets, where a moving domain wall also has a finite tilt angle [21]. Additionally, in the linear response regime, there is no distortion of the domain wall width for AFMs.

In conclusion, we have derived equations of motion for the collective coordinates corresponding to soft modes of antiferromagnetic textures to the linear order in currents, magnetization, and external magnetic field. In contrast to ferromagnets, the dynamics are second order in time derivatives, e.g., the effective particles described by the soft coordinates acquire a mass, and have no first-order contribution from time-independent external magnetic fields. We have applied our theory to a one-dimensional model of a slowly varying antiferromagnetic texture pinned at 90° at the edges, and have found the natural frequency and deviations of the center coordinate in terms of the system parameters. The results show that the dissipative (nonadiabatic) current-induced torque is crucial for the dynamics of the antiferromagnetic textures.

This work was supported by EU-ICT-7 Contract No. 257159 "MACALO". O. A. T. also acknowledges support from the NSF under Grants No. DMR-0757992 and No. ONR-N000141110780.

[1] A. H. MacDonald and M. Tsoi, Phil. Trans. R. Soc. A **369**, 3098 (2011).

[2] J. M. Logan, H. C. Kim, D. Rosenmann, Z. Cai, R. Divan, O. G. Shpyrko, and E. D. Isaacs, Appl. Phys. Lett. **100**, 192405 (2012).

[3] B. G. Park, J. Wunderlich, X. Martí, V. Holý, Y. Kurosaki, M. Yamada, H. Yamamoto, A. Nishide, J. Hayakawa, H. Takahashi, A. B. Shick, and T. Jungwirth, Nat. Mater. **10**, 347 (2011); D. Herranz, R. Guerrero, R. Villar, F. G. Aliev, A. C. Swaving, R. A. Duine, C. van Haesendonck, and I. Vavra, Phys. Rev. B **79**, 134423 (2009); A. B. Shick, S. Khmelevskyi, O. N. Mryasov, J. Wunderlich, and T. Jungwirth, Phys. Rev. B **81**, 212409 (2010).

[4] P. Rovillain, R. de Sousa, Y. Gallais, A. Sacuto, M. A. Méasson, D. Colson, A. Forget, M. Bibes, A. Barthélémy, and M. Cazayous, Nat. Mater. **9**, 975 (2010).

[5] A. V. Kimel, B. A. Ivanov, R. V. Pisarev, P. A. Usachev, A. Kirilyuk, and T. Rasing, Nat. Phys. **5**, 727 (2009).

[6] T. Jungwirth, V. Novák, X. Martí, M. Cukr, F. Máca, A. B. Shick, J. Mašek, P. Horodyská, P. Němec, V. Holý, J. Zemek, P. Kužel, I. Němec, B. L. Gallagher, R. P. Campion, C. T. Foxon, and J. Wunderlich, Phys. Rev. B **83**, 035321 (2011).

[7] A. Brataas, A. D. Kent, and H. Ohno, Nat. Mater. **11**, 372 (2012).

[8] A. S. Núñez, R. A. Duine, P. Haney, and A. H. MacDonald, Phys. Rev. B **73**, 214426 (2006); R. A. Duine, P. M. Haney, A. S. Núñez, and A. H. MacDonald, Phys. Rev. B **75**,

014433 (2007); P. M. Haney, D. Waldron, R. A. Duine, A. S. Núñez, H. Guo, and A. H. MacDonald, Phys. Rev. B **75**, 174428 (2007); H. Gomonay and V. Loktev, J. Magn. Soc. Jpn. **32**, 535 (2008); P. M. Haney and A. H. MacDonald, Phys. Rev. Lett. **100**, 196801 (2008); H. V. Gomonay and V. M. Loktev, Phys. Rev. B **81**, 144427 (2010); H. V. Gomonay, R. V. Kunitsyn, and V. M. Loktev, Phys. Rev. B **85**, 134446 (2012).

[9] Z. Wei, A. Sharma, A. S. Nunez, P. M. Haney, R. A. Duine, J. Bass, A. H. MacDonald, and M. Tsoi, Phys. Rev. Lett. **98**, 116603 (2007); R. Jaramillo, T. F. Rosenbaum, E. D. Isaacs, O. G. Shpyrko, P. G. Evans, G. Aeppli, and Z. Cai, Phys. Rev. Lett. **98**, 117206 (2007); S. Urazhdin and N. Anthony, Phys. Rev. Lett. **99**, 046602 (2007).

[10] E. M. Lifshitz and L. P. Pitaevskii, *Statistical Physics*, Course of Theoretical Physics (Pergamon, Oxford, 1980), Vol. 9.

[11] K. M. D. Hals, Y. Tserkovnyak, and A. Brataas, Phys. Rev. Lett. **106**, 107206 (2011).

[12] N. L. Schryer and L. R. Walker, J. Appl. Phys. **45**, 5406 (1974).

[13] O. A. Tretiakov, D. Clarke, G.-W. Chern, Y. B. Bazaliy, and O. Tchernyshyov, Phys. Rev. Lett. **100**, 127204 (2008); D. J. Clarke, O. A. Tretiakov, G.-W. Chern, Y. B. Bazaliy, and O. Tchernyshyov, Phys. Rev. B **78**, 134412 (2008).

[14] V. G. Bar'yakhtar, B. A. Ivanov, and M. V. Chetkin, Sov. Phys. Usp. **28**, 563 (1985).

[15] A. Brataas, Y. Tserkovnyak, and G. E. W. Bauer, Phys. Rev. B **84**, 054416 (2011).

[16] M. Bode, E. Y. Vedmedenko, K. von Bergmann, A. Kubetzka, P. Ferriani, S. Heinze, and R. Wiesendanger, Nat. Mater. **5**, 477 (2006); P. A. A. van der Heijden, C. H. W. Swüste, W. J. M. de Jonge, J. M. Gaines, J. T. W. M. van Eemeren, and K. M. Schep, Phys. Rev. Lett. **82**, 1020 (1999); F. Y. Yang and C. L. Chien, Phys. Rev. Lett. **85**, 2597 (2000).

[17] Y. Xu, S. Wang, and K. Xia, Phys. Rev. Lett. **100**, 226602 (2008).

[18] D. Spišák and J. Hafner, Phys. Rev. B **61**, 11 569 (2000).

[19] R. Y. Umetsu, A. Sakuma, and K. Fukamichi, Appl. Phys. Lett. **89**, 052504 (2006).

[20] A. C. Swaving and R. A. Duine, J. Phys. Condens. Matter **24**, 024223 (2012).

[21] G. Tatara, H. Kohno, and J. Shibata, Phys. Rep. **468**, 213 (2008).

Paper II

"Antiferromagnetic Domain Wall Motion Induced by Spin Waves"
Erlend G. Tveten, Alireza Qaiumzadeh, and Arne Brataas,
Physical Review Letters **112**, 147204 (2014).

Antiferromagnetic Domain Wall Motion Induced by Spin Waves

Erlend G. Tveten, Alireza Qaiumzadeh, and Arne Brataas
Department of Physics, Norwegian University of Science and Technology, NO-7491 Trondheim, Norway
(Received 18 November 2013; published 10 April 2014)

Spin waves in antiferromagnets are linearly or circularly polarized. Depending on the polarization, traversing spin waves alter the staggered field in a qualitatively different way. We calculate the drift velocity of a moving domain wall as a result of spin wave-mediated forces and show that the domain wall moves in opposite directions for linearly and circularly polarized waves. The analytical results agree with micromagnetic simulations of an antiferromagnetic domain wall driven by a localized, alternating magnetic field.

DOI: 10.1103/PhysRevLett.112.147204 PACS numbers: 75.50.Ee, 75.78.Fg, 85.75.-d

Antiferromagnets (AFMs) are promising candidates for future spintronic devices for the following reasons: (1) They can be integrated with ferromagnetic components, 2)) switching occurs at very high frequencies, and (3) there are no stray fields, allowing small independent devices to be created [1,2]. The dynamics of AFMs are fundamentally different from those of ferromagnets (FMs) because the equations of motion are second order in frequency rather than first order [3,4]. Furthermore, AFMs are affected by both charge and spin currents, as was recently shown theoretically [5] and experimentally [6]. The antiferromagnetic order can be probed, e.g., via the anisotropic tunneling magnetoresistance effect [7]. Additionally, a change in the spin texture of the AFM affects both the longitudinal and Hall resistivities [8].

In AFMs, domains usually result from crystal imperfections [9], but they may also inherit the domain structure of the ferrimagnetic precursor layer as they undergo a phase transition to the antiferromagnetic phase [10]. Antiferromagnetic domains [11] and several forms of domain wall (DW) structures in AFMs have been observed [12]. Furthermore, DWs in AFMs can also be induced, controlled, and engineered by exchange bias pinning forces [3,13].

Progress in the field of antiferromagnetic spintronics requires the development of novel methods for exciting AFMs at the nanoscale. Many AFMs are insulating and cannot be affected by currents in the bulk; however, other approaches can be employed to excite an AFM. We suggest the use of antiferromagnetic spin waves (SWs) as a new and exciting way of manipulating the order of AFMs. The advantage to this method is that SWs in AFMs operate coherently in the THz regime [14], which is orders of magnitude faster than the frequency of typical ferromagnetic SWs.

In this Letter, we demonstrate that SWs move DWs in AFMs. We show that this phenomenon is considerably richer than the analogous SW-DW interaction in FMs due to the inherent complexity of antiferromagnetic SWs [15]. In contrast to SW-driven DW motion in FMs, we find that the direction of DW motion in AFMs is governed by the nature of the SW excitation modes. This behavior enables superior control of DW motion induced by SWs in AFMs compared to the same phenomena in FMs.

Spin-polarized currents can induce magnetization dynamics in magnetic materials [16]. However, DWs in FMs can also be moved by the transfer of spin angular momentum from traveling SWs, eliminating the additional dissipation cost associated with the electric current. Several theoretical [17], experimental [18], and numerical [19] studies have demonstrated that DW motion from magnonic spin transfer is possible. The reciprocal phenomenon has also been reported: DW motion in FMs induces local excitations of SWs [20].

In AFMs, circularly polarized SWs carry spin angular momentum whereas linearly polarized SWs do not. In a scenario in which a circularly polarized SW passes through an antiferromagnetic DW, the spin angular momentum flow associated with its motion is reversed. However, because the total spin angular momentum is conserved and antiferromagnetic DWs cannot absorb the constant transferred flux of spin angular momentum, we show that this scenario does not arise. Instead, circularly polarized SWs are reflected so that linear momentum is passed to the DWs. Here, we demonstrate that linearly polarized SWs, carrying no spin angular momentum, can pass through DWs without any reflection, as shown schematically in Fig. 1. As a result of this radical difference in the behavior of circularly and linearly polarized SWs, DWs move in opposite directions in response to the different modes of SW excitations.

The magnetizations on adjacent sublattices in an AFM are equal in magnitude but are oppositely directed. We consider a two-spin lattice, where the antiferromagnetic order parameter is defined as $\mathbf{l}(\mathbf{r},t) = \mathbf{m}_1 - \mathbf{m}_2$, and we introduce the normalized *staggered* vector field $\mathbf{n}(\mathbf{r},t) = \mathbf{l}(\mathbf{r},t)/l$, where $l = |\mathbf{l}(\mathbf{r},t)|$. The total magnetization field $\mathbf{m}(\mathbf{r},t) = \mathbf{m}_1 + \mathbf{m}_2$ is zero at equilibrium for AFMs. We also make use of the constraint $\mathbf{n}\cdot\mathbf{m} = 0$, which is valid in the exchange approximation.

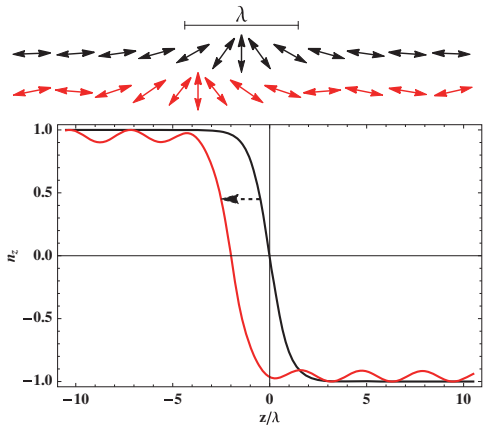

FIG. 1 (color online). Sketch of an antiferromagnetic DW displaced to the left as a result of linearly polarized SW excitations, where the SWs travel through the DW without reflection.

The equations of motion for the staggered field and the magnetization are as follows [4]:

$$\dot{\mathbf{n}} = (\gamma \mathbf{f}_m - G_1 \dot{\mathbf{m}}) \times \mathbf{n}, \tag{1}$$

$$\dot{\mathbf{m}} = (\gamma \mathbf{f}_n - G_2 \dot{\mathbf{n}}) \times \mathbf{n} + (\gamma \mathbf{f}_m - G_1 \dot{\mathbf{m}}) \times \mathbf{m}, \tag{2}$$

where γ is the gyromagnetic ratio and G_1 and G_2 are phenomenological Gilbert damping constants. The effective fields $\mathbf{f}_m = -\delta_{\mathbf{m}} U$ and $\mathbf{f}_n = -\delta_{\mathbf{n}} U$ are functional derivatives of the free energy U of the AFM with respect to the magnetization and the staggered order, respectively.

We consider a one-dimensional texture, e.g., an insulating antiferromagnetic nanowire. In this case, the free energy is $U = \int d\mathbf{r}[a\mathbf{m}^2/2 + A(\nabla \mathbf{n})^2/2 - K_z n_z^2/2]$, where a and A are the homogeneous and inhomogeneous exchange constants, respectively; a and A are related through $a \sim A/(l^2 d^2)$ [21], where d is the lattice constant of the AFM. K_z denotes the easy axis anisotropy along the wire, which is defined as the z axis. We consider a DW created by pinning the AFM to adjacent FMs in different directions in the left and right reservoirs. The equilibrium shape of the DW is now determined by the competition between the exchange energy A and the anisotropy energy K_z.

To study the interaction between SWs and a DW, we perform a unitary transformation of the present coordinate system into the coordinate system of the DW, making use of the spherical unit vectors $\hat{r} = [\sin\theta\cos\phi, \sin\theta\sin\phi, \cos\theta]$, $\hat{\theta} = [\cos\theta\cos\phi, \cos\theta\sin\phi, -\sin\theta]$, and $\hat{\phi} = [-\sin\phi, \cos\phi, 0]$. For a Walker DW [22], the equilibrium solution of Eqs. (1) and (2) is given by $m = 0$ and $\theta_0 = 2\arctan \times \exp(\xi)$. ξ depends on time through the DW center position, $r_w(t)$; $\xi = (z - r_w)/\lambda$, where the DW width is defined as $\lambda = \sqrt{A/K_z}$. We also treat the out-of-plane angle $\phi_w(t)$ as a dynamic variable in the same manner as $r_w(t)$.

SWs in AFMs are linear deviations of the staggered order $\mathbf{n}(\xi, t)$ and the magnetization $\mathbf{m}(\xi, t)$ around their equilibrium textures. The SW-DW interaction requires that we expand $\mathbf{n}(\xi, t)$ and $\mathbf{m}(\xi, t)$ to second order for small excitations h around the equilibrium DW texture $\hat{r}$,

$$\mathbf{n}(\xi, t) = \left[1 - \frac{h^2}{2}(n_\theta^2(\xi, t) + n_\phi^2(\xi, t))\right]\hat{r} + h[n_\theta(\xi, t)\hat{\theta} + n_\phi(\xi, t)\hat{\phi}], \tag{3}$$

$$\mathbf{m}(\xi, t) = h^2 m_r^{(2)}\hat{r} + [h m_\theta(\xi, t) + h^2 m_\theta^{(2)}(\xi, t)]\hat{\theta} + [h m_\phi(\xi, t) + h^2 m_\phi^{(2)}(\xi, t)]\hat{\phi}, \tag{4}$$

where the notations $n_{\theta(\phi)}$ and $m_{\theta(\phi)}$ describe first-order excitations in the $\hat{\theta}(\hat{\phi})$ direction of the staggered field and the magnetization, respectively. We also include the second-order excitations in the magnetization $m_{\theta(\phi)}^{(2)}$ and $m_r^{(2)} = -(m_\theta n_\theta + m_\phi n_\phi)$.

Using the *Ansätze* Eqs. (3) and (4) in Eqs. (1) and (2) and expanding the staggered field to the first order in h, we arrive at the equation of motion for SW excitations

$$\ddot{n}_{\theta(\phi)} = aK_z\gamma^2[\partial_\xi^2 n_{\theta(\phi)} + (2\,\mathrm{sech}^2(\xi) - 1)n_{\theta(\phi)}] - a\gamma G_2 \dot{n}_{\theta(\phi)}. \tag{5}$$

For simplicity, we have assumed that G_2 dominates G_1, simplifying the description of the SW dynamics. This assumption has been made only in the analytical treatment and is not included in the numerical results presented below. We conclude that excitations in the directions $\hat{\theta}$ and $\hat{\phi}$ are decoupled in AFMs, which is fundamentally different from the behavior of SWs in FMs [17]. This result implies that both linearly and circularly polarized antiferromagnetic SWs exist.

Using $n_{\theta(\phi)}(\xi, t) = n_{\theta(\phi)}(\xi)\exp(-i\omega t)$, Eq. (5) reads

$$\hat{H} n_{\theta(\phi)}(\xi) = q^2 n_{\theta(\phi)}(\xi), \tag{6}$$

where the operator $\hat{H} = [-\partial_\xi^2 - 2\,\mathrm{sech}^2(\xi)]$. The eigenvalues $q^2 = [\omega^2/(\gamma^2 a K_z) - 1 + i\omega G_2/(\gamma K_z)]$ define the dispersion relation of the antiferromagnetic SWs. Equation (6) is a time-independent Schrödinger-type equation with the Pöschl-Teller potential. This potential is reflectionless and offers exact solutions in the form of traveling wave eigenfunctions [23].

When q is purely imaginary, the solutions to Eq. (6), $n_{\theta_0(\phi_0)} = \rho_0\,\mathrm{sech}(\xi)$, where ρ_0 is an arbitrary amplitude, describe localized states, centered around the DW. These "Goldstone modes" [24] are distortions of the DW caused by the system being forced out of equilibrium and are naturally included in the formalism by considering the DW

center $r_w(t)$ and chirality $\phi_w(t)$ to be collective dynamic variables of the system.

For complex q, the solutions to Eq. (6) represent propagating wave excitations superimposed on the staggered field texture. These solutions can be written as $n_{\theta(\phi)}(\xi,t) = \rho_k e^{i\Omega}(\tanh(\xi) - iq)$, where ρ_k is the wave-vector-dependent SW amplitude. $\Omega = q\xi - \omega t$ so that $\mathrm{Re}\{\Omega\}$ is the general phase of the wavelike excitations. Similar bound and travelling SW modes are also present in antiferromagnetic Bloch DWs [9].

We use the *Ansatz* that the accelerations of the DW center coordinate $\ddot{r}_w(t)$ and chirality $\ddot{\phi}_w(t)$ are proportional to the square of the amplitude of the SWs and, thus, are second-order effects for the small excitation parameter h.

In the following, we assume that the antiferromagnetic SWs are linearly polarized transverse to the plane of the DW, along $\hat{\phi}$ [$n_\theta = 0$ with $\phi(0) = 0$]. Circularly polarized SWs demand a different treatment and are discussed later. After combining Eqs. (1) and (2), inserting the effective fields $\mathbf{f}_n = K_z n_z \hat{z} + A\partial_z^2 \mathbf{n}$ and $f_m = -am$, expanding to order h^2, and integrating over space, we find that $\ddot{\phi}_w + a\gamma G_2 \ddot{\phi}_w = 0$, and the equation of motion for the DW coordinate r_w is

$$\ddot{r}_w + a\gamma G_2 \dot{r}_w = \frac{a\gamma^2 K_z}{\pi} \int_{-\infty}^{\infty} d\xi \langle n_\phi^2 \rangle \mathrm{sech}(\xi)\tanh(\xi), \quad (7)$$

where $\langle n_\phi^2 \rangle$ denotes a temporal average. By carrying out this average, we disregard temporal oscillations of the coordinate r_w as the DW moves.

Equation (7) (without dissipation) is a result of the conservation of linear momentum density. As an explanation, let us consider the Lagrangian density of the AFM $\mathcal{L} = \dot{\mathbf{n}}^2/(2a\gamma^2) - A(\nabla \mathbf{n})^2/2 + K_z n_z^2/2$ [25]. Noether's theorem implies a continuity equation for the linear momentum density along z, $dT_{zt}/dt + dT_{zz}/dz = 0$, where $T_{zj}(j = z, t) = (\partial_z q \partial_{\partial_j q} - \delta_{zj})\mathcal{L}$ is defined as in Ref. [26] and $q = \theta, \phi, n_\phi$. After integration and time averaging, we find that the continuity equation is identical to Eq. (7) (without dissipation).

The real part of the SW solutions for a small dissipation G_2 is

$$\mathrm{Re}\{n_\phi\} \approx \frac{\rho_k}{(1+k^2\lambda^2)^{1/2}} e^{-Q(\xi+|\xi_0|)/2} \times [\cos(k\lambda\xi - \omega t)\tanh(\xi) + k\lambda \sin(k\lambda\xi - \omega t)], \quad (8)$$

where $Q = G_2\omega/(\gamma K_z k\lambda)$, $\xi_0 = (r_w - z_0)/\lambda$, z_0 is the position of the excitation source, and $k = [\omega^2/(a\gamma^2 K_z) - 1]^{1/2}/\lambda$ is the real wave vector of the monochromatic SWs at the driving frequency ω. The SW amplitude depends on the form of the excitation source $H_{\mathrm{ext}}(z,t)$ through its spatial Fourier transform: $\rho_k = \omega \mathcal{F}_k\{H_{\mathrm{ext}}(z,t)\}/(a\gamma A k)$.

TABLE I. Dimensionless numerical constants.

Constant	Composition	Value
$\tilde{a}$	al^2d^2/A	1
$\tilde{G}_1$	$G_1 l$	0.002
$\tilde{G}_2$	G_2/l	0.002
$\tilde{K}_z$	$K_z d^2/A$	5^{-2}
$\tilde{h}$	$h/(al)$	0.05
$\tilde{z}_0$	z_0/d	−70

Inserting Eq. (8) into Eq. (7) and solving for the steady-state ($\ddot{r}_w \to 0$) velocity, we obtain

$$\dot{r}_w = -\rho_k^2 e^{-Q|\xi_0|} \frac{(1+3k^2\lambda^2)\omega}{6k}. \quad (9)$$

Equation (9), which is our first central result, shows that the steady-state DW drift velocity induced by linearly polarized SWs is independent of the dissipation G_2 for high frequencies ω. In the long-wavelength limit, when $k\lambda \to 0$, the DW velocity becomes large when the driving frequency is close to resonance, $\omega \to \omega_0 = (a\gamma^2 K_z)^{1/2}$. Naturally, the expansion in terms of a low dissipation G_2 breaks down close to this limit.

To verify Eq. (9), we conduct a micromagnetic simulation of Eqs. (1) and 2 for a one-dimensional antiferromagnetic nanowire with a Néel DW in the x-z plane as the initial condition. We add the external magnetic field source term $\mathbf{H}_{\mathrm{ext}}(z,t)$ to the free energy, $U \to U - \int d\mathbf{r}\mathbf{H}_{\mathrm{ext}} \cdot \mathbf{m}$. We then write Eqs. (1) and (2) in dimensionless form by scaling the time axis by $\tilde{t} = (\gamma a l)^{-1}$ and the z axis by the lattice constant d. The simulation is based on the numerical method of lines with a time step control that is adaptive. The length of the wire is set to 1000 lattice constants, and the DW is initally positioned at $z = 0$. We impose absorbing boundary conditions at $z \le -400$ and $z \ge 400$. The SWs are excited in the region $z = [-72, -68]$ by a homogeneous and dimensionless magnetic field source $h_{\mathrm{ext}}(t) = \tilde{h}\sin(\tilde{\omega}t)\hat{x}$, where $\tilde{\omega} = \omega/\omega_0$. DW widths in AFMs are expected to be small [12], and therefore, we choose $\lambda = 5d$. Other dimensionless constants are listed in Table I.

Figure 2 shows the simulated DW velocity as a function of excitation frequency. The velocity is given in units of $v_0 = \gamma A/(ld)$. For frequencies close to ω_0 the long-wavelength resonance peak is easily discernible. The velocity drops to zero for $\tilde{\omega} \approx 4$, which is a result of the step shape of the excitation source.

Although we consider an antiferromagnetic nanowire with easy axis anisotropy, we estimate the magnitude of the DW velocity using parameters for the antiferromagnetic insulator NiO, which has easy plane anisotropy in the bulk. We use $A_{\mathrm{NiO}} \approx 5 \times 10^{-13}$ J/m, $d_{\mathrm{NiO}} \approx 4.2$ Å, and a magnetic moment per sublattice of $1.7\mu_B$ [27], with μ_B being the Bohr magneton. With these parameters $v_0 \approx 500$ m/s,

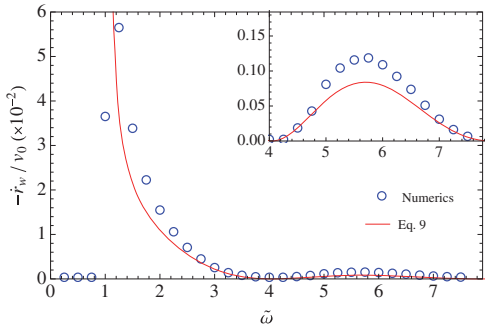

FIG. 2 (color online). Negative DW velocity $-\dot{r}_w$ in units of $v_0 = \gamma A/(ld)$, as a function of the applied excitation field frequency $\tilde{\omega}$, for linearly polarized SWs. The DW is attracted towards the SW source. Blue circles represent the results of numerical simulations, and the red line indicates the analytical result based on Eq. (9).

and the resonance frequency $\omega_0 \approx 200$ GHz. The DW drift velocity induced by long-wavelength linearly polarized SWs in NiO is then approximately 5–10 m/s directed toward the SW source.

Next, we discuss the very different interactions that arise between circularly polarized SWs and DWs. Numerically, when we excite circularly polarized antiferromagnetic SWs, $h_{\text{ext}}(t) = \tilde{h}[\sin(\tilde{\omega}t)\hat{x} + \cos(\tilde{\omega}t)\hat{y}]$, we observe that the SWs are reflected from the DW structure (SW behavior not shown). The DW now moves in the same direction as the incoming SWs. This DW behavior is opposite to that observed for linearly polarized SWs. Additionally, circularly polarized SWs also cause the DW to acquire a net angular velocity $\dot{\phi}_w$.

To elucidate this phenomenon, consider Eq. (2) with the effective fields inserted but without dissipation,

$$\dot{\mathbf{m}} = -\gamma \mathbf{n} \times K_z n_z \hat{z} - \nabla \mathbf{J}_m, \tag{10}$$

where $\mathbf{J}_m = \gamma A \mathbf{n} \times \nabla \mathbf{n}$ is defined as the *spin wave spin current* [28] through the AFM. The z component of Eq. (10) has the form of a conservation law for spin angular momentum $\partial_t m_z + \partial_z J_{m_z} = 0$, where $J_{m_z}(\xi) = \gamma A(n_\theta \partial_\xi n_\phi - n_\phi \partial_\xi n_\theta)\tanh(\xi)/\lambda$. The spin wave spin current vanishes for linearly polarized SWs, whereas circularly polarized SWs carry $J_{m_z} = \pm \gamma A k \rho_k^2$, where the sign depends on the SW helicity. After integration over space, we find

$$\partial_t M_z = -[J_{m_z}(\infty) - J_{m_z}(-\infty)], \tag{11}$$

where M_z is the total magnetization in the z direction.

There are two possibilities for circularly polarized SWs. In the first scenario, the SWs are transmitted through the DW, causing the spin current to change its sign after transmission. In this case, the right-hand side of Eq. (11) is finite, which leads to the buildup of a local magnetic moment around the DW. In the second scenario, the SWs are reflected, and the right-hand side of Eq. (11) vanishes. Only the second scenario is possible in the steady state because the strong exchange interaction in the AFM counteracts the buildup of an increasing local magnetic moment.

Having established that circularly polarized SWs are reflected, we calculate the DW velocity by means of linear momentum transfer from reflected SW packets to the DW. From the Lagrangian density, we calculate the linear momentum density in the z direction $T_{zt} = \partial_z q \partial_{\dot{q}} \mathcal{L}$ [26], with $q = \theta, \phi, n_\theta, n_\phi$. After integrating over space, we find that the total linear momentum in the z direction $P_z = \int dz T_{zt}$ can be split into a DW part and a SW part: $P_z^{\text{DW}} = 2\dot{r}/(a\gamma^2\lambda)$ and $P_z^{\text{SW}} = \int dz (n_\theta^2 + n_\phi^2) k\omega/(a\gamma^2)$. When considering SW packets, the continuity equation for linear momentum density in the z direction becomes a conservation law for the total linear momentum P_z, according to Noether's theorem, and we find $0 = dP_z/dt = d/dt(P_z^{\text{DW}} + P_z^{\text{SW}})$. A train of reflected SW packets exerts a force $\Delta P_z^{\text{SW}}/\Delta t = \rho_k^2 k\omega(v_g - \dot{r}_w)/(a\gamma^2)$, where $v_g = a\gamma^2 Ak/\omega$ is the SW group velocity. Balancing this force to the force on the DW, $dP_z^{\text{DW}}/dt = 2(\ddot{r}_w + a\gamma^2 G_2 \dot{r}_w)/(a\gamma^2\lambda)$, gives the resulting DW velocity in steady state as

$$\dot{r}_w = \frac{v_g}{1 + \frac{a\gamma G_2}{\rho_k^2 \lambda k\omega}}, \tag{12}$$

which is our second and final central result. For low damping, the DW is accelerated to the SW group velocity v_g, which is several hundred meters per second for typical AFMs. Therefore, the DW motion induced by circularly polarized SWs is oppositely directed and much faster than the motion caused by linearly polarized SWs. Numerically,

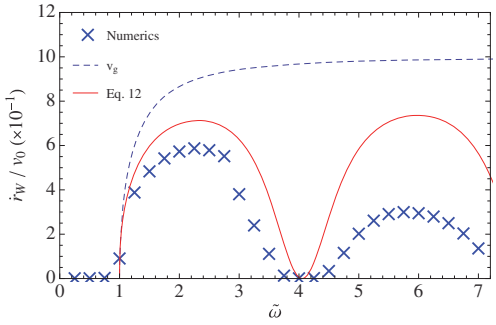

FIG. 3 (color online). DW velocity $\dot{r}_w$ as a function of the applied field frequency $\tilde{\omega}$ for circularly polarized SWs. The DW is pushed away from the SW source due to reflection. Blue crosses represent the results from numerical simulations, the red line indicates the analytical result based on Eq. (12), and the dashed blue line shows the group velocity v_g of the SWs.

we see in Fig. 3 that Eq. (12) captures the DW motion well, especially at low applied frequencies. We speculate that the assumption of total SW reflection will break down for higher frequencies.

In conclusion, we have investigated the manner in which antiferromagnetic SWs move DWs in AFMs. Linearly polarized SWs drive DWs towards the SW source, analogous to the effect of magnon spin transfer torque in FMs. In contrast to the ferromagnetic case, where the DW moves due to the conservation of angular momentum, the SW-driven antiferromagnetic DW motion can be understood as arising from the conservation of linear momentum density. Circularly polarized antiferromagnetic SWs are scattered by the DW to prevent the buildup of a local magnetic moment around the DW center. This behavior causes the DW to move away from the SW source at velocities of several hundred meters per second.

[1] A. H. MacDonald and M. Tsoi, Phil. Trans. R. Soc. A **369**, 3098 (2011).

[2] R. Duine, Nat. Mater. **10**, 344 (2011).

[3] E. G. Tveten, A. Qaiumzadeh, O. A. Tretiakov, and A. Brataas, Phys. Rev. Lett. **110**, 127208 (2013).

[4] K. M. D. Hals, Y. Tserkovnyak, and A. Brataas, Phys. Rev. Lett. **106**, 107206 (2011).

[5] A. S. Núñez, R. A. Duine, P. Haney, and A. H. MacDonald, Phys. Rev. B, **73**, 214426 (2006); R. A. Duine, P. M. Haney, A. S. Núñez, and A. H. MacDonald, Phys. Rev. B **75**, 014433 (2007); P. M. Haney, D. Waldron, R. A. Duine, A. S. Núñez, H. Guo, and A. H. MacDonald, Phys. Rev. B, **75**, 174428 (2007); P. M. Haney and A. H. MacDonald, Phys. Rev. Lett. **100**, 196801 (2008); H. V. Gomonay and V. M. Loktev, Phys. Rev. B **81**, 144427 (2010); H. V. Gomonay, R. V. Kunitsyn, and V. M. Loktev, Phys. Rev. B **85**, 134446 (2012); R. Cheng and Q. Niu, Phys. Rev. B **86**, 245118 (2012).

[6] Z. Wei, A. Sharma, A. S. Nunez, P. M. Haney, R. A. Duine, J. Bass, A. H. MacDonald, and M. Tsoi, Phys. Rev. Lett. **98**, 116603 (2007); R. Jaramillo, T. F. Rosenbaum, E. D. Isaacs, O. G. Shpyrko, P. G. Evans, G. Aeppli, and Z. Cai, Phys. Rev. Lett. **98**, 117206 (2007); S. Urazhdin and N. Anthony, Phys. Rev. Lett. **99**, 046602 (2007).

[7] B. G. Park, J. Wunderlich, X. Martí, V. Holý, Y. Kurosaki, M. Yamada, H. Yamamoto, A. Nishide, J. Hayakawa, H. Takahashi, A. B. Shick, and T. Jungwirth, Nat. Mater. **10**, 347 (2011); X. Marti, I. Fina, C. Frontera, J. Liu, P. Wadley, Q. He, R. J. Paull, J. D. Clarkson, J. Kudrnovský, I. Turek, J. Kuneš, D. Yi, J.-H. Chu, C. T. Nelson, L. You, E. Arenholz, S. Salahuddin, J. Fontcuberta, T. Jungwirth, and R. Ramesh, Nat. Mater. **13**, 367 (2014); X. Martí, B. G. Park, J. Wunderlich, H. Reichlová, Y. Kurosaki, M. Yamada, H. Yamamoto, A. Nishide, J. Hayakawa, H. Takahashi, and T. Jungwirth Phys. Rev. Lett. **108**, 017201 (2012); D. Herranz, R. Guerrero, R. Villar, F. G. Aliev, A. C. Swaving, R. A. Duine, C. van Haesendonck, and I. Vavra, Phys. Rev. B **79**, 134423 (2009); A. B. Shick, S. Khmelevskyi, O. N. Mryasov, J. Wunderlich, and T. Jungwirth, Phys. Rev. B **81**, 212409 (2010).

[8] R. K. Kummamuru and Y.-A. Soh, Nature (London) **452**, 859 (2008); Y.-A. Soh and R. K. Kummamuru, Phil. Trans. R. Soc. A **369**, 3646 (2011).

[9] D. I. Paul, Phys. Rev. **126**, 78 (1962).

[10] O. Bezencenet, D. Bonamy, R. Belkhou, P. Ohresser, and A. Barbier, Phys. Rev. Lett. **106**, 107201 (2011).

[11] F. Nolting, A. Scholl, J. Stohr, J. W. Seo, J. Fompeyrine, H. Siegwart, J. P. Locquet, S. Anders, J. Luning, E. E. Fullerton, M. F. Toney, M. R. Scheinfein, and H. A. Padmore, Nature (London) **405**, 767 (2000).

[12] M. Bode, E. Y. Vedmedenko, K. von Bergmann, A. Kubetzka, P. Ferriani, S. Heinze, and R. Wiesendanger, Nat. Mater. **5**, 477 (2006).

[13] J. M. Logan, H. C. Kim, D. Rosenmann, Z. Cai, R. Divan, O. G. Shpyrko, and E. D. Isaacs, Appl. Phys. Lett. **100**, 192405 (2012).

[14] T. Kampfrath, A. Sell, G. Klatt, A. Pashkin, S. Mahrlein, T. Dekorsy, M. Wolf, M. Fiebig, A. Leitenstorfer, and R. Hubers, Nat. Photonics **5**, 31 (2011).

[15] F. Keffer, H. Kaplan, and Y. Yafet, Am. J. Phys. **21**, 250 (1953).

[16] A. Brataas, A. D. Kent, and H. Ohno, Nat. Mater. **11**, 372 (2012).

[17] A. Mikhailov and A. I. Yaremchuk, JETP Lett. **39**, 296 (1984); D. Hinzke and U. Nowak, Phys. Rev. Lett. **107**, 027205 (2011); P. Yan, X. S. Wang, and X. R. Wang, *ibid.* **107**, 177207 (2011); A. A. Kovalev and Y. Tserkovnyak, Europhys. Lett. **97**, 67002 (2012).

[18] W. Jiang, P. Upadhyaya, Y. Fan, J. Zhao, M. Wang, L.-T. Chang, M. Lang, K. L. Wong, M. Lewis, Y.-T. Lin, J. Tang, S. Cherepov, X. Zhou, Y. Tserkovnyak, R. N. Schwartz, and K. L. Wang, Phys. Rev. Lett. **110**, 177202 (2013).

[19] D.-S. Han, S.-K. Kim, J.-Y. Lee, S. J. Hermsdoerfer, H. Schultheiss, B. Leven, and B. Hillebrands, Appl. Phys. Lett. **94**, 112502 (2009).

[20] D. Bouzidi and H. Suhl, Phys. Rev. Lett. **65**, 2587 (1990); J.-i. Kishine and A. S. Ovchinnikov, Phys. Rev. B **81**, 134405 (2010).

[21] V. G. Bar'yakhtar, B. A. Ivanov, and M. V. Chetkin, Sov. Phys. Usp. **28**, 563 (1985).

[22] N. L. Schryer and L. R. Walker, J. Appl. Phys. **45**, 5406 (1974).

[23] J. Lekner, Am. J. Phys. **75**, 1151 (2007).

[24] Y. Le Maho, J.-V. Kim, and G. Tatara, Phys. Rev. B **79**, 174404 (2009).

[25] A. Andreev and V. I. Marchenko, Sov. Phys. Usp. **23**, 21 (1980); F. D. M. Haldane, Phys. Rev. Lett. **50**, 1153 (1983).

[26] P. Yan, A. Kamra, Y. Cao, and G. E. W. Bauer, Phys. Rev. B **88**, 144413 (2013).

[27] T. Archer, C. D. Pemmaraju, S. Sanvito, C. Franchini, J. He, A. Filippetti, P. Delugas, D. Puggioni, V. Fiorentini, R. Tiwari, and P. Majumdar, Phys. Rev. B **84**, 115114 (2011).

[28] Y. Kajiwara, K. Harii, S. Takahashi, J. Ohe, K. Uchida, M. Mizuguchi, H. Umezawa, H. Kawai, K. Ando, K. Takanashi, S. Maekawa, and E. Saitoh, Nature (London) **464**, 262 (2010).

Paper III

"Electron-magnon scattering in magnetic heterostructures far out of equilibrium"

Erlend G. Tveten, Arne Brataas, and Yaroslav Tserkovnyak,
Physical Review B **92**, 180412(R) (2015).

PHYSICAL REVIEW B **92**, 180412(R) (2015)

Electron-magnon scattering in magnetic heterostructures far out of equilibrium

Erlend G. Tveten* and Arne Brataas
Department of Physics, Norwegian University of Science and Technology, NO-7491 Trondheim, Norway

Yaroslav Tserkovnyak
Department of Physics and Astronomy, University of California, Los Angeles, California 90095, USA

(Received 1 April 2015; published 23 November 2015)

We present a theory of out-of-equilibrium ultrafast spin dynamics in magnetic heterostructures based on the *s*-*d* model of ferromagnetism. Both in the bulk and across interfaces, the exchange processes between the itinerant *s* and the localized *d* electrons are described by kinetic rate equations for electron-magnon spin-flop scattering. In our treatment, the magnon distribution function remains nonthermalized on the relevant time scales of the demagnetization process, and the relaxation of the out-of-equilibrium spin accumulation among itinerant electrons provides the principal channel for dissipation of spin angular momentum from the combined electronic system.

DOI: 10.1103/PhysRevB.92.180412 PACS number(s): 72.25.Mk, 72.10.Di, 72.20.Pa, 75.40.Gb

Controlling spin flow in magnetic heterostructures at ultrafast time scales using femtosecond laser pulses opens intriguing possibilities for spintronics [1]. These laser-induced perturbations [2,3] stir up the most extreme regime of spin dynamics, which is governed by the highest energy scale associated with magnetic order: the microscopic spin exchange that controls the ordering temperature T_C. In contrast, at microwave frequencies the ferromagnetic dynamics in the bulk are well described by the Landau-Lifshitz-Gilbert (LLG) phenomenology [4], which has been successfully applied to the problem of the ferromagnetic resonance (FMR) [5]. At finite temperatures below T_C, the spin Seebeck and Peltier effects [6,7] describe the coupled spin and heat currents across interfaces in magnetic heterostructures. Despite their different appearances, the microwave, thermal, and ultrafast spin dynamics are all rooted in the exchange interactions between electrons. It is thus natural to try to advance a microscopic understanding of the ultrafast dynamics based on the established phenomena at lower energies.

Although some attempts have been made [8,9] to extend the LLG phenomenology to describe ultrafast demagnetization in bulk ferromagnets, no firm connection exists between the ultrafast spin generation at interfaces and the microwave spin-transfer and spin-pumping effects [10] or the thermal spin Seebeck and Peltier effects. In this Rapid Communication, we unify the energy regimes of microwave, thermal, and ultrafast spin dynamics in magnetic heterostructures from a common microscopic point of view, so that the parameters that control the high and low energy limits of spin relaxation originate from the same electron-magnon interactions. In addition to the unified framework, this Rapid Communication's unique contributions are the history-dependent, nonthermalized magnon distribution function and the crucial role of the out-of-equilibrium spin accumulation among itinerant electrons as the bottleneck that limits the dissipation of spin angular momentum from the combined electronic system.

The first reports on ultrafast demagnetization in Ni [11] challenged the conventional view of low-frequency magnetization dynamics at temperatures well below T_C. A multitude of mechanisms and scenarios have been suggested to explain the observed quenching of the magnetic moment. Some advocate direct coherent spin transfer induced by the irradiating laser light as the source of demagnetization [12]. Alternative theories argue that ultrafast spin dynamics arise indirectly through incoherent heat transfer to the electron system [13,14]. Recent experiments have demonstrated that nonlocal laser irradiation also induces ultrafast demagnetization [15], and atomistic modeling [16] supports the view that heating of magnetic materials is sufficient to induce ultrafast spin dynamics.

Terahertz (THz) magnon excitations in metallic ferromagnets have recently been proposed as an important element of ultrafast demagnetization by several authors [17,18]. The elementary interaction that describes these excitations is the electron-magnon scattering. Our theory is based on kinetic equations for the low-frequency spin and charge transport associated with the microwave magnetization dynamics in heterostructures [19] and with the linear spin-caloritronic response [7,20]. We extend these theories to treat far-from-equilibrium spin dynamics, in which transport is dominated by magnons and hot electrons. Electron-magnon scattering plays a critical role in this regime. We base our understanding of this interaction on the *transverse spin diffusion* [21] in the bulk and the *spin-mixing physics*, e.g., spin transfer and spin pumping [19,22], at the interfaces.

In our approach, we assume that the localized spins that result in the experimentally detectable macroscopic magnetization [23] are distinct from the itinerant electrons at the energy scales of interest. According to the accepted description of relaxation in ferromagnetic metals, the loss of energy and angular momentum from localized *d* electrons is mediated by the exchange interaction to the itinerant *s* electrons. The spin transfer from *d* to *s* states is accompanied by the relaxation of the *s* electron spins to the lattice through an incoherent spin-flip process caused by the spin-orbit coupling. Mitchell formulated such a model several decades ago to describe the longitudinal relaxation of ferromagnetic metals [24]. A similar description was later employed to describe Gilbert damping in ferromagnets at low frequencies [25,26].

In the following, we start by outlining the basic quantum-kinetic formalism for ultrafast spin dynamics in bulk ferromagnetic metals. Later, we show that the ferromagnet

*Corresponding author: erlend.tveten@ntnu.no

(F) | normal-metal (N) interfacial spin transport due to electron-magnon interactions follows a similar essential structure, unifying the bulk and interfacial spin dynamics in magnetic heterostructures. The Hamiltonian that describes F is $\hat{H} = \hat{H}_0 + \hat{H}_{sd}$, where $\hat{H}_0$ consists of decoupled s- and d-electron energies, including the kinetic energy of the itinerant electron bath, the d-d exchange energy, dipolar interactions, and the crystalline and Zeeman fields. The s-d interaction is

$$\hat{H}_{sd} = J_{sd} \sum_j \mathbf{S}_j^d \cdot \mathbf{s}(\mathbf{r}_j), \tag{1}$$

where J_{sd} is the exchange energy and $\mathbf{S}_j^d$ $[\mathbf{s}(\mathbf{r}_j)]$ is the d-electron (s-electron) spin vector (spin density) at lattice point j. We express the s-d interaction in terms of bosonic and fermionic creation and annihilation operators:

$$\hat{H}_{sd} = \sum_{qkk'} V_{qkk'} a_q c_{k\uparrow}^\dagger c_{k'\downarrow} + \text{H.c.}, \tag{2}$$

where $a_q^\dagger$ (a_q) is the Holstein-Primakoff creation (annihilation) operator for magnons with wave number q and $c_{k\sigma}^\dagger$ ($c_{k\sigma}$) is the creation (annihilation) operator for s electrons with momentum k and spin σ. $\hat{H}_{sd}$ describes how an electron flips its spin while creating or annihilating a magnon with momentum q and spin $\hbar$. The scattering strength is determined by the matrix element $V_{qkk'}$.

In Eq. (2), we have disregarded terms of the form $\sim a_q^\dagger a_{q'} c_{k\sigma}^\dagger c_{k'\sigma}$, which describe multiple-magnon scattering and do not contribute to a net change in magnetization along the spin-quantization axis. We have also disregarded higher-order terms associated with the Holstein-Primakoff expansion. Fully addressing magnonic correlation effects in the ultrafast regime would require a rigorous approach, e.g., using nonequilibrium Keldysh formalism [27]. However, when the s-d coupling (1) is not the dominant contribution to $\hat{H}$, we follow a mean-field approach and use Fermi's golden rule to compute the spin transfer between the s and d subsystems. We assume that all relevant energy scales are much smaller than the Fermi energy $\epsilon_F \equiv k_B T_F$ of the itinerant s electrons. In this limit, the electronic continuum remains largely degenerate, with electron-hole pairs present predominantly in the vicinity of the Fermi level.

We orient the coordinate system such that the localized spin density points in the negative z direction at equilibrium, with saturation value S (in units of $\hbar$). In the presence of a magnon density n_d, the longitudinal spin density becomes $S_z = n_d - S$. The magnons are assumed to follow a quadratic dispersion relation $\epsilon_q = \hbar\omega_q = \epsilon_0 + Aq^2$, where ϵ_0 is the magnon gap and A parametrizes the stiffness of the ferromagnet. $\langle a_q^\dagger a_{q'} \rangle = n(\epsilon_q)\delta_{qq'}$ defines the magnon distribution function $n(\epsilon_q)$, which is related to the total magnon density through $n_d = \int_{\epsilon_0}^{\epsilon_b} d\epsilon_q \mathcal{D}(\epsilon_q) n(\epsilon_q)$, where $\mathcal{D}(\epsilon_q) = \sqrt{\epsilon_q - \epsilon_0}/(4\pi^2 A^{3/2})$ is the magnon density of states. The integral over $\mathcal{D}(\epsilon_q)$ is cut off at an energy corresponding to the bandwidth, $\epsilon_b \sim k_B T_C$, which is the magnon energy at the edge of the Brillouin zone.

Because of the s-d interaction (1), the itinerant s electrons have a finite spin density at equilibrium (see Fig. 1). One of the key driving forces of the out-of-equilibrium spin dynamics is the spin accumulation $\mu_s \equiv \delta\mu_\uparrow - \delta\mu_\downarrow$. The bands for spin-up and spin-down electrons are split by $\Delta_{xc} \sim J_{sd} S a^3$, where a is the lattice constant of F. By introducing a dynamic exchange splitting, we can write $\mu_s = \delta n_s / D + \delta\Delta_{xc}$ [28], where δn_s is the out-of-equilibrium spin density of the s electrons, $D = 2D_\uparrow D_\downarrow/(D_\uparrow + D_\downarrow)$, and $D_{\uparrow(\downarrow)}$ is the density of states for spin-up (spin-down) electrons at the Fermi level. Because the mean-field band splitting due to the s-d exchange vanishes when the d orbitals are fully depolarized, $\delta\Delta_{xc}/\Delta_{xc} = \pm n_d/S$, where the sign determines whether the s and d orbitals couple ferromagnetically ($-$) or antiferromagnetically ($+$).

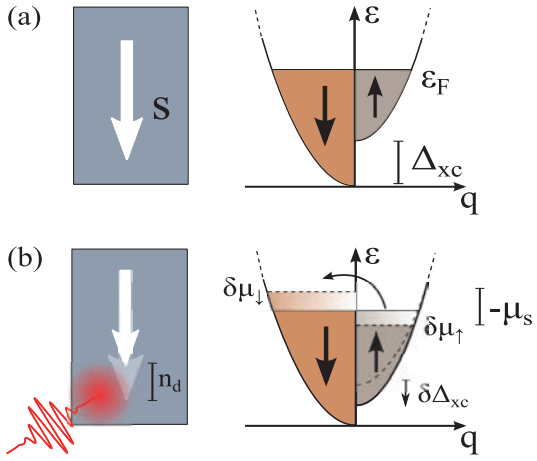

FIG. 1. (Color online) (a) Sketch of the density of s electron states in a ferromagnetic metal with saturation spin density S. At equilibrium, the exchange splitting Δ_{xc} shifts the bands for spin-up and spin-down electrons. (b) A laser pulse heats the s electron bath. The out-of-equilibrium spin accumulation $\mu_s = \delta\mu_\uparrow - \delta\mu_\downarrow$ results from two different mechanisms: (1) electron-magnon scattering induces a spin density among the s electrons, and (2) the mean-field exchange splitting is shifted by $\delta\Delta_{xc}$ by the induced magnon density n_d.

The rate of spin transfer (per unit volume) between the s and d subsystems due to electron-magnon spin-flop processes is determined from Eq. (2) by Fermi's golden rule [22]:

$$I_{sd} = \int_{\epsilon_0}^{\epsilon_b} d\epsilon_q \Gamma(\epsilon_q)(\epsilon_q - \mu_s)\mathcal{D}(\epsilon_q)[n_{\text{BE}}(\epsilon_q - \mu_s) - n(\epsilon_q)], \tag{3}$$

where $\Gamma(\epsilon_q)$ parametrizes the scattering rate at energy ϵ_q. In the derivation of Eq. (3) we have assumed that the kinetic energy of the itinerant electrons and the empty states (holes) thermalize rapidly due to Coulombic scattering and that they are distributed according to Fermi-Dirac statistics. Correspondingly, after standard manipulations [29], it can be shown that the electron-hole pairs follow the Bose-Einstein (BE) distribution function, $n_{\text{BE}}(\epsilon_q - \mu_s) = \{\exp[\beta_s(\epsilon_q - \mu_s)] - 1\}^{-1}$, at the electron temperature $T_s = 1/(k_B\beta_s)$. The number of available scattering states is influenced by the spin accumulation μ_s, as expected.

In contrast to the low-energy treatment in Ref. [22], the derivation of Eq. (3) does not constrict the form of the magnonic distribution $n(\epsilon_q)$ to the thermalized BE distribution

function. When the time scale of the s-d scattering is faster than the typical rates associated with magnon-magnon interactions, magnons are *not* internally equilibrated shortly after rapid heating of the electron bath, as also predicted by atomistic modeling [30]. Consequently, the occupation of the magnon states can deviate significantly from the BE distribution on the time scale of the demagnetization process. Our treatment of this central aspect differs from that of Ref. [31], in which the excited magnons are assumed to be instantly thermalized with an effective spin temperature and zero chemical potential and the thermally activated electron bath is assumed to be unpolarized.

The s-d scattering rate can be phenomenologically expanded as $\Gamma(\epsilon_q) = \Gamma_0 + \chi(\epsilon_q - \epsilon_0)$, where Γ_0 (which vanishes in the simplest Stoner limit [21]) parametrizes the scattering rate of the long-wavelength magnons and $\chi(\epsilon_q - \epsilon_0) \propto q^2$ describes the enhanced scattering of higher-energy magnons due to transverse spin diffusion [21]. In general, one might expect other terms of higher order in q to be present in this expansion as well. We will, however, limit ourselves to extrapolating $\Gamma(\epsilon_q)$ up to the bandwidth ϵ_b, which should be sufficient for qualitative purposes.

Neglecting any direct relaxation of magnons to the static lattice or its vibrations (i.e., phonons), $\partial_t n_d = I_{sd}/\hbar$. The equations of motion for the s-electron spin accumulation and the d-electron magnon distribution function are

$$\partial_t \mu_s = -\frac{\mu_s}{\tau_s} + \frac{\rho}{\hbar} I_{sd}, \tag{4}$$

$$\partial_t n(\epsilon_q) = \frac{\Gamma(\epsilon_q)}{\hbar}(\epsilon_q - \mu_s)[n_{\rm BE}(\epsilon_q - \mu_s) - n(\epsilon_q)], \tag{5}$$

where ρ determines the feedback of the demagnetization on μ_s and τ_s is the spin-orbit relaxation time for the s-electron spin density relaxing to the lattice. τ_s is typically on the order of picoseconds [32] and represents the main channel for the dissipation of angular momentum out of the combined electronic system. In general, τ_s also depends on the kinetic energy of the hot electrons after laser-pulse excitation. However, this discussion is beyond the scope of this Rapid Communication, and we assume that τ_s is independent of energy. $\rho = \rho_D + \rho_\Delta = -1/D \pm \Delta_{xc}/S$ includes effects arising from both the out-of-equilibrium spin density and the dynamic exchange splitting. For ferromagnetic $(-)$ s-d coupling, these effects add up, whereas for antiferromagnetic $(+)$ coupling, they compete.

At low temperatures, low-frequency excitations result in purely transverse spin dynamics. In the classical picture of rigid magnetic precession, the transverse relaxation time τ_2 is determined by the longitudinal relaxation time τ_1 as follows: $1/\tau_2 = 1/(2\tau_1) = \alpha\omega$, where α is the Gilbert damping parameter and ω is the precession frequency. Indeed, in the limit $(q, T_s) \to 0$, Eq. (3) yields

$$\partial_t n_d \to -\frac{\Gamma_0}{\hbar}\epsilon_0 n_d, \tag{6}$$

which is identical to the LLG phenomenology, indicating that $\epsilon_0 = \hbar\omega$ and thus $\Gamma_0 = 2\alpha$. This result establishes the important link between the scattering rate Γ_0 in this treatment and the Gilbert damping parameter that is accessible through FMR experiments.

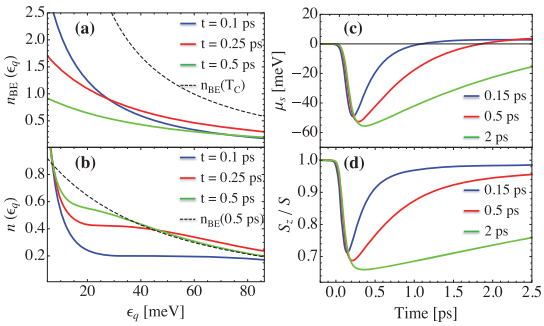

FIG. 2. (Color online) Numerical solutions of Eqs. (4) and (5) after T_s is increased from 10^2 to 10^3 K (T_C) within 50 fs with a decay time of 2 ps. $\epsilon_0 = 5$ meV, $A = 0.6$ meV nm^2, $\rho = 6$ meV nm^3, $\tau_s = 2$ ps, and $\alpha^* = 10\alpha = 0.1$. (a) The itinerant electron-hole pair distribution $n_{\rm BE}(\epsilon - \mu_s)$ is rapidly depleted by the spin accumulation μ_s that is built up via electron-magnon scattering. (b) In the magnon distribution $n(\epsilon_q)$ the high-energy magnon states are rapidly populated, whereas the low-energy states remain unaffected on short time scales. (c) Time evolution of the spin accumulation $\mu_s(t)$ and (d) the longitudinal spin density $-S_z(t)$ with different decay times of T_s: 0.15, 0.5, and 2 ps.

In the opposite high-frequency limit, pertinent to ultrafast demagnetization experiments, we consider F to be in a low-temperature equilibrium state before being excited by a THz laser pulse at $t = 0$, upon which the effective temperature of the itinerant electron bath instantly increases such that $T_s \gtrsim T_C$. This regime is clearly beyond the validity of the LLG phenomenology, which is designed to address the low-energy extremum of magnetization dynamics. Dissipation in the LLG equation, including relaxation terms based on the stochastic Landau-Lifshitz-Bloch treatment [14,33], is subject to a simple Markovian environment without any feedback or internal dynamics. This perspective must be refined for high frequencies when no subsystem can be viewed as a featureless reservoir for energy and angular momentum.

To appreciate the nonthermalized nature of the excited magnons, we consider the limit in which μ_s is small compared with ϵ_0 and no magnons are excited $[n(\epsilon_q) = 0]$ for $t < 0$. After rapid heating of the itinerant electrons at $t = 0$, the time evolution of the magnonic distribution follows

$$n(\epsilon_q, t) \approx n_{\rm BE}(\epsilon_q, t)[1 - e^{-\Gamma(\epsilon_q)\epsilon_q t/\hbar}]. \tag{7}$$

This result implies that, initially, the high-energy states are populated much faster than low-energy states. When μ_s becomes sizable, the coupled equations (4) and (5) must be solved subject to a suitable $T_s(t)$. Figures 2(a) and 2(b) present numerical solutions of (4) and (5) when T_s is increased from 10^2 to 10^3 K within 50 fs with a decay time of 2 ps. By comparison, internal magnon-magnon interactions equilibrate the distribution function on the time scale $\tau_{\rm eq}^{-1} \sim \hbar^{-1}\epsilon_m[\epsilon_m/(k_B T_C)]^3$ [22], where ϵ_m is a characteristic energy of the thermal magnon cloud. For short times, I_{sd} [Eq. (3)] dominates the magnon dynamics, and we expect the magnon population to significantly differ from the thermalized BE distribution.

When $T_s > T_C$, the thermally excited electron-hole pairs are populated in accordance with the classical Rayleigh-Jeans distribution, $n_{\rm BE}(\epsilon_q - \mu_s) \to k_B T_s/(\epsilon_q - \mu_s)$. Assuming, for simplicity, that the expansion for $\Gamma(\epsilon_q)$ is valid throughout the Brillouin zone, Eq. (3) yields $\partial_t n_d|_{t\to 0} = I_{sd}(0)/\hbar = [\Gamma_0 + 3\chi(\epsilon_b - \epsilon_0)/5]k_B T_s S/\hbar$. Thus, the demagnetization rate is initially proportional to the temperature of the electron bath but is reduced by the lack of available scattering states for high-energy magnons within the time scale of the demagnetization process. This finding conflicts with the results obtained from a Langevin treatment of the LLG equation [34], in which the magnetization relaxation rate is proportional to the temperature difference at *all times*. Figures 2(c) and 2(d) illustrate the time evolution of the out-of-equilibrium spin accumulation $\mu_s(t)$ and the longitudinal spin density $-S_z(t)$ for different decay times of T_s.

In the ultrafast regime, the electron-magnon spin-flop scattering is governed by the *effective* Gilbert damping parameter $\alpha^* \equiv \chi(\epsilon_b - \epsilon_0)$. Experimental investigations of the magnon relaxation rates on Co and Fe surfaces confirm that high-q magnons have significantly shorter lifetimes than low-q magnons [18]. It is reasonable to assume that the same effects are also present in the bulk. The initial relaxation time scale in the ultrafast regime is $\tau_i \sim (\alpha^* \hbar^{-1} k_B T_s)^{-1}$. This generalizes the result of Koopmans *et al.* [8] for the ultrafast relaxation of the longitudinal magnetization to arbitrary α^* based on the transverse spin diffusion [21]. The notion of magnons becomes questionable when the intrinsic linewidth approaches the magnon energy, which corresponds to $\alpha^* \sim 1$. Staying well below this limit and consistent with Refs. [18,21], we use $\alpha^* = 0.1$. For $T_C = 10^3$ K the initial relaxation time scale $\tau_i \sim 10^2(T_C/T_s)$ fs, which is generally consistent with the demagnetization rates observed for ultrafast demagnetization in Fe [35].

We now show that the interfacial scattering follows a structure similar to that of the bulk scattering in a unified description based on the electron-magnon interaction. Figure 3 presents a schematic illustration of an F|N interface. In magnetic heterostructures and for stand-alone ferromagnets on a conducting substrate, the demagnetization dynamics of F are also affected by the spin accumulation in N $\mu_{\rm N}(x)$, which can impact how nonlocal laser irradiation (e.g., the heating of N alone) induces ultrafast demagnetization of F [15]. By adding terms of the form $\sim \sum_{qkk'} U_{qkk'} a_q \tilde{c}^\dagger_{k\uparrow} \tilde{c}_{k'\downarrow}$ to $\hat{H}_{sd}$, where $\tilde{c}^\dagger_{k\uparrow}$ ($\tilde{c}_{k'\downarrow}$) describes the creation (annihilation) of an electron with spin up (down) at the F|N interface, the *interfacial* spin transfer (per unit area) due to electron-magnon spin-flop scattering is [22]

$$I_i = \int_{\epsilon_0}^{\epsilon_b} d\epsilon_q \Gamma^i(\epsilon_q)\big(\epsilon_q - \mu_{\rm N}^0\big)\mathcal{D}(\epsilon_q)\big[n_{\rm BE}\big(\epsilon_q - \mu_{\rm N}^0\big) - n(\epsilon_q)\big], \tag{8}$$

where $\mu_{\rm N}^0 \equiv \mu_{\rm N}(0)$ is the spin accumulation at the interface and $\Gamma^i(\epsilon_q)$ parametrizes the interfacial scattering rate.

The scattering of coherent long-wavelength magnons at the F|N interface can be described in the language of spin pumping/spin Seebeck effects [22], parametrized by the spin-mixing conductance $g_{\uparrow\downarrow}$ (per unit area) [19]. Motivated by $\Gamma(\epsilon_q)$ in the bulk, we write for the interfacial scattering rate $\Gamma^i(\epsilon_q) = g^*_{\uparrow\downarrow}(\epsilon_q)/(\pi S)$, where $g^*_{\uparrow\downarrow}$ reduces to $g_{\uparrow\downarrow}$ for low-energy scattering, $\epsilon_q \to \epsilon_0$. The interface scattering [Eq. (8)] dominates the microwave spin relaxation in thin ferromagnetic layers of thickness $d_{\rm F} \lesssim 10$ nm [19,37]. This trend should continue for higher frequencies and is relevant for ultrafast spin dynamics in thin magnetic layers in heterostructures [1]. We expect the energy dependence of the effective spin-mixing conductance to be relatively weak compared to that of the bulk scattering $\Gamma(\epsilon_q)$, which can be severely constrained at low energies due to momentum conservation [21]. For a finite temperature bias δT across the interface and for magnons thermalized at the temperature $T < T_C$, the connection to the thermal spin Seebeck and Peltier effects is made by identifying $\mathcal{S} = \partial_T I_i$ and $\Pi = T\mathcal{S}/\hbar$ [20] as the Seebeck and Peltier coefficients, respectively.

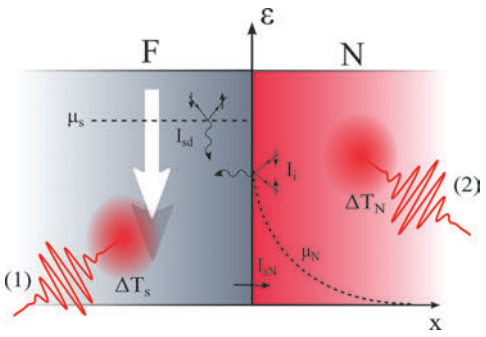

FIG. 3. (Color online) Sketch of a metallic ferromagnet (F) coupled to a normal metal (N). In the ultrafast regime, both the rapid heating of s electrons in F by ΔT_s [labeled (1)] and the heating of N by $\Delta T_{\rm N}$ [labeled (2)] can demagnetize F. I_{sd} [Eq. (3)] induces the spin accumulation μ_s in F, whereas I_i [Eq. (8)] induces the spin accumulation $\mu_{\rm N}^0$ at the F|N interface. Subsequently, $\mu_{\rm N}(x)$ diffuses into N until it vanishes due to spin-flip dissipation to the lattice. The additional interfacial spin current $I_{s{\rm N}}$, due to the thermodynamic biases $\delta\mu = \mu_s - \mu_{\rm N}^0$ and $\delta T = T_s - T_{\rm N}$, can be described by conventional thermoelectric parameters for longitudinal spin-dependent transport [36].

In conclusion, we have extended the concepts of transverse spin diffusion in bulk ferromagnets and the interfacial spin-mixing physics to address the ultrafast spin dynamics observed in rapidly heated magnetic heterostructures. In the ultrafast regime, the relative importance of the bulk scattering, parametrized by α^*, and the interfacial scattering, parametrized by $g^*_{\uparrow\downarrow}$, can be extracted from measurements of demagnetization strength and spin currents in magnetic heterostructures. For metallic ferromagnets in the bulk, our analysis shows that treating the magnonic subsystems as quasiequilibrated and parametrized by an effective temperature is insufficient to describe the far-from-equilibrium spin dynamics induced by pulsed laser heating. The magnon distribution function remains nonthermalized on the relevant time scale of the demagnetization process, in which the relaxation of the out-of-equilibrium spin accumulation μ_s limits the dissipation of spin angular momentum from the combined electronic system.

The authors thank A. V. Kimel, G. E. W. Bauer, J. Barker, S. Bender, H. Skarsvåg, and E. Fjærbu for valuable discussions.

[1] A. Melnikov, I. Razdolski, T. O. Wehling, E. T. Papaioannou, V. Roddatis, P. Fumagalli, O. Aktsipetrov, A. I. Lichtenstein, and U. Bovensiepen, Phys. Rev. Lett. **107**, 076601 (2011); E. Turgut, C. La-o-vorakiat, J. M. Shaw, P. Grychtol, H. T. Nembach, D. Rudolf, R. Adam, M. Aeschlimann, C. M. Schneider, T. J. Silva, M. M. Murnane, H. C. Kapteyn, and S. Mathias, *ibid.* **110**, 197201 (2013); G.-M. Choi, B.-C. Min, K.-J. Lee, and D. G. Cahill, Nat. Commun. **5**, 4334 (2014).

[2] A. Kirilyuk, A. V. Kimel, and T. Rasing, Rev. Mod. Phys. **82**, 2731 (2010).

[3] A. Kirilyuk, A. V. Kimel, and T. Rasing, Rep. Prog. Phys. **76**, 026501 (2013).

[4] E. M. Lifshitz and L. P. Pitaevskii, *Statistical Physics, Part 2*, 3rd ed., Course of Theoretical Physics Vol. 9 (Pergamon, Oxford, 1980); T. L. Gilbert, IEEE Trans. Magn. **40**, 3443 (2004).

[5] C. Kittel, Phys. Rev. **73**, 155 (1948).

[6] K. Uchida, J. Xiao, H. Adachi, J. Ohe, S. Takahashi, J. Ieda, T. Ota, Y. Kajiwara, H. Umezawa, H. Kawai, G. E. W. Bauer, S. Maekawa, and E. Saitoh, Nat. Mater. **9**, 894 (2010); J. Xiao, G. E. W. Bauer, K.-C. Uchida, E. Saitoh, and S. Maekawa, Phys. Rev. B **81**, 214418 (2010).

[7] G. E. W. Bauer, E. Saitoh, and B. J. van Wees, Nat. Mater. **11**, 391 (2012).

[8] B. Koopmans, J. J. M. Ruigrok, F. Dalla Longa, and W. J. M. de Jonge, Phys. Rev. Lett. **95**, 267207 (2005).

[9] J. Walowski, G. Müller, M. Djordjevic, M. Münzenberg, M. Kläui, C. A. F. Vaz, and J. A. C. Bland, Phys. Rev. Lett. **101**, 237401 (2008).

[10] A. Brataas, A. D. Kent, and H. Ohno, Nat. Mater. **11**, 372 (2012).

[11] E. Beaurepaire, J.-C. Merle, A. Daunois, and J.-Y. Bigot, Phys. Rev. Lett. **76**, 4250 (1996).

[12] J. P. van der Ziel, P. S. Pershan, and L. D. Malmstrom, Phys. Rev. Lett. **15**, 190 (1965); G. P. Zhang and W. Hübner, *ibid.* **85**, 3025 (2000); J.-Y. Bigot, M. Vomir, and E. Beaurepaire, Nat. Phys. **5**, 515 (2009).

[13] B. Koopmans, G. Malinowski, F. Dalla Longa, D. Steiauf, M. Fähnle, T. Roth, M. Cinchetti, and M. Aeschlimann, Nat. Mater. **9**, 259 (2010). A. J. Schellekens and B. Koopmans, Phys. Rev. B, **87**, 020407 (2013).

[14] J. H. Mentink, J. Hellsvik, D. V. Afanasiev, B. A. Ivanov, A. Kirilyuk, A. V. Kimel, O. Eriksson, M. I. Katsnelson, and Th. Rasing, Phys. Rev. Lett. **108**, 057202 (2012).

[15] A. Eschenlohr, M. Battiato, P. Maldonado, N. Pontius, T. Kachel, K. Holldack, R. Mitzner, A. Föhlisch, P. M. Oppeneer, and C. Stamm, Nat. Mater. **12**, 332 (2013).

[16] T. A. Ostler, J. Barker, R. F. L. Evans, R. W. Chantrell, U. Atxitia, O. Chubykalo-Fesenko, S. El Moussaoui, L. Le Guyader, E. Mengotti, L. J. Heyderman, F. Nolting, A. Tsukamoto, A. Itoh, D. Afanasiev, B. A. Ivanov, A. M. Kalashnikova, K. Vahaplar, J. Mentink, A. Kirilyuk, T. Rasing, and A. V. Kimel, Nat. Commun. **3**, 666 (2012).

[17] C. Illg, M. Haag, and M. Fähnle, Phys. Rev. B **88**, 214404 (2013).

[18] Y. Zhang, T.-H. Chuang, K. Zakeri, and J. Kirschner, Phys. Rev. Lett. **109**, 087203 (2012).

[19] A. Brataas, Y. V. Nazarov, and G. E. W. Bauer, Phys. Rev. Lett. **84**, 2481 (2000); Y. Tserkovnyak, A. Brataas, and G. E. W. Bauer, *ibid.* **88**, 117601 (2002); Y. Tserkovnyak, A. Brataas, G. E. W. Bauer, and B. I. Halperin, Rev. Mod. Phys. **77**, 1375 (2005).

[20] S. Hoffman, K. Sato, and Y. Tserkovnyak, Phys. Rev. B **88**, 064408 (2013).

[21] Y. Tserkovnyak, E. M. Hankiewicz, and G. Vignale, Phys. Rev. B **79**, 094415 (2009).

[22] S. A. Bender, R. A. Duine, and Y. Tserkovnyak, Phys. Rev. Lett. **108**, 246601 (2012); S. A. Bender, R. A. Duine, A. Brataas, and Y. Tserkovnyak, Phys. Rev. B **90**, 094409 (2014); S. A. Bender and Y. Tserkovnyak, *ibid.* **91**, 140402 (2015).

[23] C. La-O-Vorakiat, E. Turgut, C. A. Teale, H. C. Kapteyn, M. M. Murnane, S. Mathias, M. Aeschlimann, C. M. Schneider, J. M. Shaw, H. T. Nembach, and T. J. Silva, Phys. Rev. X, **2**, 011005 (2012).

[24] A. H. Mitchell, Phys. Rev. **105**, 1439 (1957).

[25] B. Heinrich, D. Fraitová, and V. Kamberský, Phys. Status Solidi, **23**, 501 (1967).

[26] Y. Tserkovnyak, G. A. Fiete, and B. I. Halperin, Appl. Phys. Lett. **84**, 5234 (2004).

[27] Y. Meir and N. S. Wingreen, Phys. Rev. Lett. **68**, 2512 (1992); A.-P. Jauho, N. S. Wingreen, and Y. Meir, Phys. Rev. B **50**, 5528 (1994).

[28] B. Y. Mueller, A. Baral, S. Vollmar, M. Cinchetti, M. Aeschlimann, H. C. Schneider, and B. Rethfeld, Phys. Rev. Lett. **111**, 167204 (2013).

[29] H. Bruus and K. Flensberg, *Many-Body Quantum Theory in Condensed Matter Physics*, 2nd ed. (Oxford University Press, Oxford, 2002).

[30] J. Barker, U. Atxitia, T. A. Ostler, O. Hovorka, O. Chubykalo-Fesenko, and R. W. Chantrell, Sci. Rep. **3**, 3262 (2013).

[31] A. Manchon, Q. Li, L. Xu, and S. Zhang, Phys. Rev. B **85**, 064408 (2012).

[32] R. Meservey and P. M. Tedrow, Phys. Rev. Lett. **41**, 805 (1978).

[33] D. A. Garanin, Phys. Rev. B **55**, 3050 (1997); U. Atxitia, O. Chubykalo-Fesenko, J. Walowski, A. Mann, and M. Münzenberg, *ibid.* **81**, 174401 (2010).

[34] W. F. Brown, Phys. Rev. **130**, 1677 (1963); R. Kubo and N. Hashitsume, Prog. Theor. Phys. Suppl. **46**, 210 (1970).

[35] T. Kampfrath, R. G. Ulbrich, F. Leuenberger, M. Münzenberg, B. Sass, and W. Felsch, Phys. Rev. B **65**, 104429 (2002); E. Carpene, E. Mancini, C. Dallera, M. Brenna, E. Puppin, and S. De Silvestri, *ibid.* **78**, 174422 (2008); A. Weber, F. Pressacco, S. Günther, E. Mancini, P. M. Oppeneer, and C. H. Back, *ibid.* **84**, 132412 (2011); S. Mathias, C. La-O-Vorakiat, P. Grychtol, P. Granitzka, E. Turgut, J. M. Shaw, R. Adam, H. T. Nembach, M. E. Siemens, S. Eich, C. M. Schneider, T. J. Silva, M. Aeschlimann, M. M. Murnane, and H. C. Kapteyn, Proc. Natl. Acad. Sci. USA **109**, 4792 (2012).

[36] M. Hatami, G. E. W. Bauer, Q. Zhang, and P. J. Kelly, Phys. Rev. Lett. **99**, 066603 (2007).

[37] S. Mizukami, Y. Ando, and T. Miyazaki, Jpn. J. Appl. Phys. **40**, 580 (2001); Phys. Rev. B **66**, 104413 (2002); Y. Liu, Z. Yuan, R. J. H. Wesselink, A. A. Starikov, and P. J. Kelly, Phys. Rev. Lett. **113**, 207202 (2014).

Paper IV

"Heat transport between antiferromagnetic insulators and normal metals"
Arne Brataas, Hans Skarsvåg, Erlend G. Tveten, and Eirik L. Fjærbu,
Physical Review B **92**, 180414(R) (2015).

PHYSICAL REVIEW B **92**, 180414(R) (2015)

Heat transport between antiferromagnetic insulators and normal metals

Arne Brataas,* Hans Skarsvåg, Erlend G. Tveten, and Eirik Løhaugen Fjærbu
Department of Physics, Norwegian University of Science and Technology, NO-7491 Trondheim, Norway
(Received 22 June 2015; revised manuscript received 6 November 2015; published 30 November 2015)

Antiferromagnetic insulators can become active spintronics components by controlling and detecting their dynamics via spin currents in adjacent metals. This cross talk occurs via spin transfer and spin pumping, phenomena that have been predicted to be as strong in antiferromagnets as in ferromagnets. Here, we demonstrate that a temperature gradient drives a significant heat flow from magnons in antiferromagnetic insulators to electrons in adjacent normal metals. The same coefficients as in the spin-transfer and spin-pumping processes also determine the thermal conductance. However, in contrast to ferromagnets, the heat is not transferred via a spin Seebeck effect which is absent in antiferromagnetic insulator-normal metal systems. Instead, the heat is proportional to a large staggered spin Seebeck effect.

DOI: 10.1103/PhysRevB.92.180414 PACS number(s): 72.25.Mk, 72.10.Di, 72.20.Pa, 73.50.Lw

In spintronics, the properties which make antiferromagnets markedly different from ferromagnets also make them attractive in a more dynamic role. Antiferromagnets operate at much higher frequencies and may empower terahertz circuits. They also have no magnetic stray fields, which therefore enables denser spintronics circuits. Antiferromagnets are usually passive spintronics components. However, they can play a role as active components despite their lack of a macroscopic magnetic moment [1–13] and even when they are insulating [10,12,13].

We demonstrate that the thermal coupling between antiferromagnetic insulators (AFIs) and normal metals is relatively strong. The strong thermal coupling facilitates several outcomes: The interface coupling can lead to efficient cooling of antiferromagnetic spintronics devices, might function as heat sensors, and can reveal valuable information about the high-frequency spin excitations in dc measurements that are complicated to extract with other techniques.

Antiferromagnets can produce pure spin currents as large as those produced by ferromagnets. We recently showed that spin pumping may be as operative from antiferromagnets as from ferromagnets [13], in apparent contradiction to naive intuition. Furthermore, the efficiency of spin pumping from antiferromagnets to normal metals implies, via Onsager reciprocity relations, that there is a considerable spin-transfer torque on antiferromagnets from a spin accumulation in adjacent normal metals. However, in the absence of external magnetic fields, the spin Seebeck effect in antiferromagnet-normal metal systems vanishes [14]. This fact seems to indicate that spins in antiferromagnets decouple from, or are only weakly connected to, heat currents and temperature gradients in adjacent normal metals.

To the contrary, we find that the thermal coupling constant is orders of magnitude stronger than its ferromagnetic counterpart. This radical difference is caused by the large exchange field in antiferromagnets that governs the heat transfer rather than the much smaller anisotropy fields or external magnetic fields in ferromagnets. The thermal coupling between antiferromagnetic insulators and normal metals is associated with a staggered spin Seebeck effect rather than via the spin Seebeck effect.

Spin caloritronics determines how spins are coupled to currents and temperature gradients [15]. Measurements of important thermoelectric properties in ferromagnetic insulators, such as the spin Seebeck effect [16], are central to this field. In the spin Seebeck effect, a temperature gradient transfers a magnon spin current in a ferromagnet into an itinerant spin current in a normal metal [17,18]. This process is active even in insulating ferromagnets [19]. The spin Peltier effect is reciprocal to the spin Seebeck effect; a heat current generates a spin accumulation [20,21]. These fascinating thermoelectric properties can be useful to control the heat flow in spintronics devices and in devices that recycle waste heat.

In explaining our calculations, we interpret the theories on the spin Seebeck effect [15–18,22] as a combination of three mechanisms. First, a precessing magnetization can pump a spin current across a ferromagnet-normal metal junction [23–25]. Spin pumping gives rise to an increased magnetization dissipation rate [23,26,27]. Second, the enhanced dissipation implies that there is also an enhanced spin current noise in terms of a fluctuating spin-transfer torque [28]. At equilibrium, there is no thermal bias and the dc spin current vanishes because the temperature-driven spin pumping and a fluctuating spin-transfer torque exactly compensate each other. Third, a temperature difference alters this balance and causes a net spin current [17,18,22].

In this picture, to compute the heat transfer between AFIs and normal metals, we first establish the fluctuating spin transfer and staggered spin transfer in such hybrid systems. Both quantum *and* thermal fluctuations are required to determine the magnon occupations. Subsequently, we use these results to define the thermal gradient-driven (staggered) spin currents, which we then use to evaluate the heat current from the AFI to the normal metal. We focus on insulating antiferromagnets where the transport properties are magnon driven. Generalizations to conducting antiferromagnets are straightforward.

We model the AFI as a two sublattice system with spatiotemporal magnetizations $\mathbf{M}_1$ and $\mathbf{M}_2$. The dynamics are described by the staggered magnetizations $\mathbf{L} = \mathbf{M}_1 - \mathbf{M}_2 = L\mathbf{n}$ and the magnetization $\mathbf{M} = \mathbf{M}_1 + \mathbf{M}_2 = L\mathbf{m}$. These fields satisfy the constraints $\mathbf{n}^2 + \mathbf{m}^2 = 1$ and $\mathbf{n} \cdot \mathbf{m} = 0$. At

*Arne.Brataas@ntnu.no

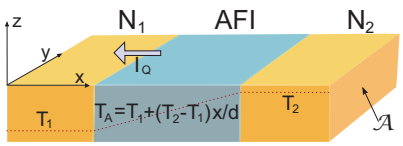

FIG. 1. (Color online) An AFI sandwiched between two normal metals N_1 and N_2. The left normal metal (N_1) is a good spin sink. The electrons in the right normal metal (N_2) are decoupled from the magnons, e.g., the interface coupling is weak and/or there is no spin-memory loss. A heat current between the normal metals flows in response to an applied temperature gradient across the AFI. The cross section is $\mathcal{A}$ and d is the AFI thickness. The heat flow I_Q is along the longitudinal coordinate x.

equilibrium, the staggered field is homogeneous and constant in time, $|\mathbf{L}| = L$, and the magnetization vanishes, $\mathbf{M} = 0$, i.e., $\mathbf{n}^2 = 1$ and $\mathbf{m} = 0$. We consider an easy-axis AFI that is described by the energy $E = \int d\mathbf{r}[\varepsilon(\mathbf{r}) + \varepsilon_s(\mathbf{r})]$, where the energy density is

$$\varepsilon = \frac{L}{\gamma}\left[\frac{1}{2}\omega_E(\mathbf{m}^2 - \mathbf{n}^2) - \frac{1}{2}\omega_A\left(m_z^2 + n_z^2\right)\right], \tag{1}$$

with the exchange frequency ω_E and the smaller anisotropy frequency ω_A, $\omega_A \ll \omega_E$. When $\mathbf{n}$ and $\mathbf{m}$ spatially vary, the stiffness contributions are

$$\varepsilon_s = \frac{L}{2\gamma}\omega_A \sum_{i=x,y,z}[(\lambda_n \partial_i \mathbf{n})^2 + (\lambda_m \partial_i \mathbf{m})^2], \tag{2}$$

where λ_n and λ_m are exchange lengths associated with $\mathbf{n}$ and $\mathbf{m}$, respectively. The dynamic equations are

$$\dot{\mathbf{n}} = \boldsymbol{\omega}_m \times \mathbf{n} + \boldsymbol{\omega}_n \times \mathbf{m} + \boldsymbol{\tau}_n, \tag{3a}$$

$$\dot{\mathbf{m}} = \boldsymbol{\omega}_n \times \mathbf{n} + \boldsymbol{\omega}_m \times \mathbf{m} + \boldsymbol{\tau}_m, \tag{3b}$$

where the effective fields are $\boldsymbol{\omega}_n = -(\gamma/L)\delta\varepsilon/\delta\mathbf{n}$ and $\boldsymbol{\omega}_m = -(\gamma/L)\delta\varepsilon/\delta\mathbf{m}$. In Eqs. (3a) and (3b), the dissipation and fluctuation torques $\boldsymbol{\tau}_m$ and $\boldsymbol{\tau}_n$ are essential to describe spin caloritronics effects.

We consider a thin-film AFI of thickness d sandwiched between two normal metals, the left one of which is a good spin sink (e.g., Pt), and the right is only weakly coupled or has little or no spin-memory loss (see Fig. 1). We assume planar AFI-normal metal interfaces of cross section $\mathcal{A}$. The coordinate $\mathbf{r} = (x, \boldsymbol{\rho})$ is decomposed into a perpendicular coordinate x ($0 \leqslant x \leqslant d$) and the two-dimensional (2D) in-plane coordinates $\boldsymbol{\rho}$. The fluctuation-dissipation torques have bulk and (spin-pumping-induced) interface contributions, $\tau_\nu(\mathbf{r}) = \tau_\nu^{(b)}(\mathbf{r}) + \delta(x - x_I)\tau_\nu^{(p)}(\boldsymbol{\rho})$, where $x_I = 0^+$ is infinitesimally near the interface on the AFI side close to the spin sink and the subscript ν denotes the product of either the subindex n or m and a Cartesian component x, y, or z. The bulk torques arise from the magnon-phonon interaction. At the AFI-N interface, the torques are governed by spin pumping induced by the coupling of the magnetic moments to itinerant electrons in adjacent normal metals. In finding the torques, we introduce dissipation in a similar way as in Ref. [7] and further generalize this description to include quantum and thermal fluctuations. The resulting fluctuation-dissipation torques are

$$\boldsymbol{\tau}_n = (\mathbf{h}_m - \alpha\dot{\mathbf{m}}) \times \mathbf{n} + (\mathbf{h}_n - \alpha\dot{\mathbf{n}}) \times \mathbf{m}, \tag{4a}$$

$$\boldsymbol{\tau}_m = (\mathbf{h}_n - \alpha\dot{\mathbf{n}}) \times \mathbf{n} + (\mathbf{h}_m - \alpha\dot{\mathbf{m}}) \times \mathbf{m}, \tag{4b}$$

for both bulk and interface contributions where we have suppressed the superscript [(b) or (p)] in $\boldsymbol{\tau}$, $\mathbf{h}$, and α. The bulk Gilbert damping constant is $\alpha^{(b)}$. $\alpha^{(p)}$ is a measure of the spin-pumping-induced enhanced dissipation; for homogeneous macrospin excitations the enhanced damping constant is $\alpha^{(b)} + \alpha^{(p)}/d$ [25].

The fluctuation-dissipation theorem implies the existence of the fluctuating forces $\mathbf{h}_m$ and $\mathbf{h}_n$. The average of the independent fluctuating forces $\mathbf{h}_m$ and $\mathbf{h}_n$ and the cross correlations between different fields vanish, but the variance is

$$\left\langle h_\nu^{(p)}(\boldsymbol{\rho}t) h_\nu^{(p)}(\boldsymbol{\rho}'t')\right\rangle = \frac{\gamma\alpha^{(p)}R(t-t',T_1)}{L\pi}\delta(\boldsymbol{\rho}-\boldsymbol{\rho}'), \tag{5a}$$

$$\left\langle h_\nu^{(b)}(\mathbf{r}t) h_\nu^{(b)}(\mathbf{r}'t')\right\rangle = \frac{\gamma\alpha^{(b)}R(t-t',T_A)}{L\pi}\delta(\mathbf{r}-\mathbf{r}'). \tag{5b}$$

The correlation function $R(t,T)$ depends on the (local) temperature. As demonstrated for ferromagnets in Ref. [28], the spin-current fluctuations associated with spin pumping depend on the temperature in the normal metal close to the interface, T_1. We posit that the one-to-one correspondence between spin pumping in ferromagnets and antiferromagnets [13] implies that the spin-current fluctuations in antiferromagnets obeys the same relationship, as in Eq. (5a). In the bulk of the AFI, the phonon-induced fluctuations associated with the bulk Gilbert damping depend on the temperature profile in the antiferromagnet $T_A(x)$, as in Eq. (5b). The correlation function only describes white noise in the (classical) high-temperature limit, $R(t,T) \approx 2\pi k_B T\delta(t)$. However, for the purpose of computing the heat current, we need to take into account the quantum behavior of the fluctuations, which we describe after Eq. (15).

The effective fields determined by Eqs. (1) and (2) are

$$\boldsymbol{\omega}_n = \omega_E\mathbf{n} + \omega_A(\mathbf{n}\cdot\hat{z})\hat{z} + \omega_A(\lambda_n\nabla)^2\mathbf{n}, \tag{6a}$$

$$\boldsymbol{\omega}_m = -\omega_E\mathbf{m} + \omega_A(\mathbf{m}\cdot\hat{z})\hat{z} + \omega_A(\lambda_m\nabla)^2\mathbf{m}. \tag{6b}$$

In the absence of bulk (electron-magnon) Gilbert damping represented by α, the energy current density $\mathbf{j}_E$ is defined via the continuity equation $\langle\partial_t(\varepsilon + \varepsilon_s)\rangle + \nabla\cdot\mathbf{j}_E = 0$. Because there is no change in external parameters (e.g., spin accumulation) in the system, the energy current can be identified as the heat current. From this continuity equation and by using the dynamic equations (3), with the interface surface normal $\hat{x}$, we find that the total heat current $I_Q = \int d\boldsymbol{\rho}(-\hat{x}\cdot\mathbf{j}_E)$ across the normal-metal–AFI interface is

$$I_Q = \frac{L}{\gamma}\left\langle\omega_A\lambda_n^2\partial_x\mathbf{n}\cdot\partial_t\mathbf{n} + \omega_A\lambda_m^2\partial_x\mathbf{m}\cdot\partial_t\mathbf{m}\right\rangle|_{x=0}. \tag{7}$$

I_Q contains products of the deviations from equilibrium of the staggered field and the magnetization. It is therefore sufficient to carry out the computation of $\mathbf{n}$ and $\mathbf{m}$ in linear response.

We use a circular basis so that $n_\pm = n_x \pm in_y$ and $m_\pm = m_x \pm im_y$ are first-order corrections with respect to the

equilibrium configuration $\mathbf{n} = \hat{z}$ and $\mathbf{m} = 0$. Next, we Fourier transform in the transverse coordinate $\boldsymbol{\rho}$ and time t so that any function $c(x,\boldsymbol{\rho},t) = \sum_{\mathbf{q}} \int d\omega \tilde{c}(x,\mathbf{q},\omega) \exp i(\omega t - \mathbf{q}\cdot\boldsymbol{\rho})$. Using Eq. (3), the linearized dynamic equations of motion become

$$\left\{i\alpha^{(b)}\omega + \omega_A\left[1+\lambda_m^2\left(\mathbf{q}^2 - \partial_x^2\right)\right] + 2\omega_E\right\}\tilde{m}_\pm = \pm\omega\tilde{n}_\pm + \tilde{h}^{(b)}_{m\pm}(x), \tag{8a}$$

$$\left\{i\alpha^{(b)}\omega + \omega_A\left[1+\lambda_n^2\left(\mathbf{q}^2 - \partial_x^2\right)\right]\right\}\tilde{n}_\pm = \pm\omega\tilde{m}_\pm + \tilde{h}^{(b)}_{n\pm}(x). \tag{8b}$$

In the coupled dynamic equations (8), the stiffness contributions (2) can be interpreted as arising from the continuity equations for the staggered field and the magnetizations, $(\partial_t \mathbf{n})_s + \sum_i \partial_i \mathbf{j}_{n,i} = 0$ and $(\partial_t \mathbf{m})_s + \sum_i \partial_i \mathbf{j}_{m,i} = 0$. In linear response, the staggered spin current and spin current along the x direction are $\mathbf{j}_{n,x} = \omega_A\lambda_m^2\hat{z}\times\partial_x\mathbf{m}$ and $\mathbf{j}_{m,x} = \omega_A\lambda_n^2\hat{z}\times\partial_x\mathbf{n}$. The boundary conditions for the linearized equation of motion (8) are obtained by integrating the dynamic equations (3) across the AFI-N interface. This results in the continuity of the staggered spin and spin currents in linearized forms at $x = 0$:

$$\omega_A\lambda_m^2\frac{\partial\tilde{m}_\pm}{\partial x} = i\omega\alpha^{(p)}\tilde{m}_\pm - \tilde{h}^{(p)}_{m,\pm}, \tag{9a}$$

$$\omega_A\lambda_n^2\frac{\partial\tilde{n}_\pm}{\partial x} = i\omega\alpha^{(p)}\tilde{n}_\pm - \tilde{h}^{(p)}_{n,\pm}. \tag{9b}$$

Similarly, at $x = d$, there is no loss of currents and the boundary conditions are $\omega_A\lambda_m^2\partial\tilde{m}_\pm/\partial x = 0$ and $\omega_A\lambda_n^2\partial\tilde{n}_\pm/\partial x = 0$.

In typical antiferromagnets, ω_E is much larger than all other energy scales and we may employ the so-called exchange approximation. This implies that we may disregard smaller terms in the equation of motion (8a) so that it greatly simplifies to $\tilde{m}_\pm = \omega\tilde{n}_\pm/2\omega_E$. By inserting this relation into Eq. (8b), we find the equation of motion in the exchange approximation

$$\lambda_n^2\left(q_x^2 + \partial_x^2\right)\tilde{n}_\pm = -\frac{\tilde{h}^{(b)}_{n\pm}}{\omega_A}, \tag{10}$$

which can be solved with the boundary conditions of Eq. (9b). In the exchange approximation, to the lowest order in the dissipation, we have introduced the longitudinal wave number q_x. The complex wave number q_x is implicitly defined via the relation $\omega = \omega_R + i/t^{(b)}$, where the bulk resonance frequency and the bulk lifetime are determined by

$$\omega_R^2 = 2\omega_A\omega_E\left[1+\lambda_n^2\left(q_x^2+q_y^2+q_z^2\right)\right], \tag{11a}$$

$$1/t^{(b)} = \alpha^{(b)}\omega_E. \tag{11b}$$

The central results we will obtain can be interpreted in terms of the eigenstates with the associated eigenfrequencies and lifetimes in a thin-film antiferromagnet. The eigenstates are determined by expressing $\tilde{n}_\pm = A_\pm\exp(iq_x x) + B_\pm\exp(-iq_x x)$ in Eq. (10) when the right-hand side (the fluctuations) vanishes. The only nontrivial solution that satisfies both the boundary conditions of Eq. (9b) at $x = 0$ (with no fluctuations) and $\partial\tilde{n}_\pm/\partial x = 0$ at $x = d$ is determined by the secular equation $s(q_x) = 0$, where

$$s(q_x) = \frac{q_x\lambda_n^2\omega_A}{d\omega}\tan(q_x d) - i\frac{\alpha^{(p)}}{d}. \tag{12}$$

In the absence of spin pumping and bulk damping, the solutions of $s(q_x) = 0$ are standing waves where $q_x = N\pi/d$ and N is an integral number. When spin pumping is weak, the second term in Eq. (12) is small and the solutions of $s(q_x) = 0$ can be expanded around the solutions obtained in the absence of spin pumping. For the higher modes, when $N \neq 0$, we expand the wave vector q_x to the first order in the deviations from $N\pi/d$ and insert the resulting imaginary part of the wave vector into the dispersion relation of Eq. (11a) to find the spin-pumping lifetime $t_N^{(p)}$. For $N = 0$, we carry out a second-order expansion in terms of the small parameter $q_x d$ around 0 and insert this result into the dispersion of Eq. (11a) to find the lifetime $t_0^{(p)}$. We compute that

$$1/t_0^{(p)} = \frac{\alpha^{(p)}}{d}\omega_E, \tag{13a}$$

$$1/t_{N\neq 0}^{(p)} = 2\frac{\alpha^{(p)}}{d}\omega_E. \tag{13b}$$

In a striking contrast to ferromagnets, the spin-pumping-induced scattering rate $1/t^{(p)}$ (13) is proportional to the exchange energy. Similar expressions for the spin-pumping rates in ferromagnets scale with the ferromagnetic spin-wave energy, which is several orders of magnitude smaller than the exchange energy. We know that the spin-pumping-induced effective Gilbert damping coefficients $\alpha^{(p)}$ in insulating antiferromagnet–normal-metal systems are comparable to those of insulating ferromagnet–normal-metal systems (Ref. [29]). We will see that the short spin-pumping-induced AFI lifetimes of Eq. (13) imply a large heat conductance between AFIs and normal metals. Interestingly, we find that the spin-pumping-induced relaxation rate of the higher modes is twice as large as the uniform, but independent of the transverse (2D) wave vector $\mathbf{q}$. This ratio agrees with our previous result for the spin-pumping-induced ratio in thin-film ferromagnets and can be used to distinguish the spin-wave modes [29].

Next, we solve the linearized dynamic equation (8) with the fluctuating bulk forces and subject to the boundary condition (9b) where the fluctuating spin-pumping-induced forces appear. To compute the heat current, we represent the solution at $x = 0$ as $\tilde{m}_+ = \chi^{(p)}_{m+}\tilde{h}^{(p)}_{n+} + \int_0^d dx\,\chi^{(b)}_{m+}(x)\tilde{h}^{(b)}_{n+}(x)$ and $\omega_A\lambda_n^2\partial_x\tilde{n}_+/d = \chi^{(p)}_{n'+}\tilde{h}^{(p)}_{n+} + \int_0^d dx\,\chi^{(b)}_{n'+}(x)\tilde{h}^{(b)}_{n+}(x)$. We find that $\chi^{(p)}_{m+} = -1/[2d\omega_E s(q_x)]$, $\chi^{(b)}_{m+} = \chi^{(p)}_{m+}\cos q_x(d-x)/\cos q_x d$, $\chi^{(p)}_{n'+} = -q_x\lambda^2\omega_A\tan q_x d/d^2\omega s(q_x)$, and $\chi^{(b)}_{n'+} = -i\alpha^{(p)}\cos q_x(d-x)/d^2 s(q_x)\cos q_x d$.

We evaluate the variance of the fluctuating forces and find the heat current, $I_Q = -(2d\omega_E/\pi)\mathrm{Im}\sum_{\mathbf{q}}\int_{-\infty}^{\infty}d\omega[\eta_Q^{(p)} + \eta_Q^{(b)}]$, where the spin-pumping and bulk contributions are

$$\eta_Q^{(p)} = \chi^{(p)}_{m+}\left(\chi^{(p)}_{n'+}\right)^*\alpha^{(p)}\tilde{R}(\omega,T_1), \tag{14a}$$

$$\eta_Q^{(b)} = \int_0^d dx\,\chi^{(b)}_{m+}(x)\left[\chi^{(b)}_{n'+}(x)\right]^*\alpha^{(b)}\tilde{R}(\omega,T_A(x)). \tag{14b}$$

At equilibrium, $T_A(x) = T_1$, the heat current vanishes, $I_Q = 0$, as expected. In linear response, the temperature varies linearly in the AFI so that $T_A(x) = T_1 + (T_2 - T_1)x/d$. We then compute that the heat current is $I_Q = (T_2 - T_1)\kappa_Q$, where

$$\kappa_Q = \sum_{q_y,q_z} \int_{-\infty}^{\infty} d\omega \frac{\alpha^{(b)} \frac{\alpha^{(p)}}{d}}{\pi |s(q_x)|^2} \zeta(q_x) \frac{\partial \tilde{R}(\omega,T)}{\partial T} \qquad (15)$$

and $\zeta(q_x) = 2\int_0^d dx |\frac{\cos q_x(d-x)}{\cos q_x d}|^2 \frac{x}{d^2}$. By following the same methods, we also compute that the temperature-driven spin current, i.e., the spin Seebeck effect, vanishes, in agreement with Ref. [14]. However, we find that the temperature-driven staggered spin current is finite. Furthermore, the heat current is directly proportional to the staggered spin current.

By comparing the equilibrium expectation value of the spin-wave internal energy with the quantum-mechanical result for a magnon gas or, alternatively, by using the fluctuation-dissipation theorem represented by Eq. (4.9) in Ref. [30], we identify that the correlation function $R(\omega,T)$ represents the mean energy at the temperature T of an oscillator at natural frequency ω, $\tilde{R}(\omega,T) = \frac{1}{2}\hbar|\omega| + \hbar\omega f(|\omega|,T)$, where $f(\omega,T)$ is the Bose-Einstein distribution function.

When damping is small, and the spin-pumping-induced damping is smaller than the bulk damping, we can expand the poles of the denominator of Eq. (15) around the spin-wave resonance $q_x d = n\pi$ in a similar way as in Ref. [22]. This results in an intuitive expression:

$$I_Q = \sum_{N=0}^{\infty} \frac{1}{t_N^{(p)}} \int_0^{\infty} d\omega\, D_N(\omega)\hbar\omega\{f(\omega,T_2)[1 - f(\omega,T_1)] - f(\omega,T_1)[1 - f(\omega,T_2)]\}. \qquad (16)$$

The heat current that flows between the normal metals via the antiferromagnet, at each frequency, is proportional to the spin-pumping-induced spin-wave relaxation rate $1/t_N^{(p)}$, the mode-dependent density of states, $D_N(\omega) = \sum_{q_y,q_z} 2\delta[\omega - (2\omega_A\omega_E\{1 + \lambda_n^2[(\frac{N\pi}{d}) + q_y^2 + q_z^2]\})^{1/2}]$. Furthermore, the heat current is determined by the Bose-Einstein occupation of the magnons and the electron-hole pairs in the normal metal. This expression (16) reveals that the thermal coupling between normal metals and AFIs is relatively strong. The heat current is proportional to the spin-pumping-induced spin-wave scattering rates that are proportional to the exchange energy and the Gilbert damping coefficient and therefore are orders of magnitude larger than in ferromagnets. At high temperature, we find $I_Q = \mathcal{A}\pi^2(k_B T_1)^3 k_B(T_2 - T_1)\alpha^{(p)}/(15\sqrt{2}A_{\rm ex}^{3/2}\sqrt{\omega_E}\hbar^{3/2})$, where $A_{\rm ex} = \hbar\omega_A\lambda_n^2$ is the exchange stiffness. For example, using material parameters from Refs. [31,32], we find $\kappa/\mathcal{A} \sim 10^7$ W/m^2 for $RbMnF_3$, whereas a calculation for F-N yields a value $\sim 10^5$W/m^2 for yttrium iron garnet, both at 30 K and assuming a spin mixing conductance $g = 5 \times 10^{18}$ m^{-2}.

Phonons also mediate heat currents between AFIs and normal metals. Experimentally, the magnon-induced heat current we predict here can be separated from the phonon heat current by the different material, temperature, and length dependence. For instance, at temperatures below the magnon gap, magnons do not contribute to the heat conductance. Also, different measurements in systems with normal metals that couple strongly or weakly to the antiferromagnets can be compared. Finally, one can use an external magnetic field to change the magnon dispersion and consequently the spin-wave density of states governing magnon-induced heat current of Eq. (16).

In conclusion, we demonstrated a strong thermal coupling between antiferromagnetic insulators and normal metals. The heat current is directly proportional to the staggered spin current.

We acknowledge support from the Research Council of Norway, Project No. 216700.

[1] A. S. Nunez, R. A. Duine, P. Haney, and A. H. MacDonald, Phys. Rev. B **73**, 214426 (2006).
[2] Z. Wei, A. Sharma, A. S. Nunez, P. M. Haney, R. A. Duine, J. Bass, A. H. MacDonald, and M. Tsoi, Phys. Rev. Lett. **98**, 116603 (2007).
[3] S. Urazhdin and N. Anthony, Phys. Rev. Lett. **99**, 046602 (2007).
[4] P. M. Haney and A. H. MacDonald, Phys. Rev. Lett. **100**, 196801 (2008).
[5] Y. Xu, S. Wang, and K. Xia, Phys. Rev. Lett. **100**, 226602 (2008).
[6] H. V. Gomonay and V. M. Loktev, Low Temp. Phys. **34**, 198 (2008).
[7] K. M. D. Hals, Y. Tserkovnyak, and A. Brataas, Phys. Rev. Lett. **106**, 107206 (2011).
[8] B. G. Park, J. Wunderlich, X. Marti, Y. Kurosaki, M. Yamada, H. Yamamoto, A. Nishide, J. Hayakawa, H. Takahashi, A. B. Shick, and T. Jungwirth, Nat. Mater. **10**, 347 (2011).
[9] X. Marti, B. G. Park, J. Wunderlich, H. Reichlova, Y. Kurosaki, M. Yamada, H. Yamamoto, A. Nishide, J. Hayakawa, H. Takahashi, and T. Jungwirth, Phys. Rev. Lett. **108**, 017201 (2012).
[10] E. G. Tveten, A. Qaiumzadeh, O. A. Tretiakov, and A. Brataas, Phys. Rev. Lett. **110**, 127208 (2013).
[11] X. Marti, I. Fina, C. Frontera, J. Liu, P. Wadley, Q. He, R. J. Paull, J. D. Clarkson, J. Kudrnovsky, I. Turek, J. Kunes, D. Yi, J-H. Chu, C. T. Nelson, L. You, E. Arenholz, S. Salahuddin, J. Foncuberta, T. Jungwirth, and R. Ramesh, Nat. Mater. **13**, 367 (2014).
[12] E. G. Tveten, A. Qaiumzadeh, and A. Brataas, Phys. Rev. Lett. **112**, 147204 (2014).
[13] R. Cheng, J. Xiao, Q. Niu, and A. Brataas, Phys. Rev. Lett. **113**, 057601 (2014).
[14] Y. Ohnuma, H. Adachi, E. Saitoh, and S. Maekawa, Phys. Rev. B **87**, 014423 (2013).
[15] G. E. W. Bauer, E. Saitoh, and B. J. van Wees, Nat. Mater. **11**, 391 (2012).
[16] K. Uchida, S. Takahashi, K. Harii, J. Ieda, W. Koshibae, K. Ando, S. Maekawa, and E. Saitoh, Nature (London) **455**, 778 (2008).
[17] J. Xiao, G. E. W. Bauer, K.-C. Uchida, E. Saitoh, and S. Maekawa, Phys. Rev. B **81**, 214418 (2010).

[18] H. Adachi, J.-I. Ohe, S. Takahashi, and S. Maekawa, Phys. Rev. B **83**, 094410 (2011).
[19] K. Uchida, J. Xiao, H. Adachi, J. Ohe, S. Takahashi, J. Ieda, T. Ota, Y. Kajiwara, H. Umezawa, H. Kawai, G. E. W. Bauer, S. Maekawa, and E. Saitoh, Nat. Mater. **9**, 894 (2010).
[20] J. Flipse, F. L. Bakker, A. Slachter, F. K. Dejene, and B. J. van Wees, Nat. Nanotechnol. **7**, 166 (2012).
[21] J. Flipse, F. K. Dejene, D. Wagenaar, G. E. W. Bauer, J. B. Youssef, and B. J. van Wees, Phys. Rev. Lett. **113**, 027601 (2014).
[22] S. Hoffman, K. Sato, and Y. Tserkovnyak, Phys. Rev. B **88**, 064408 (2013).
[23] Y. Tserkovnyak, A. Brataas, and G. E. W. Bauer, Phys. Rev. Lett. **88**, 117601 (2002).
[24] A. Brataas, Y. Tserkovnyak, G. E. W. Bauer, and B. I. Halperin, Phys. Rev. B **66**, 060404 (2002).
[25] Y. Tserkovnyak, A. Brataas, G. E. W. Bauer, and B. I. Halperin, Rev. Mod. Phys. **77**, 1375 (2005).
[26] S. Mizukami, Y. Ando, and T. Miyazaki, Jpn. J. Appl. Phys. **40**, 580 (2001).
[27] R. Urban, G. Woltersdorf, and B. Heinrich, Phys. Rev. Lett. **87**, 217204 (2001).
[28] J. Foros, A. Brataas, Y. Tserkovnyak, and G. E. W. Bauer, Phys. Rev. Lett. **95**, 016601 (2005).
[29] A. Kapelrud and A. Brataas, Phys. Rev. Lett. **111**, 097602 (2013).
[30] H. B. Callen and T. A. Welton, Phys. Rev. **83**, 34 (1951).
[31] C. G. Windsor and R. W. H. Stevenson, Proc. Phys. Soc., London **87**, 501 (1966).
[32] S. Klingler, A. V. Chumak, T. Mewes, B. Khodadadi, C. Mewes, C. Dubs, O. Surzhenko, B. Hillebrands, and A. Conca, J. Phys. D: Appl. Phys. **48**, 015001 (2015).

Paper V

"Intrinsic magnetization of antiferromagnetic textures"
Erlend G. Tveten, Tristan Müller, Jacob Linder, and Arne Brataas,
Physical Review B **93**, 104408 (2016).

Intrinsic magnetization of antiferromagnetic textures

Erlend G. Tveten,[1,*] Tristan Müller,[2] Jacob Linder,[1] and Arne Brataas[1]
[1]*Department of Physics, Norwegian University of Science and Technology, NO-7491 Trondheim, Norway*
[2]*JARA-Institute for Quantum Information, RWTH Aachen University, D-52074 Aachen, Germany*
(Received 22 June 2015; revised manuscript received 13 January 2016; published 9 March 2016)

Antiferromagnets (AFMs) exhibit intrinsic magnetization when the order parameter spatially varies. This intrinsic spin is present even at equilibrium and can be interpreted as a twisting of the homogeneous AFM into a state with a finite spin. Because magnetic moments couple directly to external magnetic fields, the intrinsic magnetization can alter the dynamics of antiferromagnetic textures under such influence. Starting from the discrete Heisenberg model, we derive the continuum limit of the free energy of AFMs in the exchange approximation and explicitly rederive that the spatial variation of the antiferromagnetic order parameter is associated with an intrinsic magnetization density. We calculate the magnetization profile of a domain wall and discuss how the intrinsic magnetization reacts to external forces. We show conclusively, both analytically and numerically, that a spatially inhomogeneous magnetic field can move and control the position of domain walls in AFMs. By comparing our model to a commonly used alternative parametrization procedure for the continuum fields, we show that the physical interpretations of these fields depend critically on the choice of parametrization procedure for the discrete-to-continuous transition. This can explain why a significant amount of recent studies of the dynamics of AFMs, including effective models that describe the motion of antiferromagnetic domain walls, have neglected the intrinsic spin of the textured order parameter.

DOI: 10.1103/PhysRevB.93.104408

I. INTRODUCTION

Measuring the ordered state of antiferromagnets (AFMs) is complicated by the absence of macroscopic magnetization. The promise of AFMs as candidates for active roles in spintronics logic elements have increased the interest in addressing this problem [1,2]. In particular, the observation of tunneling anisotropic magnetoresistance in AFMs [3–6] represents a clear experimental procedure to detect the antiferromagnetic order. Furthermore, current-induced torques on the antiferromagnetic order have been theoretically predicted [7–10] and experimentally indicated in spin valve systems [11]. Also, the ferromagnetic concept of spin pumping has been generalized to AFMs [12]. The possibility of manipulating the antiferromagnetic order parameter by external forces has fueled renewed theoretical interest in domain-wall motion in AFMs due to both charge [13–15] and spin [16–18] currents. However, the reports on current-induced domain-wall motion [19] are based on indirect observations and not confirmed by other methods or groups. Therefore, there is no straightforward method to reliably detect the dynamics of textures in the antiferromagnetic order.

In this paper, we discuss the intrinsic magnetization associated with an inhomogeneous antiferromagnetic order parameter. We describe the origin of the intrinsic spin and discuss whether it can be exploited to detect antiferromagnetic texture dynamics, e.g., domain-wall motion. To revisit this topic, which was pioneered for one-dimensional systems in Refs. [20–22], we construct the continuum free-energy functional for AFMs from the discrete Heisenberg Hamiltonian in the exchange approximation. We use the Hamiltonian approach to show that the intrinsic magnetization due to textures in the order parameter arises from a parity-breaking term in the energy functional that is absent in a commonly used alternative parametrization of the continuum fields. We clarify the mapping between the two different parametrizations and explain how the intrinsic magnetization can be easily missed in models which are based on the alternative parametrization. We further describe the shape of the intrinsic magnetization density for an antiferromagnetic domain wall and discuss its physical significance as a twisting of the homogeneous spinless AFM into a state with a finite spin. The intrinsic magnetization adds up in two- and three-dimensional extended domain-wall systems and can affect the dynamics of domain walls subject to external magnetic fields and spin-polarized currents. We discuss how these consequences can go beyond that of the purely quantum topological effects [23] observed in one-dimensional spin chains.

Studies of domains in AFMs and descriptions of the shape and properties of antiferromagnetic domain walls date back several decades [24–26]. However, most of the experimental evidence of such domains was restricted to studies of AFMs in which the collinearity of the sublattices is broken due to Dzyaloshinskii-Moriya (DM) anisotropy. In these studies, when the DM field or the external field vanishes, so does the equilibrium magnetization of the AFM. Consequently, the detection of domain walls and their dynamics in compensated AFMs remains an experimental challenge. However, antiferromagnetic domain walls are known to exist and have been experimentally observed, e.g., in monolayers of antiferromagnetic Fe [27], in the elemental AFM Cr [28], and in the antiferromagnetic insulator NiO [29]. Antiferromagnetic domains and domain walls can also be tailored by manipulating the ferrimagnetic precursor layer before cooling the AFM below the Néel temperature [30]. Observation of individual domains in AFMs can be done, e.g., using x-ray magnetic linear dichroism [31,32].

A key aspect of detecting the *dynamics* of antiferromagnetic domain walls is whether such solitons of staggered magnetic order are associated with a spatially constricted magnetization

*Corresponding author: erlend.tveten@ntnu.no

density. Reference [20] argued that such a magnetization exists and that the earlier studies of antiferromagnetic spin chains missed certain parity-breaking terms in the transition from the discrete spin model to the continuum approximation. The antiferromagnetic Heisenberg Hamiltonian has been mapped to the nonlinear σ model for the continuous staggered order parameter [24,25]. However, in Haldane's seminal work on large-spin Heisenberg AFMs [25], no apparent parity-breaking terms survived the transition to the continuum model. In *Haldane's mapping* [33,34], the continuum field that is conjugate to the antiferromagnetic order parameter describes the dynamic magnetization only (see Sec. II D). Using a slightly different parametrization of the antiferromagnetic order and the magnetization field, Ivanov *et al.* [21,22] later demonstrated that the energy functional based on the one-dimensional antiferromagnetic Heisenberg model indeed contains a parity-breaking term in the continuum limit and that this term must be taken into account to describe the equilibrium magnetization of a domain wall. The parity-breaking term included in Refs. [21,22] is not equivalent to the well-known "topological Θ terms" [35,36], which arise in effective σ-model Lagrangians for one-dimensional antiferromagnetic spin chains and are responsible for quantum effects such as Haldane's conjecture [25,33,36]. The recently increased interest in AFMs as active spintronics components has spawned a number of effective models for antiferromagnetic dynamics [13,15–18]. These recent models mostly adopt the nonlinear σ model without introducing a Hamiltonian that includes parity-breaking terms that lead to the intrinsic magnetization of antiferromagnetic textures. The absence of parity-breaking terms in these models may be due to different definitions of the continuum fields, or these terms may have been disregarded in the transition to the continuum limit due to specialized symmetry requirements, which only hold for homogeneous AFMs. Whether the intrinsic magnetization of extended two- and three-dimensional systems can lead to qualitatively new physics for the dynamics of antiferromagnetic textures under the influence of external forces remains an open question that we seek to address in this paper.

The intrinsic magnetization of antiferromagnetic textures is small. A domain wall in a one-dimensional antiferromagnetic spin chain exhibits intrinsic magnetization that is in total no larger than the spin of one sublattice [20,21]. It is therefore unlikely that such a small magnetic moment can be directly detected in the near future. However, the presence of the small spin of domain walls in one-dimensional spin chains manifests itself through quantum effects [23,37]. In higher-dimensional extended systems, such as synthetic AFMs, the magnetization of a textured multilayer may be of appreciable size [38]. Furthermore, in thin films or in bulk AFMs, which is the focus of our study, the intrinsic magnetization of a transverse domain wall is additive in the perpendicular directions. The result is a macroscopic magnetization that can be more easily excited and detected and that can influence the dynamics of AFMs beyond that of purely quantum effects.

The paper is organized as follows. In Sec. II, we take the continuum limit of the Heisenberg Hamiltonian, describe the origin of the intrinsic magnetization, and discuss the consequences for the antiferromagnetic dynamic equations. We also compare our model to Haldane's alternative mapping of the continuum fields. This comparison demonstrates that the continuum fields in these two parametrization procedures have critically different physical interpretations. In Sec. III, we describe the magnetization profile of a domain wall and discuss generalizations to higher-dimensionsal systems. We show how the intrinsic magnetization leads to qualitatively new physics and that the domain wall can be moved by a spatially inhomogeneous magnetic field that couples to the intrinsic magnetization. In Sec. IV, we present numerical results for the motion and control of an antiferromagnetic domain wall and show that we can create potential wells for the domain wall with spatially constricted magnetic fields. In Sec. V, we discuss the experimental consequences of the intrinsic magnetization for extended systems in two (2D) and three (3D) dimensions. Section VI concludes the discussion.

II. THEORY

Our starting point is the Heisenberg Hamiltonian due to the exchange coupling between classical spin vectors on a lattice [39]

$$H = J \sum_{\langle \boldsymbol{\alpha},\boldsymbol{\beta}\rangle} \mathbf{S}_{\boldsymbol{\alpha}} \cdot \mathbf{S}_{\boldsymbol{\beta}}, \tag{1}$$

where the positive exchange energy $J > 0$ describes an antiferromagnetic ground state. $\langle \boldsymbol{\alpha},\boldsymbol{\beta}\rangle$ denotes a sum over all nearest-neighbor lattice sites described by the two sublattices $\boldsymbol{\alpha}$ and $\boldsymbol{\beta}$, where each spin at $\boldsymbol{\alpha}$ has N_n nearest neighbors of type $\boldsymbol{\beta}$, and vice versa. $\boldsymbol{\alpha}$ and $\boldsymbol{\beta}$ are D-dimensional vectors, where D is the dimensionality of the AFM. We proceed by describing the simplest model, the $D = 1$ antiferromagnetic linear spin chain with easy-axis anisotropy, and later generalize our results to 2D and 3D in the Appendix. The focus of our subsequent sections is on extended 3D AFMs in which the order parameter varies along one dimension only.

A. Free-energy functional for 1D

We consider a linear spin chain with $2N$ atomic lattice sites, where the spins on half of the lattice sites, denoted by α, minimize their energy by pointing in the opposite direction of the spins on their $N_n = 2$ nearest-neighbor lattice sites, denoted by β, and vice versa. For the AFM, we impose the boundary conditions that the spin on the left end of the spin chain is of type α, whereas the right end of the chain is occupied by a β site. Therefore, in the ground state, the AFM is fully compensated, and the total spin vanishes. We define the z axis as the magnetic easy axis. The classical Heisenberg Hamiltonian including the easy-axis anisotropy is

$$H_{1\mathrm{D}} = J \sum_{\langle \alpha,\beta\rangle}^{N,N} \mathbf{S}_{\alpha} \cdot \mathbf{S}_{\beta} - K\left(\sum_{\alpha}^{N} S_{\alpha z}^2 + \sum_{\beta}^{N} S_{\beta z}^2\right), \tag{2}$$

where K is the anisotropy energy. In typical easy-axis AFMs, the exchange energy dominates, $|J| \gg |K|$. The classical ground state of the Hamiltonian (2) is degenerate, $(\mathbf{S}_{\alpha},\mathbf{S}_{\beta})_0 \rightarrow \pm(S\hat{z}, -S\hat{z})$, where S (in units of $\hbar$) is the spin on a single atomic lattice site. We now introduce the standard definitions (see Sec. II D for a comparison with an alternative definition that is occasionally mistaken to be equivalent to the present

model) of the magnetic and staggered order parameters $\mathbf{m}_i$ and $\mathbf{l}_i$ on a two-sublattice linear lattice parametrized by i:

$$\mathbf{m}_i = \frac{\mathbf{S}^i_\alpha + \mathbf{S}^i_\beta}{2S}, \tag{3a}$$

$$\mathbf{l}_i = \frac{\mathbf{S}^i_\alpha - \mathbf{S}^i_\beta}{2S}, \tag{3b}$$

where we have paired the sublattice spins $\mathbf{S}^i_\alpha$ and $\mathbf{S}^i_\beta$ at unit cell i running over a total of N antiferromagnetic unit cells. In this convention, $\mathbf{m}_i^2 + \mathbf{l}_i^2 = 1$ and the spins in unit cell i can be expressed as follows:

$$\mathbf{S}^i_\alpha = S(\mathbf{m}_i + \mathbf{l}_i), \tag{4a}$$

$$\mathbf{S}^i_\beta = S(\mathbf{m}_i - \mathbf{l}_i). \tag{4b}$$

After introducing the magnetization vector $\mathbf{m}_i$ and the staggered order parameter $\mathbf{l}_i$, the Heisenberg Hamiltonian (2) reduces to a sum over antiferromagnetic lattice points:

$$\begin{aligned} H_{1D} = {} & JS^2 \sum_i^{N-1} (\mathbf{m}_i - \mathbf{l}_i)[(\mathbf{m}_i + \mathbf{l}_i) + (\mathbf{m}_{i+1} + \mathbf{l}_{i+1})] \\ & + JS^2\left(\mathbf{m}_N^2 - \mathbf{l}_N^2\right) \\ & - KS^2 \sum_i^N \left[(\mathbf{m}_i + \mathbf{l}_i)_z^2 + (\mathbf{m}_i - \mathbf{l}_i)_z^2\right]. \end{aligned} \tag{5}$$

We continue by using the identities $2\mathbf{m}_i\mathbf{m}_{i+1} = \mathbf{m}_i^2 + \mathbf{m}_{i+1}^2 - (\mathbf{m}_{i+1} - \mathbf{m}_i)^2$ and $(\mathbf{l}_i\mathbf{m}_{i+1} - \mathbf{m}_i\mathbf{l}_{i+1}) = \mathbf{l}_i(\mathbf{m}_{i+1} - \mathbf{m}_i) - \mathbf{m}_i(\mathbf{l}_{i+1} - \mathbf{l}_i)$ to rewrite the bulk part of Eq. (5) as follows:

$$\begin{aligned} H_{1D} \approx {} & 2JS^2 \sum_i^N \left(\mathbf{m}_i^2 - \mathbf{l}_i^2\right) \\ & + \frac{JS^2}{2} \sum_i^{N-1} [(\mathbf{l}_{i+1} - \mathbf{l}_i)^2 - (\mathbf{m}_{i+1} - \mathbf{m}_i)^2] \\ & + JS^2 \sum_i^{N-1} [\mathbf{m}_i(\mathbf{l}_{i+1} - \mathbf{l}_i) - \mathbf{l}_i(\mathbf{m}_{i+1} - \mathbf{m}_i)] \\ & - 2KS^2 \sum_i^N \left(m_{i,z}^2 + l_{i,z}^2\right), \end{aligned} \tag{6}$$

where we have disregarded the vanishingly small energy contribution $-JS^2(\mathbf{m}_1^2 + \mathbf{m}_N^2 - \mathbf{n}_1^2 - \mathbf{n}_N^2)/2$ from the unit cells at the edges.

Next, we go to the large-N limit and take the continuum approximation, allowing us to write $H_{1D} \approx \int (d_i/\Delta)\mathcal{H}(\mathbf{l},\mathbf{l}',\mathbf{m},\mathbf{m}')$, where Δ is the length of the antiferromagnetic unit cell and $\mathbf{l}'$ and $\mathbf{m}'$ are the (dimensionless) spatial derivatives of the staggered field and the magnetization, respectively. d_i is an infinitesimal length element along the spin chain. For $D = 1$, $\Delta = 2d$, where d is the nearest-neighbor spacing in the linear chain. The energy density (apart from a constant and in units of energy) is

$$\begin{aligned} \mathcal{H}_{1D}(\mathbf{l},\mathbf{l}',\mathbf{m},\mathbf{m}') = {} & JS^2[4|\mathbf{m}|^2 + |\mathbf{l}'|^2 - |\mathbf{m}'|^2 \\ & + (\mathbf{m}\cdot\mathbf{l}' - \mathbf{l}\cdot\mathbf{m}')] - KS^2[(\mathbf{l}\cdot\hat{z})^2 + (\mathbf{m}\cdot\hat{z})^2]. \end{aligned} \tag{7}$$

We note that the fourth exchange term in Eq. (7) has an unusual parity-breaking form [35,40] and is an odd function of the order parameter $\mathbf{l}$.

In the models of AFMs that we consider, the two-sublattice linear lattice in 1D, the centered squared lattice in 2D, and the body-centered-cubic lattice in 3D, the Heisenberg Hamiltonian is not invariant under sublattice exchange ($\alpha \leftrightarrow \beta$) if the order parameter is spatially inhomogeneous (see Fig. 1). However, there is an ambiguity in the pairing of spins $\mathbf{S}^i_\alpha$ and $\mathbf{S}^i_\beta$ and the definition of the order parameter $\mathbf{l}_i$ in Eq. (3b). One might as well choose $\tilde{\mathbf{l}}_i = -\mathbf{l}_i$ as the order parameter, and consequently, one usually demands that the bulk Hamiltonian is invariant under the transformations $\mathbf{l}_i \to -\mathbf{l}_i$ and $\mathbf{m}_i \to \mathbf{m}_i$ [41] because the two possible choices of the order parameter are physically equivalent. Under these transformations, the definitions of $\mathbf{S}^i_\alpha$ and $\mathbf{S}^i_\beta$ in Eqs. (4) also change, and the fourth exchange term in Eq. (7) undergoes an additional sign change. The energy functional is therefore invariant with respect to the two equivalent definitions of the order parameter but not invariant under sublattice exchange. In the latter case, the ordering of the spins changes, resulting in a larger exchange energy penalty for inhomogeneous AFMs. A simplified sketch of this energy difference is shown in Fig. 1 for a 6-spin chain with a 90° texture. The permutation of the two sublattices α and β leads to a more disordered phase that costs additional exchange energy. This result generalizes to an arbitrary number of spins in a linear textured spin chain.

To describe the order-parameter dynamics of the AFM, it is useful to work in the exchange approximation [41] $|J| \gg |K|$ and consider slowly varying antiferromagnetic textures. In this case, $|\mathbf{m}|^2 \ll |\mathbf{l}|^2$, and we can disregard terms that are

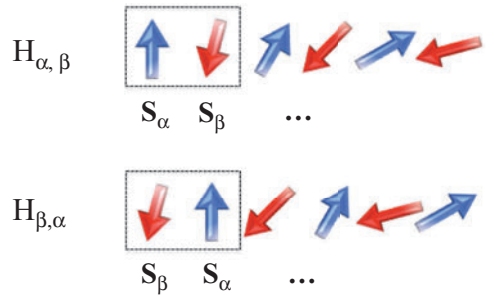

FIG. 1. For a simple linear spin chain with antiferromagnetic exchange coupling, the Heisenberg Hamiltonian is not invariant under sublattice exchange, $\mathbf{S}_\alpha \leftrightarrow \mathbf{S}_\beta$, if the order parameter is spatially inhomogeneous. (Top) A simplified sketch of a 6-spin 90° texture. Exchanging the spins on sublattices α and β (bottom) creates a more disordered phase that costs additional exchange energy, hence, $H_{\alpha,\beta} < H_{\beta,\alpha}$. In the continuum limit, this energy difference is captured by the parity-breaking term in the antiferromagnetic energy functional.

of higher order than $|\mathbf{m}|^2$, such as the magnetic anisotropy energy term and the magnetic stiffness term in Eq. (7). We choose the spin chain axis to be along the z axis and introduce the normalized staggered vector field $\mathbf{n}(z,t) \equiv \mathbf{l}(z,t)/|\mathbf{l}(z,t)|$. We can consequently write the energy density as a function of the deviations $\partial_z\mathbf{n}$ ($\equiv \partial\mathbf{n}/\partial z$) and $\mathbf{m}$ from the ground state. After integrating by parts, we arrive at the free-energy density for the linear antiferromagnetic spin chain to the lowest order in deviations from an equilibrium state [22]:

$$\mathcal{H}_{1D}(\mathbf{n},\partial_z\mathbf{n},\mathbf{m}) = \frac{a}{2}|\mathbf{m}|^2 + \frac{A}{2}|\partial_z\mathbf{n}|^2 + L(\mathbf{m}\cdot\partial_z\mathbf{n}) - \frac{K_z}{2}(\mathbf{n}\cdot\hat{z})^2 . \tag{8}$$

The equation has the following parameters: the homogeneous exchange energy $a = 8JS^2$, the exchange stiffness terms $A = \Delta^2 JS^2$ and $L = 2\Delta JS^2$, and the anisotropy energy $K_z = 2KS^2$. Here, a finite L lifts the degeneracy of the sublattice exchange.

B. Free-energy functional for $D > 1$

In the Appendix, we generalize the free energy of Eq. (8) to 2D and 3D for the centered squared and the body-centered-cubic unit cell, respectively. We find that the generalized free-energy density in the exchange approximation is given by

$$\mathcal{H}(\mathbf{n},\partial_i\mathbf{n},\mathbf{m}) = \frac{a}{2}|\mathbf{m}|^2 + \frac{A}{2}\left[\sum_i |\partial_i\mathbf{n}|^2 + \frac{1}{2}\sum_{i\neq j}(\partial_i\mathbf{n}\cdot\partial_j\mathbf{n})\right] + L\sum_i(\mathbf{m}\cdot\partial_i\mathbf{n}) - \frac{K_z}{2}(\mathbf{n}\cdot\hat{z})^2, \tag{9}$$

where $a = 4N_D JS^2$, $A = N_D\Delta^2 JS^2/2$, $L = N_D\Delta JS^2$, $K_z = 2KS^2$, and N_D is the number of nearest neighbors. $N_1 = 2$, $N_2 = 4$ for the squared lattice, and N_3 depends on the choice of unit cell, 6 for the simple cubic cell and 8 for the body-centered-cubic cell. The stiffness part of the above Hamiltonian density contains two apparent anisotropic terms: $\sim(\partial_i\mathbf{n}\cdot\partial_j\mathbf{n})$ and $\sim(\mathbf{m}\cdot\partial_i\mathbf{n})$. However, in the following, we show that after eliminating the degrees of freedom associated with $\mathbf{m}$, the effective Lagrangian reduces to the nonlinear σ model and the resulting antiferromagnetic spin-wave dispersion remains isotropic.

This isotropic dispersion is in contrast to the anisotropic dispersion relation resulting from the exchange term identified by Lifshitz and Pitaevskii [41], which is similar but not identical to the third term in Eq. (9). Lifshitz and Pitaevskii consider only the small deviation $\mathbf{n}_\perp$ ($\mathbf{n} \to \mathbf{n}_0 + \mathbf{n}_\perp$) from the equilibrium homogeneous antiferromagnetic spin configuration and add the exchange term $\sim(\mathbf{m}\cdot\partial_z\mathbf{n}_\perp - \mathbf{n}_\perp\cdot\partial_z\mathbf{m})$ to the free-energy density. Compared to Eq. (7), this also results in a surface anisotropy $\sim(\mathbf{n}_0\cdot\partial_z\mathbf{m})$, which (after integration over the space) favors magnetization buildup on the edges of the AFM. Consequently, the dispersion relation for this model is anisotropic. The parity-breaking exchange term ($\sim L$) in the above free-energy density (7) differs from the term of Lifshitz and Pitaevskii because it involves $\mathbf{n}$ rather than $\mathbf{n}_\perp$ and does not violate the isotropic dispersion relation of antiferromagnetic spin waves due to small variations in the staggered field $\mathbf{n}$. This is also the case for $D > 1$. Neglecting the parity-breaking term as being of leading order in the exchange energy would imply that an AFM at equilibrium exhibits no intrinsic magnetization, even when textures in the staggered field are present.

C. Lagrangian density and equations of motion

The equations of motion for the staggered field $\mathbf{n}$ and the magnetization field $\mathbf{m}$ can be found from, e.g., linear combinations of the equations of motion for the sublattice spins $\mathbf{S}_\alpha$ and $\mathbf{S}_\beta$ [20]. Equivalently, we may proceed by constructing the Lagrangian density and directly compute the dynamic equations for $\mathbf{n}$ and $\mathbf{m}$ from the variation of the Lagrangian with respect to these fields. Our starting point is the generalized free-energy density in the exchange approximation (9). The Lagrangian density can be constructed as $\mathcal{L} = \mathcal{K} - \mathcal{H}$, where $\mathcal{K}$ is the kinetic energy term. Analogous to the procedure for constructing the kinetic term for a single spin in a ferromagnet [42,43], $\mathcal{K}$ can be constructed from the Berry phase of the spin *pair* $\mathbf{S}_\alpha + \mathbf{S}_\beta$ that constitutes the antiferromagnetic unit cell:

$$\int \mathcal{K}\,dV = -S\hbar\left[\sum_\alpha \mathbf{A}_\alpha\cdot\dot{\mathbf{S}}_\alpha + \sum_\beta \mathbf{A}_\beta\cdot\dot{\mathbf{S}}_\beta\right], \tag{10}$$

where it is convenient to choose the gauge potential $\mathbf{A}_{\alpha(\beta)}$ such that the spin-pair Berry phase vanishes in the strictly antiparallel configuration $\mathbf{S}_\alpha = -\mathbf{S}_\beta$. One such choice is $\mathbf{A}_{\alpha(\beta)} = -\hat{\phi}_{\alpha(\beta)}\cos\theta_{\alpha(\beta)}/\sin\theta_{\alpha(\beta)}$ in the spherical coordinate system, where θ is the polar angle and $\hat{\phi}$ is a unit vector along the azimuth. This gauge is identical to that which is normally used to describe the kinetic energy of a single spin in ferromagnets [43] and generalized to a two-sublattice model with antiparallel spin configuration. By expanding the spin-pair Berry phase in small deviations from the antiparallel configuration, $\theta_\beta \to \pi - (\theta_\alpha + \delta\theta)$ and $\phi_\beta \to \pi + (\phi_\alpha + \delta\phi)$, and transferring back to the $[\mathbf{n},\mathbf{m}]$ basis, the kinetic term in the continuum approximation is given by [21,25]

$$\mathcal{K} = \rho\mathbf{m}(\dot{\mathbf{n}}\times\mathbf{n}), \tag{11}$$

where $\rho = 2S\hbar$ is the magnitude of the staggered spin angular momentum per unit cell and we have disregarded terms of the order $|\mathbf{m}|^4$ and higher.

Varying the Lagrangian with respect to the magnetization $\mathbf{m}$ and the staggered field $\mathbf{n}$ gives the coupled Landau-Lifshitz equations of motion

$$\dot{\mathbf{n}} = \omega_\mathbf{m}\times\mathbf{n}, \tag{12a}$$

$$\dot{\mathbf{m}} = \omega_\mathbf{n}\times\mathbf{n} + \omega_\mathbf{m}\times\mathbf{m}, \tag{12b}$$

where damping is typically phenomenologically introduced [13]. In the transverse basis, where $|\mathbf{n}|^2 = 1$, no term of the form $\sim(\omega_\mathbf{n}\times\mathbf{m})$ (as present in the dynamics of $\mathbf{l}$ in, e.g., Ref. [10]) appears in Eq. (12a), which is valid in the exchange approximation and includes terms up to second order in small deviations from equilibrium. The effective magnetic and staggered fields (in units of s^{-1}) are defined as functional

derivatives of the total free energy H:

$$\rho\omega_{\mathbf{m}} \equiv -\frac{\delta H}{\delta \mathbf{m}} = -a\mathbf{m} - L\partial^i \mathbf{n}, \tag{13a}$$

$$\rho\omega_{\mathbf{n}} \equiv -\frac{\delta H}{\delta \mathbf{n}} = A\left(\nabla^2\mathbf{n} + \frac{1}{2}\partial^i\partial^j\mathbf{n}\right) + L\partial^i\mathbf{m} + K_z(\mathbf{n}\cdot\hat{z})\hat{z}, \tag{13b}$$

where we have defined the sum over spatial derivatives in all directions as $\partial^i \equiv \sum_{i=x,y,z}\partial/\partial i$ and $\partial^i\partial^j \equiv \sum_{i\neq j}\partial^2/(\partial i\partial j)$. In the Appendix, we discuss how these anisotropic differential operators arise in 2D and 3D.

In the absence of external forces in the effective magnetic field, Eqs. (12a) and (13a) give [21]

$$\mathbf{m} = \frac{\rho}{a}\dot{\mathbf{n}}\times\mathbf{n} - \frac{L}{a}\partial^i\mathbf{n}, \tag{14}$$

which indicates that the magnetization field $\mathbf{m}$ is simply a slave variable that follows the temporal *and* spatial evolution of the staggered field $\mathbf{n}$. We note that if we neglect the parity-breaking term in the free energy ($L \to 0$), the intrinsic magnetization of a textured AFM vanishes at equilibrium. Our analysis shows that for our particular parametrization of the continuum fields, this parity-breaking term is an important part of the transition from the discrete spin model to the continuum approximation and cannot be disregarded.

Equation (14) allows us to eliminate $\mathbf{m}$ and write an effective Lagrangian density for the staggered field and its derivatives as

$$\mathcal{L}(\mathbf{n},\dot{\mathbf{n}},\partial_i\mathbf{n}) = \frac{\rho^2}{2a}|\dot{\mathbf{n}}|^2 - \frac{A - L^2/a}{2}\sum_i|\partial_i\mathbf{n}|^2 + \frac{\rho L}{a}\sum_i\partial_i\mathbf{n}\cdot(\mathbf{n}\times\dot{\mathbf{n}}) + \frac{K_z}{2}(\mathbf{n}\cdot\hat{z})^2. \tag{15}$$

This Lagrangian density describes the anisotropic nonlinear σ model with a kinetic topological term (third term) [25,40,44–47]. This topological term is a by-product of the elimination of $\mathbf{m}$ from the Lagrangian. It can be shown that this term has the form of a total derivative [40]. Consequently, it has no effect on the effective equations of motion for $\mathbf{n}$ or the domain-wall dynamics that we describe in the next sections. We will not discuss in any detail the quantum effects of the topological term in the following.

D. Comparison with Haldane's mapping

We digress for a moment to compare the one-dimensional model described above with a commonly used alternative definition of the continuum fields known as Haldane's mapping [25,33,34] of the antiferromagnetic order parameter. We include this comparison because the different parametrizations are not equivalent and are, therefore, recurrent sources for confusion. In contrast to the Hamiltonian approach described by Eqs. (3) and (4), Haldane's parametrization maps each spin in the spin chain at cite i onto two continuum fields:

$$\mathbf{S}_i/S = (-1)^i\tilde{\mathbf{n}}_i\sqrt{1-|\tilde{\mathbf{m}}_i|^2} + \tilde{\mathbf{m}}_i, \tag{16}$$

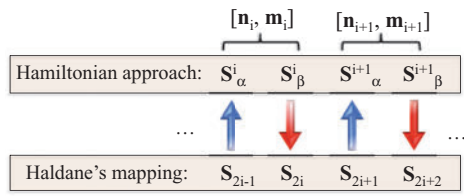

FIG. 2. In the Hamiltonian approach (top), Eqs. (3) define values for the staggered field $\mathbf{n}_i$ and the magnetization field $\mathbf{m}_i$ at the center of every antiferromagnetic unit cell labeled by i. In Haldane's mapping (bottom), every single spin is mapped onto two continuum fields: the Néel field $\tilde{\mathbf{n}}$ and the "canting" field $\tilde{\mathbf{m}}$.

where $\tilde{\mathbf{n}}$ is the unitary Néel field and $\tilde{\mathbf{m}}$ is the "canting" field. We note that this mapping introduces extra degrees of freedom, which must subsequently be reduced by limiting the Fourier components of the fields $\tilde{\mathbf{n}}$ and $\tilde{\mathbf{m}}$ to include only long-wavelength excitations [34].

Figure 2 compares the labeling of the spins in the Hamiltonian approach used in this work with that of Haldane's mapping. By equating the expressions for $\mathbf{S}^i_\alpha$ and $\mathbf{S}^i_\beta$ in Eqs. (4) and their corresponding expressions in Haldane's parametrization, we find the relationship between the continuum fields in the two different parametrizations:

$$\mathbf{m}_i + \mathbf{n}_i\sqrt{1-|\mathbf{m}_i|^2} = -\tilde{\mathbf{n}}_{2i-1}\sqrt{1-|\tilde{\mathbf{m}}_{2i-1}|^2} + \tilde{\mathbf{m}}_{2i-1}, \tag{17a}$$

$$\mathbf{m}_i - \mathbf{n}_i\sqrt{1-|\mathbf{m}_i|^2} = \tilde{\mathbf{n}}_{2i}\sqrt{1-|\tilde{\mathbf{m}}_{2i}|^2} + \tilde{\mathbf{m}}_{2i}. \tag{17b}$$

In the exchange approximation, $\mathbf{m} \ll \mathbf{n}$ and $\tilde{\mathbf{m}} \ll \tilde{\mathbf{n}}$. Keeping only the lowest-order contributions in the magnetization $\mathbf{m}$ and the canting field $\tilde{\mathbf{m}}$, it follows that

$$\mathbf{n}_i \approx -\tfrac{1}{2}(\tilde{\mathbf{n}}_{2i-1} + \tilde{\mathbf{n}}_{2i}) + \tfrac{1}{2}(\tilde{\mathbf{m}}_{2i-1} - \tilde{\mathbf{m}}_{2i}), \tag{18a}$$

$$\mathbf{m}_i \approx -\tfrac{1}{2}(\tilde{\mathbf{n}}_{2i-1} - \tilde{\mathbf{n}}_{2i}) + \tfrac{1}{2}(\tilde{\mathbf{m}}_{2i-1} + \tilde{\mathbf{m}}_{2i}), \tag{18b}$$

where we have disregarded terms of the order $|\mathbf{m}|^2$ and $|\tilde{\mathbf{m}}|^2$ and higher.

For small-angle spatial variations in the continuum fields, we use the gradient approximation to find the field values for $\tilde{\mathbf{n}}$ and $\tilde{\mathbf{m}}$ at the center of each unit cell: $\tilde{\mathbf{n}}_{i+1/2} \approx \tilde{\mathbf{n}}_i + (\Delta/4)\partial_z\tilde{\mathbf{n}}_i$ and $\tilde{\mathbf{m}}_{i+1/2} \approx \tilde{\mathbf{m}}_i + (\Delta/4)\partial_z\tilde{\mathbf{m}}_i$, where $\Delta/2 = d$ is the nearest-neighbor distance and $\tilde{\mathbf{n}}(\tilde{\mathbf{m}})_{i+1/2}$ represents the Néel (canting) field at the midpoint between the spins $\mathbf{S}_i$ and $\mathbf{S}_{i+1}$. Inserting these lowest-order gradient approximations into Eqs. (18) results in a one-to-one relationship between the continuum fields of the Hamiltonian approach and Haldane's parametrization. Correspondingly, the mapping between the two different representations reduces to $\mathbf{n} \to -\tilde{\mathbf{n}} + (\Delta/4)\partial_z\tilde{\mathbf{m}} + \mathcal{O}(|\tilde{\mathbf{m}}|^2)$ and $\mathbf{m} \to \tilde{\mathbf{m}} - (\Delta/4)\partial_z\tilde{\mathbf{n}} + \mathcal{O}(|\tilde{\mathbf{m}}|^2)$.

It is critically important that the continuum fields $\tilde{\mathbf{n}}$ and $\tilde{\mathbf{m}}$ of Haldane's mapping are not identical to the staggered and magnetization fields $\mathbf{n}$ and $\mathbf{m}$ used in this work. By inserting the mapping between the two parametrizations into the energy functional in Eq. (8) and keeping only terms of the order $|\tilde{\mathbf{m}}|^2$ in the exchange approximation, we find the continuum limit

energy functional of Haldane's mapping:

$$\mathcal{H}_{\rm Hal}(\tilde{\mathbf{n}},\partial_z\tilde{\mathbf{n}},\tilde{\mathbf{m}}) = \frac{a}{2}|\tilde{\mathbf{m}}|^2 + \frac{A}{2}|\partial_z\tilde{\mathbf{n}}|^2 - \frac{K_z}{2}(\tilde{\mathbf{n}}\cdot\hat{z})^2. \quad (19)$$

This result conclusively shows that the parity-breaking exchange term in Eq. (8), which is a result of the procedure of breaking the lattice into spin pairs, vanishes after a suitable transformation of the continuum fields, e.g., $\mathbf{m} \to \tilde{\mathbf{m}} - (\Delta/4)\partial_z\tilde{\mathbf{n}}$. In other words, when applying Haldane's mapping procedure, the parity-breaking exchange term does not appear in the energy functional. An overall requirement, however, is that the physics remains the same, including the existence of the intrinsic magnetization.

Although the Hamiltonian approach used in this work and Haldane's mapping are both valid continuum representations of spin systems with antiferromagnetic exchange coupling, a crucial difference exists for the physical interpretations of the continuum fields, which are *not* equivalent in the two representations. The equilibrium value of the canting field $\tilde{\mathbf{m}}$ of Haldane's mapping vanishes, also when $\tilde{\mathbf{n}}$ is inhomogeneous. Therefore, $\tilde{\mathbf{m}}$ represents the dynamic magnetization induced by temporal variations of the order parameter $\tilde{\mathbf{n}}$ and not the total magnetization. Consequently, the coupled equations of motion for $\tilde{\mathbf{n}}$ and $\tilde{\mathbf{m}}$ are not of the same form as Eqs. (12) and (13). In particular, the expression for the canting field $\tilde{\mathbf{m}} \sim \dot{\tilde{\mathbf{n}}} \times \tilde{\mathbf{n}}$, which is analogous to Eq. (14), does not include a term proportional to the gradient of $\tilde{\mathbf{n}}$. This fact may be an important reason why the intrinsic magnetization is easily missed in models based on Haldane's mapping.

In the Hamiltonian approach, on the other hand, $\mathbf{m}$ can be interpreted as a magnetization density in the sense that the total accumulated spin (both intrinsic and dynamical) of the AFM can be found from integration, $\mathbf{M}/S = \int \mathbf{m}\, dV$. For antiferromagnetic textures, this integral is generally nonzero even for static spin systems. Although the canting field $\tilde{\mathbf{m}}$ in Haldane's mapping does not include the intrinsic contribution to the magnetization density, the total spin can instead be found from the relation $\mathbf{M}/S \approx \sum_{i=1}^{2N}[(-1)^i\tilde{\mathbf{n}}(z_i) + \tilde{\mathbf{m}}(z_i)]$. The intrinsic magnetization can be identified as arising from the first terms in the sum. For a slowly varying $\tilde{\mathbf{n}}$ in, e.g., the $\hat{z}$ direction, $\sum_{i=1}^{2N}(-1)^i\tilde{\mathbf{n}}(z_i)\cdot\hat{z} \approx [\tilde{n}_z(z_1) - \tilde{n}_z(z_{2N})]/2$ [44], which is generally nonzero for textured AFMs. In the following analysis, we continue using the Hamiltonian approach, in which the continuum field $\mathbf{m}$ is interpreted as the total magnetization density.

E. Antiferromagnetic spin waves and spin current

To study small harmonic excitations from a homogeneous AFM, we construct the effective equation of motion for the staggered vector field $\mathbf{n}$ by combining Eqs. (12a) and (12b) while retaining the constraint $|\mathbf{n}|^2 = 1$:

$$\mathbf{n}\times(\ddot{\mathbf{n}}\times\mathbf{n}) = \frac{1}{\rho^2}\mathbf{n}\times[(aA - L^2)\nabla^2\mathbf{n} + aK_z(\mathbf{n}\cdot\hat{z})\hat{z}]\times\mathbf{n}. \quad (20)$$

The parity-breaking exchange term leads to the renormalization of the exchange stiffness $A \to A^* = (A - L^2/a) = A/2$ but otherwise leaves the equation of motion (20) invariant in linear response [48]. The topological term in Eq. (15) has no effect on the effective equations of motion for $\mathbf{n}$, as expected.

Insertion of a small harmonic excitation from the ground state in time and space $\mathbf{n}(\mathbf{r},t) \to \hat{z} + \delta\mathbf{n}_\perp \exp[i(\omega t - \mathbf{k}\cdot\mathbf{r})]$ into Eq. (20) results in the usual "relativistic" antiferromagnetic dispersion relation

$$\omega^2 = \frac{1}{\rho^2}[aA^*k^2 + aK_z], \quad (21)$$

where $k = |\mathbf{k}|$. In the isotropic limit $K_z \to 0$, which results in the familiar linear dispersion

$$\omega_i = ck, \quad (22)$$

where $c = N_D S J \Delta/(2\hbar)$ is the spin-wave phase velocity. For $\Delta = 2d/\sqrt{D}$, where d is the nearest-neighbor distance, and for hypercubic lattices, where $N_D = 2D$, Eq. (22) agrees with Eqs. (13) and (20) in the semiclassical treatment in Ref. [39], as well as with Holstein-Primakoff calculations [49,50] and Haldane's $D = 1$ result [25]. We note that the parity-breaking term ($\sim L$) does not lead to an anisotropic dispersion relation, such as the term in Lifshitz and Pitaevskii [41]. On the contrary, the inclusion of such a term is important to arrive at the correct dispersion relation in the classical continuum limit.

The intrinsic magnetic moment of antiferromagnetic textures will necessarily influence how spin currents in inhomogeneous AFMs are described. A continuity equation for the spin angular momentum transfer in the AFM caused by the exchange interaction can be constructed from Eq. (12b) as $\rho\dot{\mathbf{m}} + \sum_i \partial_i \mathbf{J}_{s,i} = 0$. The spin current polarized along i is

$$\mathbf{J}_{s,i} = A^*\partial_i\mathbf{n}\times\mathbf{n} - \frac{\rho L}{a}\dot{\mathbf{n}}, \quad (23)$$

where we have used Eq. (14) to eliminate $\mathbf{m}$. Equation (23) explicitly shows that a time-varying antiferromagnetic texture is equivalent to spin angular momentum transfer, a relationship that can be missed by models for the staggered dynamics that disregard the intrinsic magnetization. This result may have implications for antiferromagnetic spin pumping from textures [12] because the collective motion of the antiferromagnetic order parameter is equivalent to a current of spin angular momentum. In one-dimensional textures, $\rho L/a = S\hbar d$, thus indicating that textures that oscillate at frequency T^{-1} produce a spin-current corresponding approximately to a single spin moving one lattice spacing per period of oscillation T.

F. Consequences for staggered dynamics

In effective models for the dynamics of the staggered vector field $\mathbf{n}$, the magnetization field $\mathbf{m}$ plays the role of a slave variable that follows the temporal and spatial evolution of $\mathbf{n}$. When no external forces couple directly to the intrinsic spin in the AFM, the parity-breaking term in the energy functional ($\sim L$) only leads to a renormalization of the exchange stiffness and has no other effect on the dynamic equations. However, we show in the following that by including external magnetic fields or spin-polarized currents, the dynamics of the antiferromagnetic order parameter can also be altered indirectly through the excitation of the magnetization density field $\mathbf{m}$.

The spin-transfer torque on *ferromagnetic* textures is normally considered a second-order effect in AFMs when acting only on the small magnetization $\mathbf{m}(t)$ induced by the time

variation of the staggered field $\dot{\mathbf{n}}$. If AFMs also exhibit intrinsic magnetization, the spin-transfer torque from spin-polarized currents on the magnetization $\mathbf{m}$ may become more important. However, because the magnetization is first order in the spatial variation of the staggered field $\mathbf{m} \sim \partial_i \mathbf{n}$, the Berger spin-transfer torques [Eqs. (5) and (6) in Ref. [51]] are of the order $\sqrt{K/J}$ smaller than the driving forces acting directly on textures in the staggered field, first identified in Ref. [16]. In this case, the intrinsic magnetization of AFMs leads to higher-order corrections to the current-induced torques that couple directly to the staggered field. In antiferromagnetic thin films with strong surface anisotropy or in special cases in which a strained geometry suppresses the torques on the staggered field, the Berger torques on the textured magnetization could become important. We will not discuss the effects of spin-polarized currents any further in the following.

Instead, we focus on the effect of an external magnetic field $\mathbf{H}$ that couples directly to the intrinsic magnetization of antiferromagnetic textures. To illustrate this phenomenon, we add the Zeeman interaction to the free-energy density $\mathcal{H}_{\mathbf{H}} = \mathcal{H} - \rho\gamma(\mathbf{H}\cdot\mathbf{m})$, where γ is the gyromagnetic ratio. The external magnetic field induces a small magnetic moment density in the AFM, and the magnetization field $\mathbf{m}$ is altered according to

$$\mathbf{m} = \frac{\rho}{a}\dot{\mathbf{n}}\times\mathbf{n} - \frac{L}{a}\partial^i\mathbf{n} + \frac{\gamma\rho}{a}\mathbf{n}\times(\mathbf{H}\times\mathbf{n}), \tag{24}$$

where the cross products enforce the constraint $\mathbf{n}\cdot\mathbf{m} = 0$. Inserting this result in the Lagrangian gives the effective Lagrangian density for an AFM under the influence of an external magnetic field $\mathbf{H}$:

$$\begin{aligned}\mathcal{L}_{\mathbf{H}} = {} & \frac{\rho^2}{2a}(\dot{\mathbf{n}} - \gamma\mathbf{H}\times\mathbf{n})^2 - \frac{A^*}{2}\sum_i(\partial_i\mathbf{n})^2 \\ & + \frac{K_z}{2}(\mathbf{n}\cdot\hat{z})^2 + \frac{\rho L}{a}\sum_i \partial_i\mathbf{n}\cdot(\mathbf{n}\times\dot{\mathbf{n}}) \\ & - \frac{\gamma\rho L}{a}\sum_i \mathbf{H}\cdot\partial_i\mathbf{n}.\end{aligned} \tag{25}$$

This Lagrangian density agrees with that proposed in Ref. [48], with the exception of the second to last topological term and the last term, which couples the external magnetic field and textures in the antiferromagnetic order. In the following, we show how this coupling between magnetic fields and the gradient of the staggered field allows the movement of domain walls in AFMs to be controlled by spatially varying magnetic fields. This result has not been reported previously.

Utilizing the method of collective coordinates [15,52], we assume that the temporal dependence of the staggered vector field $\mathbf{n}(\mathbf{r},t)$ is held by a set of coordinates $\{a_j(t)\}$ that describe the time evolution of textures in the AFM, such that $\mathbf{n}(\mathbf{r},\{a_j(t)\})$. In this case, the time derivative of the staggered field can be written as $\dot{\mathbf{n}} = \sum_j \dot{a}_j\partial_{a_j}\mathbf{n}$. We earlier demonstrated that in AFMs, the collective coordinates can be viewed as quasiparticles with an effective mass reacting to external forces and following Newton's second law [15]. The equation of motion for the collective mode a_j is

$$M^{ij}\left(\ddot{a}_j + \frac{a\alpha}{\rho}\dot{a}_j\right) = F^i, \tag{26}$$

where $M^{ij} = (\rho^2/a)\int dV(\partial_{a_i}\mathbf{n}\cdot\partial_{a_j}\mathbf{n})$ is the effective mass, α is the phenomenological Gilbert damping parameter for AFMs, and F^i are the forces that act on the collective excitations. $F^i = F^i_{\text{int}} + F^i_{\text{ext}}$ can be split into the internal exchange forces $F^i_{\text{int}} = \partial_{a_i}H$, which are derivatives of the free energy with respect to the collective modes, and the external forces F^i_{ext}. We focus here on an external magnetic field as the only external force that acts on the AFM, giving

$$F^i_{\text{ext}} = \frac{\rho\gamma}{a}\int dV[\rho\dot{\mathbf{H}}\cdot(\mathbf{n}\times\partial_{a_i}\mathbf{n}) + L(\partial_{a_i}\mathbf{n}\cdot\partial^i\mathbf{H})], \tag{27}$$

where, in addition to the previously identified reactive force on the collective coordinates in AFMs due to time-varying magnetic fields [15], we now identify a new force induced by a spatially inhomogeneous magnetic field. This force will necessarily influence how antiferromagnetic textures are excited by external magnetic fields.

III. DOMAIN-WALL DYNAMICS

In this section, we return to systems where the order parameter varies along one dimension and discuss how the intrinsic magnetization influences the motion and detection of solitons in quasi-one-dimensional AFMs. Although the texture is assumed to vary only along one direction, the nearest neighbors to each spin may also exist along two (2D) or three (3D) axes. Later, we show how a Néel domain wall can be accelerated and controlled by a stationary and spatially inhomogeneous magnetic field.

A. Antiferromagnetic domain walls

In one-dimensional spin chains, the spatial variation of the staggered field $\mathbf{n}$ is constricted to the spin-chain axis $\hat{z}$. At equilibrium, the time evolution of the staggered field and the magnetization vanishes, $\dot{\mathbf{n}} = 0$ and $\dot{\mathbf{m}} = 0$, and Eq. (20) gives

$$\mathbf{n}_0\times\left[A^*\partial_z^2\mathbf{n}_0 + K_z(\mathbf{n}_0\cdot\hat{z})\hat{z}\right]\times\mathbf{n}_0 = 0. \tag{28}$$

By introducing spherical coordinates for the normalized staggered vector field as $\mathbf{n}_0(z) = [\sin\theta_0\cos\phi_0, \sin\theta_0\sin\phi_0, \cos\theta_0]$, a series of solutions for the above equation can be found from

$$\partial_z\phi_0 = 0, \tag{29a}$$

$$\partial_z^2\theta_0 = \frac{1}{\lambda^2}\sin\theta_0\cos\theta_0, \tag{29b}$$

where $\lambda = \sqrt{A^*/K_z}$. The trivial solution to Eqs. (29) is $\theta_0(z,t)\to 0$, which corresponds to a homogeneous AFM where all the spins are polarized along the positive/negative z direction. The excited state is given by $\theta_0 = 2\arctan[\exp(z/\lambda)]$, the Walker domain wall [53]. In this Néel configuration, $\sin\theta_0 = \pm\text{sech}(z/\lambda)$ and $\cos\theta_0 = \pm\tanh(z/\lambda)$, which ensures that $\mathbf{n}_0^2 = 1$. λ is the half-width of the domain wall. Inserting the results from the Heisenberg model, we find that the domain-wall half-width $\lambda = d\sqrt{J/K}$ is given

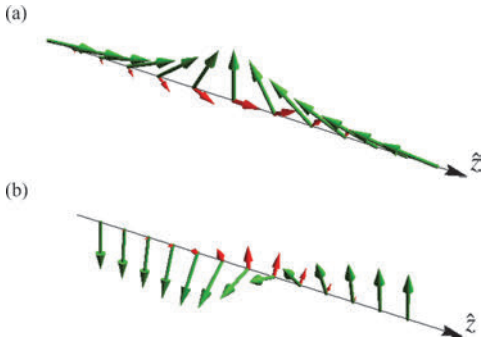

FIG. 3. Sketch of the intrinsic magnetization $\mathbf{m}(z)$ (red) (not to scale) of one-dimensional (a) Néel and (b) Bloch (not used in the calculations) domain walls in the order parameter $\mathbf{n}(z)$ (green). The equilibrium magnetization profile was calculated from Eq. (14). We note that the magnetization is so small that in a one-dimensional system, the domain-wall spin must be treated quantum mechanically. However, for higher-dimensional extended systems, the total spin of domain walls could be of appreciable size because the intrinsic magnetization is additive in the perpendicular directions.

by a competition between the exchange and anisotropy energy scales, as expected.

The intrinsic magnetization associated with the antiferromagnetic domain wall at equilibrium is given by Eq. (14) when $\dot{\mathbf{n}} = 0$:

$$\mathbf{m}_0 = -\frac{L}{a}\partial_z \mathbf{n}_0 = \pm\frac{d}{2\lambda}\begin{bmatrix} \mathrm{sech}(z/\lambda)\tanh(z/\lambda)\cos\phi_0 \\ \mathrm{sech}(z/\lambda)\tanh(z/\lambda)\sin\phi_0 \\ -\mathrm{sech}^2(z/\lambda)\end{bmatrix}, \quad (30)$$

where the sign determines whether the Néel domain wall is head-to-head or tail-to-tail. The magnetization profile of a head-to-head Néel domain wall and the profile of an antiferromagnetic Bloch domain wall are presented in Fig. 3. The total magnetic moment in the z direction contained in a head-to-head domain wall configuration is [20,21]

$$M_z^{\mathrm{dw}} = \frac{S}{d}\int dz(\mathbf{m}_0\cdot\hat{z}) = S. \quad (31)$$

This result demonstrates that domain walls in the antiferromagnetic order induce a finite magnetization proportional to the spatial derivative of the staggered field and that the direction of the magnetization depends crucially on the boundary conditions of the AFM, e.g., in the case of the Néel wall whether it is head-to-head or tail-to-tail. This result is intuitively easy to appreciate: because both edge spins (at an α and β site) point in the same direction, the 180° twist turns the homogeneous spinless AFM into a spin-S object. The domain wall is a nonlinear excitation of the homogeneous AFM and carries the spin S. The creation of a domain wall can therefore be interpreted as a twisting of the homogeneous spinless AFM into a configuration with a finite spin S that is located around the domain-wall center.

A consequence of the intrinsic magnetization of domain walls in one-dimensional spin chains is that for AFMs with half-integer S, the ground state, which is doubly degenerate, occurs for stationary domain walls [21,37] and not for precessing domain walls, as predicted in Ref. [25]. Another consequence is that the motion of domain walls in AFMs is equivalent to spin angular momentum transfer, as confirmed by Eq. (23). The identification of antiferromagnetic domain walls as single-spin carriers may become important for future applications in antiferromagnetic spintronics.

B. Domain-wall motion

We consider a (slowly) moving tail-to-tail domain-wall profile $\mathbf{n}[z,a_n(t)]$ corresponding to the dynamic soliton solution $\theta(z,t) \to 2\arctan(\exp\{[z - r_w(t)]/\lambda\})$ and $\phi(t) \to \phi_w(t)$. The domain-wall shape is assumed to be rigid, so that the temporal dynamics is held by the collective coordinates $\{a_n(t)\} \to \{\phi_w(t), r_w(t)\}$, the domain-wall tilt angle with respect to the x-z plane, and the position of the domain-wall center, respectively. Dissipation in AFMs is typically added in a phenomenological manner [13,18] and is naturally incorporated in the collective coordinate approach [15]. We add to the system a spatially varying magnetic field in the $\hat{z}$ direction, $\mathbf{H} = \{0,0,H_z(z)\}$. To the lowest order in the small external field and the velocities $\dot{\phi}_w$ and $\dot{r}_w$, we find that $\ddot{\phi}_w$ vanishes (although a constant precession $\dot{\phi}_w \neq 0$ is allowed in one-dimensional easy-axis systems) and that the domain-wall center coordinate is accelerated according to

$$\ddot{r}_w + \frac{a\alpha}{\rho}\dot{r}_w = -\frac{\gamma L}{\pi\rho\lambda}H_z^{\mathrm{int}}, \quad (32)$$

where α is the dimensionless Gilbert damping parameter of the AFM. Depending on the spatial profile of the magnetic field in the vicinity of the domain wall, the center coordinate will feel a force. The integrated magnetic field contribution is

$$H_z^{\mathrm{int}} = \int dz\left[\mathrm{sech}\left(\frac{z-r_w}{\lambda}\right)\tanh\left(\frac{z-r_w}{\lambda}\right)H_z(z)\right], \quad (33)$$

where any noneven profile $H_z(z)$ around the domain-wall center coordinate r_w gives rise to a finite acceleration of the domain wall. A homogeneous magnetic field does not accelerate the domain wall. In the steady state, the domain-wall velocity saturates at $\dot{r}_w = \gamma L H_z^{\mathrm{int}}/(\pi a\alpha\lambda)$. We note that the domain-wall velocity depends on the spatial distribution of the external magnetic field. This dependence opens up the possibility that nanoscale magnetic probes can accurately control the position of domain walls in, e.g., antiferromagnetic nanowires. In particular, a spatially constricted magnetic field can act as a potential well for the domain wall. In two-dimensional antiferromagnetic thin films, a spatially concentrated magnetic probe may attract spins from the edges of the AFM to form vortex states (see Sec. V).

IV. NUMERICAL RESULTS

To conceptually test the effect of a spatially inhomogeneous magnetic field on the dynamics of an antiferromagnetic domain wall, we have conducted numerical simulations of generalized versions of Eqs. (12a) and (12b) in which we have phenomenologically included dissipation as in Ref. [13]. We write the equations of motion in dimensionless form by scaling the time axis by $\tilde{t} = \rho/K_z$ and the spatial axis by

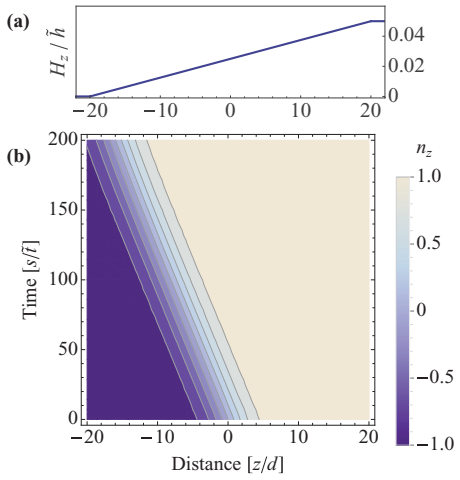

FIG. 4. (a) Magnetic field strength as a function of distance along the spin chain. The magnetic field has a constant gradient of approximately 0.4 mT per lattice constant. (b) Time evolution of an antiferromagnetic domain wall moved by the magnetic field gradient. For clarity, only the region $z\,\epsilon[-25,25]$ is shown. The domain wall slows down due to the finite dissipation when it reaches the region of the homogeneous external field. The maximum magnetic field strength is $H^{\max} \approx 10$ mT, and the Gilbert damping constant is set to $\alpha = 0.01$.

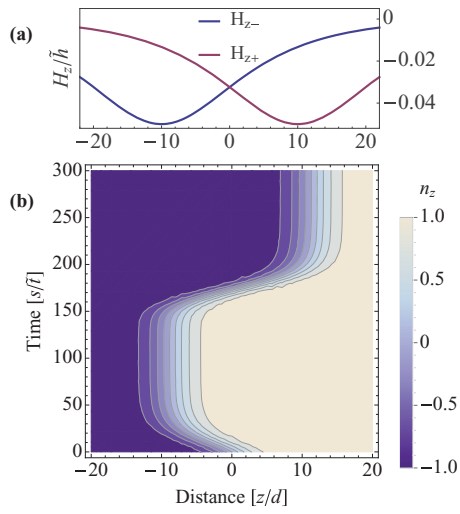

FIG. 5. (a) Magnetic field potential wells as a function of distance along the spin chain. (b) Time evolution of an antiferromagnetic domain wall controlled by the magnetic field potential wells. At $t = 0$, the domain wall is attracted toward a potential well at $z_- = -10$ due to a spatially concentrated magnetic field in the $\hat{z}$ direction with the spatial profile $H_z = H_0 \mathrm{sech}[(z - z_-)/10]\hat{z}$. In the time interval $t = 140 \rightarrow 160$, the potential well to the left is turned off, and a similar magnetic field-induced potential well is turned on to the right at $z_+ = 10$.

the nearest-neighbor distance d. We solve the dimensionless equations of motion using the numerical method of lines with an adaptive time control. The system size is $z\,\epsilon[-500,500]$ with the boundary conditions that $n_z(-500) = -1$ and $n_z(500) = 1$.

Although domain walls in insulating AFMs, such as NiO, are approximately 100 nm wide [29], we consider here the much shorter and more technologically important domain walls observed in antiferromagnetic Fe monolayers on W(001) [27], for which the geometric anisotropy is considerably larger. In such systems, the domain-wall widths are only a few lattice spacings and the intrinsic magnetization is therefore relatively more important. For spin-$\frac{1}{2}$ particles, for which the anisotropy energy per atom is 2.4 meV [54], the time unit $\tilde{t} \approx 1$ ps, the velocity unit $\tilde{v} = d/\tilde{t} \approx 300$ ms^{-1}, and the external field unit $\tilde{h} = \rho\gamma/K_z \approx 0.3$ T.

Figure 4 presents the motion of a domain-wall with half-width $\lambda = 4d$ due to a constant magnetic field gradient. Because the domain-wall spin in this particular Néel domain wall is $-S$, the wall drifts toward lower magnetic fields to minimize its energy. The domain wall quickly reaches a steady-state velocity of approximately 50 ms^{-1}. Figure 5 presents how spatially concentrated magnetic fields can control and pin the position of the domain wall. By switching the pinning potential from the left to the right side of the domain wall, the position of the wall can be accurately controlled. The velocity of the center coordinate reaches more than 100 ms^{-1}, and the transition from the left to the right pinning potential occurs in less than 100 ps.

V. HIGHER-DIMENSIONAL EXTENDED SYSTEMS

In this section, we discuss the possible experimental consequences for higher-dimensional textured systems, which typically extend in one or two perpendicular directions to the texture gradient axis. In such systems, the intrinsic magnetization can add up to a macroscopic number that is much larger than the spin on one atomic site. We also discuss the intrinsic magnetization of vortex states of the staggered order, which are two-dimensional analogs of the domain wall in the one-dimensional spin chain. At the end, we briefly discuss the effects of pinning sites on the domain-wall dynamics.

A. Antiferromagnetic vortex states

For $D = 2$ and in quasi-two-dimensional systems, such as antiferromagnetic thin films, nontrivial topological objects such as vortices [55] can form due to DM fields or external pinning. Figure 6 shows the intrinsic magnetization $\mathbf{m}(x,y)$ associated with the spatially inhomogeneous staggered vector field of such a two-dimensional object. The magnetization profile is calculated from Eq. (14). We note that the intrinsic spin of the vortex structure can be interpreted as a twisting of the spins in the homogeneous spinless AFM induced by spin rotations on the corners into a state with a finite spin located around the vortex core. The staggered vector field $\mathbf{n}(x,y)$ of this type of vortex structure is rotationally invariant around the vortex core along an axis normal to the x-y plane. The underlying spin structure, however, is not rotationally

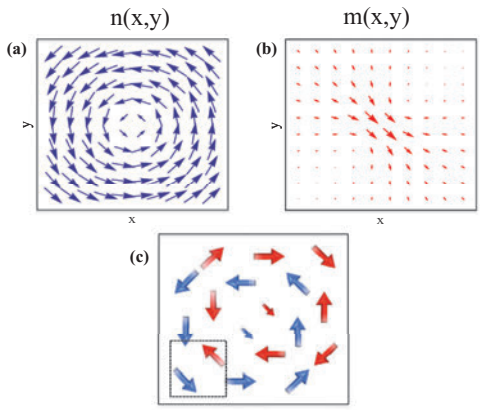

FIG. 6. (a) Sketch of a two-dimensional antiferromagnetic vortex structure in the staggered order parameter $\mathbf{n}(x,y)$ (blue vector field). The portions of the staggered field pointing in the perpendicular direction close to the vortex core have been omitted for clarity. (b) The resulting magnetization density profile $\mathbf{m}(x,y)$ (red vector field, not to scale) of the vortex state, calculated from Eq. (14). This intrinsic magnetization can be interpreted as a rearrangement of the spins on the corners so that the center of the vortex structure acquires a finite spin. (c) A simplified sketch of a vortex structure with six spins along each edge ordered in centered squared unit cells with α (blue arrows) and β (red arrows) sites. Although the vortex structure in the continuous staggered field appears invariant under the rotation of an arbitrary angle around the vortex core, the underlying spin structure is only invariant under axis inversion $[\hat{x},\hat{y}] \rightarrow [-\hat{x},-\hat{y}]$. The total integrated spin of the vortex structure is S, such as for the one-dimensional domain wall. The direction of this intrinsic spin is determined by the boundary conditions of the AFM.

invariant, which is captured by the finite magnetization density $\mathbf{m}(x,y)$ of the vortex. The total spin of the vortex is S, as in the case of a domain wall, and the direction of the intrinsic spin depends crucially on the boundary conditions of the AFM, e.g., induced via exchange bias pinning to ferromagnetic neighbors.

The topological term in the effective Lagrangian density (15) for the staggered vector field $\mathbf{n}$ can possibly indirectly influence the dynamics of two-dimensional objects in the order parameter such as vortices or skyrmions. However, the complex two-dimensional dynamics of such topological objects is beyond the scope of this paper and will not be discussed further.

B. Extended domain walls in 2D and 3D

Because the intrinsic spin of one-dimensional domain walls and two-dimensional vortices totals no more than the spin on a single atomic lattice site S, it is unlikely that the intrinsic magnetization associated with these antiferromagnetic textures can be reliably detected in the near future. Furthermore, to predict the correct excitation scheme of antiferromagnetic solitons, the intrinsic spin must be treated quantum mechanically because quantum fluctuations become important [21]. In higher-dimensional systems such as thin films or bulk AFMs, however, domain walls are not purely one-dimensional objects.

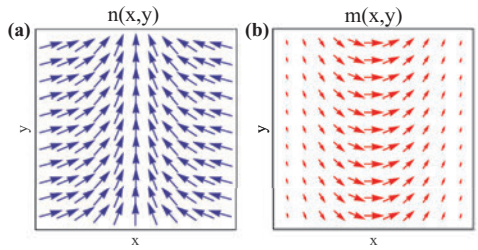

FIG. 7. (a) Sketch of a domain wall in the staggered order parameter $\mathbf{n}(x,y)$ (blue vector field) in a two-dimensional AFM, e.g., a nanostrip. The domain-wall configuration is repeated in the perpendicular direction. (b) The magnetization vector field $\mathbf{m}(z,y)$ (red vector field, not to scale) calculated from Eq. (14). Each spin chain along the horizontal direction will contribute the spin $S\hat{x}$ to the total spin of the two-dimensional domain-wall structure.

Although the order parameter can be defined as varying along one axis only, the nearest neighbors of each spin can exist along two (2D) or three (3D) perpendicular axes. In such systems, the intrinsic magnetization of the domain wall accumulates over the total number of spin chains that constitute the domain-wall structure. An example of the intrinsic magnetization of such an extended domain-wall structure in, e.g., a nanostrip is presented in Fig. 7.

In bulk AFMs with domain structures in the order parameter, the intrinsic magnetization forms planes along the domain boundaries. The total spin of these magnetization planes can be of appreciable size. In addition, for synthetic antiferromagnetic superlattices, in which the magnetization of each single ferromagnetic layer is much larger than S, the intrinsic magnetization associated with magnetic textures is accordingly larger and may be detectable [38].

C. Effect of pinning sites on domain-wall dynamics

Pinning sites for domain walls can arise from impurities or crystal defects in the underlying lattice of AFMs. Although several studies have found that pinning effects in AFMs are small [56–58], dislocations and impurities diffuse the effects on a single spin. In quasi-one-dimensional spin chains, the introduction of a single impurity atom can be enough to destroy long-ranged antiferromagnetic order and domain-wall configurations. From such a perspective, the scenario studied in Sec. IV requires a perfect spin chain in strictly one-dimensional systems. However, because three-dimensional domain boundaries are typically sums of many one-dimensional spin chains, we expect the effects of pinning from impurities to be significantly smaller for domain-wall systems that extend in the perpendicular directions than for one-dimensional spin chains.

VI. CONCLUSION

Starting from the discrete Heisenberg Hamiltonian with antiferromagnetic exchange coupling and easy-axis anisotropy, we have rederived the continuum limit of the free-energy functional in the exchange approximation and conclusively shown that textures in the antiferromagnetic order exhibit intrinsic magnetization. In recent effective

models for the dynamics of the antiferromagnetic order parameter, this intrinsic magnetization has been mostly disregarded. By comparing the Hamiltonian approach that we apply in this paper with a commonly used alternative parametrization procedure called Haldane's mapping, we have shown that the continuum fields of the two parametrization procedures have crucially different physical interpretations. As a result, the intrinsic magnetization can be easily missed in continuum models based on Haldane's mapping.

We have demonstrated that parity-breaking terms in the energy functional influence the dynamics of textured AFMs affected by external forces that couple directly to the intrinsic magnetization. For extended domain walls in 2D/3D, the influence of the intrinsic magnetization on the texture dynamics goes beyond that of the quantum effects observed for one-dimensional spin chains. By utilizing the method of collective coordinates, we have shown that a spatially inhomogeneous magnetic field represents a reactive force on antiferromagnetic textures and can move a domain wall in an antiferromagnetic nanowire. This effect is directly linked to the intrinsic magnetization of the domain wall. Numerical simulations of the coupled equations of motion for the staggered field and the magnetization field confirmed that a spatially inhomogeneous magnetic field can act as a potential well for the domain wall. Finally, we have discussed how the intrinsic magnetization of antiferromagnetic textures, which for one-dimensional domain walls are not larger than the spin on one atomic site, can be experimentally exploited in 2D and 3D. In such higher-dimensional real systems the intrinsic magnetization accumulates in the perpendicular directions and the total spin can, therefore, be of appreciable size and may be detectable.

ACKNOWLEDGMENTS

We thank H. Skarsvåg, R. A. Duine, and J.-O. Fjærestad for valuable discussions. J.L. acknowledges financial support from the Outstanding Academic Fellows programme at Norwegian University of Science and Technology and the Norwegian Research Council Grants No. 205591, No. 216700, and No. 240806.

APPENDIX: ENERGY FUNCTIONAL FOR $D > 1$

In this Appendix, we expand our calculation of the free-energy functional of AFMs to two and three dimensions to disclose the form of the parity-breaking term in higher dimensions. For $D = 2$, we use the centered rectangular unit cell, with two sublattices within each unit cell. Starting with Eq. (1), we now assume that $\boldsymbol{\alpha}$ and $\boldsymbol{\beta}$ are two-dimensional vectors and that the coordinate pair $\{i, j\}$ unambiguously defines all antiferromagnetic unit cells. Next, we define

$$\mathbf{m}_{i,j} = \frac{\mathbf{S}_\alpha^{i,j} + \mathbf{S}_\beta^{i,j}}{2S}, \tag{A1a}$$

$$\mathbf{l}_{i,j} = \frac{\mathbf{S}_\alpha^{i,j} - \mathbf{S}_\beta^{i,j}}{2S}, \tag{A1b}$$

$$\mathbf{S}_\alpha^{i,j} = S(\mathbf{m}_{i,j} + \mathbf{l}_{i,j}), \tag{A1c}$$

$$\mathbf{S}_\beta^{i,j} = S(\mathbf{m}_{i,j} - \mathbf{l}_{i,j}), \tag{A1d}$$

where we must take into account the equivalence of interchanging $\mathbf{l}_i \to -\mathbf{l}_i$, such as in the one-dimensional derivation. The Heisenberg Hamiltonian can be written as a sum over antiferromagnetic unit cells in the perpendicular i and j directions

$$\begin{aligned} H_{2\mathrm{D}} = JS^2 \sum_{i,j}^{N-1,N-1} & (\mathbf{m}_{i,j} - \mathbf{l}_{i,j})[(\mathbf{m}_{i,j} + \mathbf{l}_{i,j}) \\ & + (\mathbf{m}_{i+1,j} + \mathbf{l}_{i+1,j}) + (\mathbf{m}_{i,j+1} + \mathbf{l}_{i,j+1}) \\ & + (\mathbf{m}_{i+1,j+1} + \mathbf{l}_{i+1,j+1})] \\ & - KS^2 \sum_{i,j}^{N,N} \left[(\mathbf{m}_{i,j} + \mathbf{l}_{i,j})_z^2 + (\mathbf{m}_{i,j} - \mathbf{l}_{i,j})_z^2\right], \end{aligned} \tag{A2}$$

where we have disregarded a small energy contribution from the edge spins like in Sec. II A. Equation (A2) is a sum over the $N_D = 4$ nearest-neighbor exchange couplings and the anisotropy energies for each antiferromagnetic unit cell. We use the identities $2\mathbf{m}_{i,j}\mathbf{m}_{i+1,j} = \mathbf{m}_{i,j}^2 + \mathbf{m}_{i+1,j}^2 - (\mathbf{m}_{i+1,j} - \mathbf{m}_{i,j})^2$ and $(\mathbf{l}_{i,j}\mathbf{m}_{i+1,j} - \mathbf{m}_{i,j}\mathbf{l}_{i+1,j}) = \mathbf{l}_{i,j}(\mathbf{m}_{i+1,j} - \mathbf{m}_{i,j}) - \mathbf{m}_{i,j}(\mathbf{l}_{i+1,j} - \mathbf{l}_{i,j})$, etc., to rewrite Eq. (A2) to

$$\begin{aligned} H_{2\mathrm{D}} = {} & N_D JS^2 \sum_{i,j}^{N,N} \left(\mathbf{m}_{i,j}^2 - \mathbf{l}_{i,j}^2\right) \\ & + \frac{JS^2}{2} \sum_{i,j}^{N-1,N-1} [(\mathbf{l}_{i+1,j} - \mathbf{l}_{i,j})^2 + (\mathbf{l}_{i,j+1} - \mathbf{l}_{i,j})^2 \\ & + (\mathbf{l}_{i+1,j+1} - \mathbf{l}_{i,j})^2 - (\mathbf{m}_{i+1,j} - \mathbf{m}_{i,j})^2 \\ & - (\mathbf{m}_{i,j+1} - \mathbf{m}_{i,j})^2 - (\mathbf{m}_{i+1,j+1} - \mathbf{m}_{i,j})^2] \\ & + JS^2 \sum_{i,j}^{N-1,N-1} [\mathbf{m}_{i,j}(\mathbf{l}_{i+1,j} + \mathbf{l}_{i,j+1} + \mathbf{l}_{i+1,j+1} - 3\mathbf{l}_{i,j}) \\ & - \mathbf{l}_{i,j}(\mathbf{m}_{i+1,j} + \mathbf{m}_{i,j+1} + \mathbf{m}_{i+1,j+1} - 3\mathbf{m}_{i,j})] \\ & - 2KS^2 \sum_{i,j}^{N,N} \left(m_{i,j,z}^2 + l_{i,j,z}^2\right). \end{aligned} \tag{A3}$$

To make the transition to the continuum limit, we define the derivatives in the linear approximation

$$\lim_{|\Delta_i|\to 0} \sum_{i,j} (\mathbf{l}_{i+1,j} - \mathbf{l}_{i,j}) \approx \frac{1}{V} \int [\mathcal{J}(\mathbf{l})\boldsymbol{\Delta}_{\boldsymbol{i}}] dV, \tag{A4a}$$

$$\lim_{|\Delta_j|\to 0} \sum_{i,j} (\mathbf{l}_{i,j+1} - \mathbf{l}_{i,j}) \approx \frac{1}{V} \int [\mathcal{J}(\mathbf{l})\boldsymbol{\Delta}_{\boldsymbol{j}}] dV, \tag{A4b}$$

$$\lim_{|\Delta_{i(j)}|\to 0} \sum_{i,j} (\mathbf{l}_{i+1,j+1} - \mathbf{l}_{i,j}) \approx \frac{1}{V} \int [\mathcal{J}(\mathbf{l})\boldsymbol{\Delta}_{\boldsymbol{i}} + \mathcal{J}(\mathbf{l})\boldsymbol{\Delta}_{\boldsymbol{j}}] dV, \tag{A4c}$$

where $\mathcal{J}(\mathbf{l})$ is the Jacobian matrix of the vector field $\mathbf{l}$, $\boldsymbol{\Delta}_{\boldsymbol{i(j)}}$ is a vector between unit cells in the $\hat{i}(\hat{j})$ direction, and V is the volume of the unit cell. For the centered squared unit cell, $|\boldsymbol{\Delta}_{\boldsymbol{i}}| = |\boldsymbol{\Delta}_{\boldsymbol{j}}| \equiv \Delta$ and $V = \Delta^2$. We define similar derivatives as in Eqs. (A4) for the magnetization field $\mathbf{m}$.

The procedure is analogous when including a third dimension, e.g., for a body-centered-cubic unit cell, repeating the above calculation with $\{i,j\} \to \{i,j,k\}$. Apart from a constant contribution, the resulting free-energy density for AFMs in dimensions $D > 1$, defined here as $H_{2(3)\mathrm{D}} = \int (dV/V)\mathcal{H}_{2(3)\mathrm{D}}$, is given by

$$\begin{aligned}\mathcal{H}_{2(3)\mathrm{D}} = JS^2N_D\Big\{&2\mathbf{m}^2 + \frac{1}{2}\sum_i \Delta_i^2[(\partial_i\mathbf{l})^2 - (\partial_i\mathbf{m})^2] \\ &+ \frac{1}{4}\sum_{i\neq j}\Delta_i\Delta_j(\partial_i\mathbf{n}\cdot\partial_j\mathbf{n} - \partial_i\mathbf{m}\cdot\partial_j\mathbf{m}) \\ &+ \frac{1}{2}\sum_i \Delta_i(\mathbf{m}\cdot\partial_i\mathbf{l} - \mathbf{l}\cdot\partial_i\mathbf{m})\Big\} \\ &- KS^2[(\mathbf{l}\cdot\hat{z})^2 + (\mathbf{m}\cdot\hat{z})^2], \end{aligned} \tag{A5}$$

where we may define i and j to run over perpendicular directions $\{x,y,z\}$. The sum over first-order derivatives arises from the relation $\mathcal{J}(\mathbf{l})\boldsymbol{\Delta} = \sum_i \Delta_i\partial_j(\mathbf{l})$, where $\boldsymbol{\Delta} = \{\Delta_i,\Delta_j,\Delta_k\}$.

By considering squared or cubic lattices, $\Delta = 2d/\sqrt{D}$ and d is the nearest-neighbor distance. We can express the free-energy density in the exchange approximation $|K| \ll |J|$ as

$$\begin{aligned}\mathcal{H}_{2(3)\mathrm{D}} = &\frac{a}{2}\mathbf{m}^2 + \frac{A}{2}\left[\sum_i(\partial_i\mathbf{n})^2 + \frac{1}{2}\sum_{i\neq j}\partial_i\mathbf{n}\cdot\partial_j\mathbf{n}\right] \\ &+L\sum_i(\mathbf{m}\cdot\partial_i\mathbf{n}) - \frac{K_z}{2}(\mathbf{n}\cdot\hat{z})^2, \end{aligned} \tag{A6}$$

where $a = 4N_DJS^2$, $A = N_D\Delta^2JS^2/2$, $L = N_D\Delta JS^2$, $K_z = 2KS^2$, and N_D is the number of nearest neighbors.

In antiferromagnetic materials in which the exchange energy is anisotropic due to, e.g., more complicated unit cells, Eq. (A6) can still be used, although in this case a, A, and L must be treated as tensors.

[1] A. H. MacDonald and M. Tsoi, Philos. Trans. R. Soc. A **369**, 3098 (2011).
[2] E. V. Gomonay and V. M. Loktev, Low Temp. Phys. **40**, 17 (2014).
[3] B. G. Park, J. Wunderlich, X. Martí, V. Holý, Y. Kurosaki, M. Yamada, H. Yamamoto, A. Nishide, J. Hayakawa, H. Takahashi, A. B. Shick, and T. Jungwirth, Nat. Mater. **10**, 347 (2011).
[4] X. Martí, B. G. Park, J. Wunderlich, H. Reichlová, Y. Kurosaki, M. Yamada, H. Yamamoto, A. Nishide, J. Hayakawa, H. Takahashi, and T. Jungwirth, Phys. Rev. Lett. **108**, 017201 (2012).
[5] X. Marti, I. Fina, C. Frontera, J. Liu, P. Wadley, Q. He, R. J. Paull, J. D. Clarkson, J. Kudrnovský, I. Turek, J. Kuneš, D. Yi, J.-H. Chu, C. T. Nelson, L. You, E. Arenholz, S. Salahuddin, J. Fontcuberta, T. Jungwirth, and R. Ramesh, Nat. Mater. **13**, 367 (2014).
[6] C. Wang, H. Seinige, G. Cao, J.-S. Zhou, J. B. Goodenough, and M. Tsoi, Phys. Rev. X **4**, 041034 (2014).
[7] A. S. Núñez, R. A. Duine, P. Haney, and A. H. MacDonald, Phys. Rev. B **73**, 214426 (2006).
[8] A. C. Swaving and R. A. Duine, Phys. Rev. B **83**, 054428 (2011).
[9] J. Linder, Phys. Rev. B **84**, 094404 (2011).
[10] H. V. Gomonay and V. M. Loktev, Phys. Rev. B **81**, 144427 (2010).
[11] Z. Wei, A. Sharma, A. S. Nunez, P. M. Haney, R. A. Duine, J. Bass, A. H. MacDonald, and M. Tsoi, Phys. Rev. Lett. **98**, 116603 (2007).
[12] R. Cheng, J. Xiao, Q. Niu, and A. Brataas, Phys. Rev. Lett. **113**, 057601 (2014).
[13] K. M. D. Hals, Y. Tserkovnyak, and A. Brataas, Phys. Rev. Lett. **106**, 107206 (2011).
[14] A. C. Swaving and R. A. Duine, J. Phys.: Condens. Matter **24**, 024223 (2012).
[15] E. G. Tveten, A. Qaiumzadeh, O. A. Tretiakov, and A. Brataas, Phys. Rev. Lett. **110**, 127208 (2013).
[16] R. Cheng and Q. Niu, Phys. Rev. B **89**, 081105 (2014).
[17] E. G. Tveten, A. Qaiumzadeh, and A. Brataas, Phys. Rev. Lett. **112**, 147204 (2014).
[18] S. K. Kim, Y. Tserkovnyak, and O. Tchernyshyov, Phys. Rev. B **90**, 104406 (2014).
[19] D. Herranz, R. Guerrero, R. Villar, F. G. Aliev, A. C. Swaving, R. A. Duine, C. van Haesendonck, and I. Vavra, Phys. Rev. B **79**, 134423 (2009).
[20] N. Papanicolaou, Phys. Rev. B **51**, 15062 (1995).
[21] B. A. Ivanov and A. K. Kolezhuk, Phys. Rev. Lett. **74**, 1859 (1995).
[22] B. A. Ivanov and A. K. Kolezhuk, Fiz. Niz. Temp. **21**, 355 (1995) [Low Temp. Phys. **21**, 275 (1995)].
[23] H.-B. Braun, J. Kulda, B. Roessli, D. Visser, K. W. Kramer, H.-U. Gudel, and P. Boni, Nat. Phys. **1**, 159 (2005).
[24] I. V. Bar'yakhatar and B. A. Ivanov, Fiz. Niz. Temp. **5**, 759 (1979) [Low Temp. Phys. **5**, 361 (1979)]; Solid State Commun. **34**, 545 (1980).
[25] F. D. M. Haldane, Phys. Rev. Lett. **50**, 1153 (1983).
[26] V. G. Bar'yakhtar, B. A. Ivanov, and M. V. Chetkin, Sov. Phys.–Usp. **28**, 563 (1985).
[27] M. Bode, E. Y. Vedmedenko, K. von Bergmann, A. Kubetzka, P. Ferriani, S. Heinze, and R. Wiesendanger, Nat. Mater. **5**, 477 (2006).
[28] R. Jaramillo, T. F. Rosenbaum, E. D. Isaacs, O. G. Shpyrko, P. G. Evans, G. Aeppli, and Z. Cai, Phys. Rev. Lett. **98**, 117206 (2007).
[29] N. B. Weber, H. Ohldag, H. Gomonaj, and F. U. Hillebrecht, Phys. Rev. Lett. **91**, 237205 (2003).
[30] O. Bezencenet, D. Bonamy, R. Belkhou, P. Ohresser, and A. Barbier, Phys. Rev. Lett. **106**, 107201 (2011).
[31] S. Czekaj, F. Nolting, L. J. Heyderman, P. R. Willmott, and G. van der Laan, Phys. Rev. B **73**, 020401 (2006).
[32] E. Folven, T. Tybell, A. Scholl, A. Young, S. T. Retterer, Y. Takamura, and J. K. Grepstad, Nano Lett. **10**, 4578 (2010).

[33] D. Cabra and P. Pujol, in *Quantum Magnetism*, Lecture Notes in Physics, Vol. 645, edited by U. Schollwöck, J. Richter, D. Farnell, and R. Bishop (Springer, Berlin, 2004), pp. 253–305.
[34] A. Auerbach, *Interacting Electrons and Quantum Magnetism* (Springer, New York, 2012).
[35] I. Affleck, Nucl. Phys. **257**, 397 (1985).
[36] F. D. M. Haldane, J. Appl. Phys. **57**, 3359 (1985).
[37] B. A. Ivanov and A. K. Kolezhuk, Phys. Rev. B **56**, 8886 (1997).
[38] N. Papanicolaou, J. Phys.: Condens. Matter **10**, L131 (1998).
[39] P. W. Anderson, Phys. Rev. **86**, 694 (1952).
[40] I. Affleck, J. Phys.: Condens. Matter **1**, 3047 (1989).
[41] E. M. Lifshitz and L. P. Pitaevskii, *Statistical Physics, Course of Theoretical Physics*, Vol. 9 (Pergamon, Oxford, 1980).
[42] H.-B. Braun and D. Loss, Phys. Rev. B **53**, 3237 (1996).
[43] G. Tatara, H. Kohno, and J. Shibata, Phys. Rep. **468**, 213 (2008).
[44] E. Fradkin and M. Stone, Phys. Rev. B **38**, 7215 (1988).
[45] F. D. M. Haldane, Phys. Rev. Lett. **61**, 1029 (1988).
[46] N. Read and S. Sachdev, Nucl. Phys. B **316**, 609 (1989).
[47] N. Read and S. Sachdev, Phys. Rev. B **42**, 4568 (1990).
[48] A. F. Andreev and V. I. Marchenko, Sov.–Phys. Usp. **23**, 21 (1980).
[49] T. Oguchi, Phys. Rev. **117**, 117 (1960)
[50] M. Takahashi, Phys. Rev. B **40**, 2494 (1989).
[51] A. Brataas, A. D. Kent, and H. Ohno, Nat. Mater. **11**, 372 (2012).
[52] O. A. Tretiakov, D. Clarke, G.-W. Chern, Y. B. Bazaliy, and O. Tchernyshyov, Phys. Rev. Lett. **100**, 127204 (2008).
[53] N. L. Schryer and L. R. Walker, J. Appl. Phys. **45**, 5406 (1974).
[54] A. Kubetzka, P. Ferriani, M. Bode, S. Heinze, G. Bihlmayer, K. von Bergmann, O. Pietzsch, S. Blügel, and R. Wiesendanger, Phys. Rev. Lett. **94**, 087204 (2005).
[55] J. Wu, D. Carlton, J. S. Park, Y. Meng, E. Arenholz, A. Doran, A. T. Young, A. Scholl, C. Hwang, H. W. Zhao, J. Bokor, and Z. Q. Qiu, Nat. Phys. **7**, 303 (2011).
[56] R. P. Michel, N. E. Israeloff, M. B. Weissman, J. A. Dura, and C. P. Flynn, Phys. Rev. B **44**, 7413 (1991).
[57] O. G. Shpyrko, E. D. Isaacs, J. M. Logan, Y. Feng, G. Aeppli, R. Jaramillo, H. C. Kim, T. F. Rosenbaum, P. Zschack, M. Sprung, S. Narayanan, and A. R. Sandy, Nature (London) **447**, 68 (2007).
[58] J. M. Logan, H. C. Kim, D. Rosenmann, Z. Cai, R. Divan, O. G. Shpyrko, and E. D. Isaacs, Appl. Phys. Lett. **100**, 192405 (2012).